

OBSERVATIONS OF LOW ENERGY ELECTRONS

WITH THE OGO-A SATELLITE

by

VYTENIS M. VASYLIUNAS

A.B., Harvard College

(1962)

SUBMITTED IN PARTIAL FULFILLMENT

OF THE REQUIREMENTS FOR THE

DEGREE OF DOCTOR OF

PHILOSOPHY

at the

MASSACHUSETTS INSTITUTE OF

TECHNOLOGY

August, 1966

Signature of Author

Department of Physics, August 22, 1966

Certified by

Thesis Supervisor

Accepted by

Chairman, Departmental Committee
on Graduate Students



Room 14-0551
77 Massachusetts Avenue
Cambridge, MA 02139
Ph: 617.253.2800
Email: docs@mit.edu
<http://libraries.mit.edu/docs>

DISCLAIMER OF QUALITY

Due to the condition of the original material, there are unavoidable flaws in this reproduction. We have made every effort possible to provide you with the best copy available. If you are dissatisfied with this product and find it unusable, please contact Document Services as soon as possible.

Thank you.

Some pages in the original document contain text that runs off the edge of the page.

OBSERVATIONS OF LOW ENERGY ELECTRONS

WITH THE OGO-A SATELLITE

by

Vytenis M. Vasyliunas

Submitted to the Department of Physics on August 22, 1966, in partial fulfillment of the requirements for the degree of Doctor of Philosophy.

ABSTRACT

Electrons of energies between 125 ev and about 2000 ev were observed out to distances of 24.4 earth radii near the geomagnetic equator on the dusk side of the earth from October to December 1964 by means of a Faraday cup detector with four energy windows flown on the OGO-A satellite. In the transition region between the magnetosphere and the solar wind, fluxes of electrons varying from 10^8 $\text{cm}^{-2}\text{sec}^{-1}$ to 10^{10} $\text{cm}^{-2}\text{sec}^{-1}$ were found, the higher values occurring during magnetic storms; the differential flux of the electrons varied with energy roughly as E^{-4} to E^{-6} , indicating that the electrons were a non-Maxwellian high energy tail of a distribution peaked well below 125 ev. Weak or no fluxes were detected in the solar wind; the termination of transition region electron fluxes occurred at the shock front, except that during one magnetic storm strong fluxes were found out to some distance in front of the shock. In the magnetosphere a band of electrons of mean energy of a few hundred ev, density of order 1 cm^{-3} , and flux of order $10^9 \text{ cm}^{-2}\text{sec}^{-1}$ was found extending from the magnetosphere boundary inward to a sharp termination at 11 ± 1 earth radii, occasionally closer; crossing this termination inward, the mean energy of the electrons dropped sharply (as much as a factor of 5 in 1 earth radius distance) while the density increased slightly. This band is identified with the soft electron belt previously inferred from Lunik 1 and 2 observations by Gringauz. At distances greater than about 10 earth radii from the dawn-dusk meridian on the night side, a region of electrons of mean energy 40 to 80 ev, density 5 to 10 cm^{-3} , and flux of the order of $10^{10} \text{ cm}^{-2}\text{sec}^{-1}$ was found, but limited data prevented determining its precise boundary. Throughout the surveyed region of the magnetosphere, including both the high and low energy regimes mentioned, the electron energy density was found to be approximately the same and relatively unvarying; the total energy density of the plasma, if equipartition of energy between electrons and protons is assumed, corresponded to magnetic fields of 20 to 40 γ , comparable to the measured fields.

Thesis Supervisor: Stanislaw Olbert

Title: Associate Professor of Physics

ACKNOWLEDGMENTS

I am grateful to Prof. S. Olbert for his inspiring supervision, and to Prof. F. Scherb (now at the University of Wisconsin) who suggested the topic and supervised the first year of this work. The design and construction of the apparatus was the work of Prof. H. Bridge and of R.E. McMahon, R.H. Baker, and E.F. Lyon of Lincoln Laboratory. The operation of the spacecraft was ably handled by Dr. G. Ludwig, OGO project scientist, and the OGO project staff at Goddard Space Flight Center. Major contributions to the data processing were made by Dr. G. Gordon (now at Lincoln Laboratory). I am indebted to Dr. J.P. Heppner and Dr. M. Sugiura of Goddard Space Flight Center for opportunity to see and discuss their OGO-A magnetic field data before publication. I greatly profited from numerous discussions with Prof. H. Bridge, Prof. A.J. Lazarus, Dr. E.F. Lyon, and J. Binsack. Finally I thank my sister, Mrs. Rasa D'Entremont, for typing the thesis.

TABLE OF CONTENTS

Acknowledgments	page 3
Table of Contents	4
List of Figures	6
I. Introduction	10
II. Review of previous work	
A. General concepts	11
B. Electron observations in the magnetosphere	19
C. Electron observations in the transition region	42
III. The Experiment	
A. The flight	46
B. Apparatus	49
C. Data acquisition and processing	55
IV. Results	
A. The transition region	58
B. The magnetosphere	73
V. Conclusion	87
Appendix A. Some details of the apparatus	90
Appendix B. Orbital elements	99
Appendix C. Some details of data processing	100
Appendix D. Some concepts of geomagnetism	102
Appendix E. Coordinate systems	104
Appendix F. Critique of the electron energy calculation of Freeman et al.	108

Table I. Energy windows of the detector	page 110
Table II. Numerical coefficients for various quantities related to the model distribution function	111
Table III. Positions and times for spectra in Fig. 20	112
Table IV. Electron spectra in the magnetosphere	114
References	117
Figures	130
Biographical note	171

LIST OF FIGURES

- Fig. 1. Schematic view of the plasma and magnetic field configuration near the earth, in the noon-midnight meridian plane.
- Fig. 2. The magnetosphere according to Dungey.
- Fig. 3. The magnetosphere according to Dessler.
- Fig. 4. Projections in the solar magnetic equatorial plane of the regions scanned by several satellites carrying electron detectors.
- Fig. 5. Two possible interpretations of the observed cusp termination; above, there is a real termination of the cusp region in the equatorial plane; below, the cusp joins on smoothly to the neutral sheet and the radial termination is only apparent, caused by the satellite orbit.
- Fig. 6. A model of magnetic field configuration in the cusp region, in the noon-midnight meridian plane, on the assumption that the cusp joins on smoothly to the neutral sheet. The density of field lines indicates the field strength (except near the neutral sheet).
- Fig. 7. Equatorial plane projections of the several distinct regions recognized from 40 kev electron measurements.
- Fig. 8. Representation of the OGO-A orbit and spin axis and their relation to the ecliptic plane, in inertial space.
- Fig. 9a. Orbits 1 and 2 of OGO-A projected on the solar ecliptic XY plane.

- Fig. 9b. Same, on the XZ plane.
- Fig. 10. Orbits 25,26, and 27 projected by rotation about the dipole axis onto a magnetic meridian plane.
- Fig. 11. Schematic diagram of detector and electronics.
- Fig. 12. Modulator potential waveform.
- Fig. 13. Energy windows of the detector: relative efficiency for detecting flux of particles with $\frac{1}{2} m v^2 (\cos)^2 \theta = E$
- Fig. 14. The measurement sequence and its timing.
- Fig. 15. The angular response function.
- Fig. 16. Data coverage: the solid lines indicate the distance ranges in each orbit from which data are available.
- Fig. 17. Data for orbit 23 inbound. In this and similar plots, the lowest energy channel is at the bottom, the highest energy at the top. The quantity plotted is log of the smoothed current, with scale in amps as shown; the "50 points/inch" label should be ignored. The horizontal scales are: the lowest, U.T.; the upper bottom, geocentric distance in earth radii; the lower top, the "azimuth", the angle between the ecliptic and the projection on the dawn-dusk meridian of the radius vector to the satellite, measured counterclockwise as seen from the sun; the highest, sun-earth-probe angle.
- Fig. 18. Data for orbit 22 inbound.
- Fig. 19. Data for part of orbit 27 inbound.

- Fig. 20. Sample spectra in the transition region. The abscissa of each is $\log V_2$ of the channel, in ev; the ordinate, \log measured current, in amps. The times and positions of these spectra are listed in Table III.
- Fig. 21. The speed distribution $v^2 f(v)$, with $f(v)$ given by equation (9), normalized to 1 at the peak (courtesy of Moreno, Olbert, and Pai).
- Fig. 22a. Predicted currents in channel 1, using the model distribution; for normalization, see text.
- Fig. 22b. Same, channel 2.
- Fig. 22c. Same, channel 3.
- Fig. 22d. Same, channel 4.
- Fig. 23. Ratio of omnidirectional flux $J(E)$ to channel 4 current i_4 as function of E , for the model distribution.
- Fig. 24. Measured spectra from Fig. 20 in a $\log (i_4/i_3)$ vs. $\log (i_3/i_2)$. Circled points appear only in this figure, squared points in this and the next. Lines are constant parameter curves predicted from the model distribution.
- Fig. 25. Same, $\log (i_3/i_2)$ vs. $\log i_2/i_1$.
- Fig. 26. Qualitative (and exaggerated) sketch of electron spectrum suggested by deviations from model. (a) and (b) are the "first case", (c) the "second" (see text).
- Fig. 27. Unsmoothed data for portion of orbit 33 outbound. Channels and horizontal scales as described under Fig. 17. Vertical scale is measured signal in volts.

- Fig. 28. Data for orbit 15 inbound. Format as in Fig. 17.
- Fig. 29. Data for orbit 35 inbound.
- Fig. 30. Data for orbit 11 inbound.
- Fig. 31. Data for portion of orbit 23 inbound. Format as in Fig. 27.
- Fig. 32. Observed spatial distribution of electrons.
- Fig. 33. Examples of curve fitting to spectra in the magnetosphere.
See text for description.
- Fig. 34. Positions within magnetosphere at which spectra were analysed, and rough indication of mean energies found.
- Fig. 35. Energy vs. density plot of spectra in the magnetosphere.
Lines connecting two points indicate that only a range of values can be specified by the fitting process. The line connects (highest N - lowest E_0) with (lowest N - highest E_0); the actual allowed region is roughly a narrow ellipse with the line as major axis.
- Fig. 36. Changes of electron spectrum with distance at the earthward boundary of observed electrons on orbit 23.
- Fig. 37. Calibration curve of the electronics.

I. INTRODUCTION

Observations of charged particles have constituted one of the major scientific efforts of space exploration since its beginning. They are studied both as a significant geophysical system in its own right and for insights that their study can be expected to provide into fundamental processes in collisionless magnetic plasmas, on the one hand, and into the causes of a great variety of geomagnetic and auroral phenomena, on the other. High energy particles, that small fraction of the plasma with improbably high velocities, have been the most intensively studied to date. In recent years, extensive surveys of protons in the 100 ev to 10 kev energy range have provided information on the bulk (rather than just the high energy tail) of the positive particles in the plasma; there were no comparable surveys of plasma electrons but only brief and scattered observations, until the launchings of Vela 2 and OGO-A in the summer of 1964. The regions of space surveyed by these two satellites are nearly orthogonal surfaces: while Vela scanned a wide range of latitudes at a fixed geocentric distance of 17 earth radii, OGO-A, relatively confined in latitude to near the geomagnetic equator, scanned a range of distances from 1.3 to 24.4 earth radii. This thesis is a report on observations of electrons of energies from 125 ev to about 2000 ev with a Faraday cup flown on OGO-A.

II. REVIEW OF PREVIOUS WORK

A. General Concepts

The electromagnetic and charged-particle environment of the earth is determined largely by two factors: the permanent magnetic field of the earth and the continuous flow of a tenuous, ionized gas from the sun.

Nearly forty years before the beginning of space exploration, an intermittent flow of plasma from the sun was postulated by Lindemann (1919) to account for magnetic storms*; starting from his ideas Chapman and Ferraro (1931, 1932, 1933), in a classic series of papers, developed the first detailed theory of the interaction between the earth's magnetic field and the flowing plasma. A continuous streaming of plasma from the sun was invoked by Biermann (1951) to account for certain properties of comet tails and was later theoretically derived from a hydrodynamical model of the solar corona by Parker (1958a , 1963), who named it the solar wind. To put Parker's argument very simply, the heating of the corona inferred from observations represents an energy input too large to be balanced by radiation and heat conduction alone; hence to maintain a steady state a continuous expansion of the coronal gas, carrying energy off into space,

* See Appendix D for a brief description of magnetic storms and their phases

is required. The existence of the solar wind has been established and its gross features determined by plasma observations from a number of satellites and space probes, among them Explorer 10, Mariner 2, Explorer 18 (alias IMP-1), Explorer 21 (alias IMP-2) Vela 2,OGO-A, Mariner 4, Vela 3, and Pioneer 6 (see e.g., Bonetti et al., 1963; Snyder et al., 1963; Bridge et al., 1965, 1966; Lyon, 1966; Wolfe et al., 1966; Strong et al., 1966; Neugebauer and Snyder, 1966). The positive ion component of the solar wind consists mainly of protons, with an admixture of alpha particles ranging from 2% to 8% by number. Typically the number density of protons varies between 4 and 15 particles cm^{-3} , the bulk velocity varies between 250 and 700 km/sec, and the "thermal" spread in velocities corresponds to temperatures of the order of 10^5 °K. Magnetic measurements (see Ness et al., 1964; Wilcox and Ness, 1965; Coleman, 1966; and references therein) show an interplanetary magnetic field with magnitude ranging from 2 to 10 gammas (1 gamma = 10^{-5} gauss) and with rather variable direction; on the average, though, the field vector lies close to the ecliptic plane and points either away from or toward a direction about 45° west of the sun, in agreement with the spiral field pattern predicted by Parker's model.

The electrical conductivity of the solar wind is very high and, as a well-known consequence, the magnetic flux through any closed loop moving with the wind must remain nearly constant. Thus the solar wind cannot flow through the high-field region near the earth; there must therefore be a boundary dividing space into two regions, one containing the interplanetary plasma, the other the earth's magnetic field; electric currents flowing on the boundary (associated with the magnetic

field discontinuity there) shield the plasma from the earth's magnetic field and also interact with the field to produce the forces that balance the plasma pressure on the boundary. The region containing the geomagnetic field is called the magnetosphere, a term introduced by Gold (1959); its boundary is often called the magnetopause*. That the flow of the solar wind past the earth would produce a magnetosphere was one of the chief predictions of the Chapman-Ferraro theory. Magnetic field and plasma measurements from satellites have confirmed the existence of the magnetosphere and mapped its boundary (at least in regions not very close to the earth's magnetic dipole axis) (Heppner et al., 1963; Cahill and Amazeen, 1963; Bonetti et al., 1963; Ness et al., 1964; Ness, 1965; Lyon, 1966; Ness et al., 1966; Cahill and Patel, 1966); Figure 1 contains a sketch of the (rather non-spherical) shape found for the magnetosphere. The observations, as far as they go, are consistent with a shape having at least a rough axial symmetry about the sun-earth line (or, more precisely, about the direction of the plasma flow; the two differ only by a few degrees). Over the sunlit side of the earth the boundary is quasi-spherical and in rough agreement with theoretical calculations based on simplified models of plasma-field pressure balance (Midgley and Davis, 1963; Mead and Beard, 1964; Slutz and Winkelman, 1964; reviewed by Beard, 1964); on the night side the magnetosphere is drawn out into a long "tail" that seems to approach a constant width and shows no sign of closing even at the greatest distances yet reached by satellites, about half-way to the moon. The size of the

* "— pause" as the boundary of "— sphere" is a common meteorological usage; compare, e.g., "troposphere" and "tropopause".

magnetosphere is somewhat variable but a typical distance to its subsolar point (i.e. the point on the sun-earth line) is about 10 earth radii (abbreviated Re; 1 Re=6380 km) and a typical tail radius (Ness, 1966) is about 20 to 22 Re.

The magnetic field in the magnetosphere is of crucial significance in determining the behavior of charged particles. The principal features of the field topology inferred from observations (see especially Ness, 1965) are sketched in Fig. 1. The field line pattern can be thought of as obtained by deforming the dipole pattern of the earth's main field: in the front part of the magnetosphere the field lines are compressed; in the tail they are pulled back until they point in a direction nearly along the sun-earth line. With such an almost straight-line topology, in the tail there must be a thin region in which the field reverses direction pointing generally away from the earth below this region (over the southern hemisphere) and toward the earth above it; such a region of abrupt field reversal is generally called a neutral sheet (within it the field magnitude must be very small to avoid large stresses on the ionized matter present). The existence of a neutral sheet in the tail of the magnetosphere was demonstrated from Explorer 18 magnetic measurements by Ness (1965), who also noted that the neutral sheet lies roughly in a plane containing the sun-earth line and the line perpendicular to this and the earth's magnetic dipole axis (and hence having a diurnal roll motion about the sun-earth line) as suggested earlier by Axford et al. (1965) and Dessler and Juday (1965).

Two different theoretical approaches to the magnetospheric tail have been proposed. The model of the tail suggested by Dungey (1961) and elaborated by Levy et al. (1964) and Axford et al. (1965) is sketched in Fig. 2. Field lines from the earth become connected to the field external to the magnetosphere (assumed to have a southward component opposing the dipole field) at a neutral point near the subsolar point (thus producing a small component of the field normal to the magnetopause), are carried back by the external plasma flow and reconnect to form closed loops again at another neutral point in the tail; the resulting motion, when projected on the polar caps, agrees qualitatively with auroral current patterns (Levy et al., 1964) and the reconnection of field lines at the neutral points provides mechanisms for injecting into the magnetosphere particles needed to account for a variety of auroral and geomagnetic phenomena (Axford, 1966). The length of the tail to the neutral point is estimated by Dungey (1965) as $\sim 10^3$ Re. The model proposed by Dessler (1964; see also Dessler and Juday, 1965, and Michel and Dessler, 1965) and sketched in Fig. 3, on the other hand, is based on the assumption that field reconnection cannot be significant because of lack of sufficiently fast dissipative processes (such as collisions); the tail extends indefinitely (i.e. as far as the solar wind itself), maintained open by the pressure of hydromagnetic waves generated in the front of the magnetosphere during magnetic storms; no field lines cross the magnetopause anywhere or in other words, the field at the magnetopause is tangential to the boundary. In spite of recent extensive and occasionally heated discussions (see, e.g. the debate between Van Allen,

1966 and Dessler, 1966), at present there appears to be no clear-cut observational (or theoretical) argument to decide between the two models.

The magnetosphere presents an obstacle to solar wind flow, a blunt obstacle of typical dimension 10^5 km. Now from the values of solar wind parameters (density, magnetic field etc.) given earlier one can readily show that the speed of either "sound" waves

$$c_s = (\gamma P / \rho)^{\frac{1}{2}}$$

or Alfvén waves

$$c_A = B / (4\pi\rho)^{\frac{1}{2}}$$

is an order of magnitude less than the flow speed. (Here P is the pressure, ρ the mass density, B the magnetic field strength, γ the ratio of specific heats). Thus the solar wind is highly "supersonic", in the sense that the flow speed exceeds the speed of relevant small amplitude waves (a feature predicted by Parker). This, if the solar wind can be described by the continuum fluid equations of ordinary gasdynamic theory, at once implies that an obstacle like the magnetosphere will produce ahead of it a standing shock wave, separating the region of the flow disturbed by the obstacle from the region where the obstacle has not yet been "sensed" by the flow. That the solar wind should behave like a fluid on a length scale of 10^5 km, however, is by no means obvious, since in it the mean free path for proton-proton collisions is of the order of 10^8 km. Nevertheless, on the grounds that the long-range electromagnetic interactions in a collisionless plasma could produce the collective behavior characteristic of a fluid (a view argued by,

for example, Levy et al., 1964), several theorists, among them Axford (1962) and Kellogg (1962), predicted the existence of a shock front ahead of the magnetosphere; the expected shape of the shock was calculated from magnetohydrdynamic equations by Spreiter and Jones (1963) and more recently by Spreiter et al. (1966). Satellite observations of both plasma and magnetic fields have in fact found outside the magnetosphere a well-defined region with a sharp outer boundary (sketched in Fig. 1) that agrees approximately with the shock shape of Spreiter and Jones (see references cited earlier, and also Heppner, 1965 and Holzer et al., 1966). This transition region between the undisturbed solar wind flow and the magnetosphere, generally called simply the transition region (another term which has been occasionally used lately is magnetosheath), is characterized by turbulent, fluctuating magnetic fields and a plasma that is appreciably hotter (i.e. with a larger spread of proton random velocities) than the undisturbed solar wind; the increase in the random thermal motions takes place at the expense of the speed of bulk motion which is reduced from the solar wind value, a process sometimes described as thermalization of the plasma.

Whether or not the outer boundary of the transition region is indeed a standing shock in the conventional gasdynamic sense is at present not certain. The distinguishing feature of a shock is the transition from a supersonic flow upstream to a subsonic flow within a region bounded by the obstacle and a certain well-defined surface (the sonic surface) ahead of it. ~~In the case of a blunt obstacle like the magnetosphere, this region of subsonic flow should have its greatest width near the stagnation line (along~~

~~which the undisturbed flow is normal to the obstacle), here very nearly the sun-earth line.~~ According to the analysis of the Explorer 18 results by Olbert and coworkers (Moreno et al., 1966), even in the subsolar part of the transition region the thermal speed of the protons (related to the speed of acoustic waves) is comparable to the flow speed; whether the flow is subsonic or not depends on the precise relation between thermal and wave speeds.* This uncertainty about the applicability of continuum shock theories (emphasized by, e.g. Bernstein et al., 1964, and Wolfe et al., 1966) has not prevented the general use of the term "shock" for the outer boundary of the transition region (a loose but convenient usage that I shall follow).

The distance between the magnetopause and the shock (i.e. the width of the transition region) near the subsolar point is often called the stand-off distance, another term borrowed from theories of the gasdynamic analog, and is typically 3 - 4 earth radii.

This concludes a rather brief and sketchy account of the overall configuration of plasmas and magnetic fields around the earth, as determined through extensive observational and theoretical work, and forming the general framework within which more detailed particle observations must be considered.

*The "thermal speed" of the Explorer 18 analysis is the most probable speed of protons, whereas the wave speed is related to their rms speed; the ratio of the two is sensitive to possible departures from a Maxwellian distribution.

B. Electron Observations in the Magnetosphere

Ground-based observations and related work. - Some information about magnetospheric electrons can be obtained with ground-based equipment, by observing their effect on electromagnetic wave propagation. Historically the first and so far the most important such technique makes use of certain naturally occurring very low frequency (VLF) electromagnetic signals called whistlers. These are circularly polarized waves whose frequency (typically 1-20 kc /s) lies below the plasma frequency and above the electron gyrofrequency of the propagation medium. They originate from the electromagnetic impulse associated with lightning and propagate back and forth ("hop") between the hemispheres along magnetic field lines; different frequency components propagate at different speeds in the highly dispersive medium, changing the original "click" into the characteristic descending "whistle". The phenomenon and its application to electron studies have been extensively described in reviews by Carpenter and Smith (1964) and Helliwell (1965); more recent work is presented by Carpenter (1966) and Angerami and Carpenter (1966). The quantity observed is the signal time delay since the originating lightning impulse (identified by the "click") as a function of frequency, for each hop; there often is a frequency (called the "nose" frequency, because of the shape of the frequency-time plot) at which the delay is a minimum. Analysis in terms of the cold-plasma (magnetoionic or Appleton-Hartree) dispersion relation (described in detail by Carpenter and Smith, 1964) relates the nose frequency to the gyrofrequency near the equatorial point of the propagation

path (from which the equatorial distance of the path can be derived if the field line pattern is known) and gives the delay time as an integral along the path of the plasma frequency (and hence the square root of the electron density) times a function of the field which is strongly peaked at the equatorial point. Assuming a model for the electron density distribution along the field line that is the propagation path (common choices are $N \sim R^{-3}$ or R^{-4} where R is the radial distance; the results are not very sensitive to the precise model used), one obtains from a number of different whistlers the electron density in the geomagnetic equatorial plane as a function of radial distance (the distance is conventionally and conveniently described by the L value* of the propagation path). The electron density thus obtained decreases smoothly with increasing L , remaining in the range 100 to 1000 electrons cm^{-3} out to about $L=4$ or 5; then abruptly the density drops to about 1 cm^{-3} , remaining at this low level out to the largest distances, $L \sim 7$, accessible to whistler observations so far. Carpenter has named the abrupt decrease at $L \sim 4$ the "knee" of the density profile. That it is a real spatial feature and not the result of some peculiar time variation is dramatically demonstrated by numerous simultaneous observations of several whistlers, some propagating inside, others outside the high density region. The position of the knee shows an inverse correlation with geomagnetic activity (as measured by the K_p index**), moving closer to the earth by as much as $2R_e$ during disturbed periods.

* See Appendix E

**Explained in Appendix D

There must be a corresponding abrupt decrease in positive ion density if the medium is to be electrically neutral. Such a decrease near a distance of $4R_e$ was observed in plasma measurements from Lunik 2 and Explorer 10 (Bonetti et al., 1963), both of which, however, made only one pass through this region. More recently, repeated direct observations of the ion density knee have been made with the mass spectrometer on OGO-A by Taylor et al. (1965), who obtained densities and knee positions in general agreement with whistler results, confirmed the inverse correlation with geomagnetic activity and presented evidence that the positive ions are predominantly protons, with a 1% admixture of He^+ ions. Indirect evidence for the ion knee from the present experiment will be described in a later chapter. Measurements of very low energy (0-15 eV) electrons with retarding potential analysers on Explorers 18 and 21 (Serbu, 1965; Serbu and Maier, 1966), on the other hand, while agreeing with whistler results inside the high density region, give densities of the order of 50 cm^{-3} outside, more than a factor of 10 higher than other determinations. It should be kept in mind, however, that the average energy of the electrons detected is of the order of 1 eV, that the outside surface of the detector is maintained at potentials of +15 volts or so relative to the skin of the satellite and the efficiency for collecting electrons is known no better than within a factor of 10, and that no detailed consideration of possible contributions from a photoelectron sheath around the satellite has been published. The whistler data are thus generally reported by satellite measurements so far with some possible but not well-established discrepancies.

Whistlers are not very sensitive to electron energy spectra; attempts by Liemohn and Scarf to deduce spectra from cut-off frequencies did not lead to self-consistent results (Liemohn, 1965). Measurements by Serbu and Maier (1966) inside the high density region give electron thermal energies 0.2 to 1 ev. In the case of positive ions, the observations on Explorer 10 of a flux maximum from the direction of satellite motion (Bonetti et al., 1963) indicate that the most of ions were slower than the satellite, putting an upper limit of a few tenths of an ev on their thermal energies.

To summarize, there seems to be a region near the earth filled with relatively high density, low energy plasma and having a sharp boundary that usually coincides approximately with the L=4 magnetic shell, but moves closer to the earth during magnetically disturbed periods. The L=4 shell intersects the earth at magnetic latitude 60° , somewhat below the auroral zones. The existence of some physically significant boundary at that latitude was already inferred from a variety of ionospheric and geomagnetic phenomena by Axford and Hines (1961), before the discovery of the knee; more recently a sharp local depression of electron density in the ionosphere near L=4 has been discovered by topside sounders (Muldrew, 1965; Sharp, 1966). The origin of this region and its relation to other phenomena has yet to be theoretically understood (some suggestions have been made by, among others, Axford and Hines, 1961, and Block, 1966).

Another ground-based technique for observing electrons makes use of high frequency radio waves reflected from the moon or transmitted to or from satellites. The quantity measured is the dispersive Doppler shift

(a Doppler shift not proportional to frequency and hence not arising from relative motion) which can be related, using the magnetoionic dispersion relation to the electron density integrated along the propagation path. This technique, extensively used for ionospheric studies, has been applied to the study of the average electron content in the magnetosphere by Howard et al. (1965) and Yoh et al. (1966), who used radio waves reflected off the moon, and more recently to the study of the electron density in the solar wind by Eshleman and others (1966), who used radio transmission to the Pioneer 6 space probe and obtained an average value of $8.25 \pm 4.43 \text{ cm}^{-3}$, in fair agreement with direct proton density measurements. The lunar radar measurements yield, after subtracting the large contribution from the ionosphere, a total electron content in a column to the moon that varies, as a function of angle from the earth-sun line, by up to $6 \times 10^{16} \text{ m}^{-2}$ relative to an unknown zero level, reaching a maximum near the antisolar direction. If spread uniformly between the ionosphere and the moon, as done by Yoh et al., this gives a mean density in the tail of the magnetosphere of $\sim 200 \text{ cm}^{-3}$, inconsistent with whistler results and also objectionable on theoretical grounds (Dessler and Michel, 1966). It is certain, however, that the density is not uniform over the path and that a large contribution to the result must come from the high density region just discussed. For example, taking the density of electrons at 1000 km height as 10^4 cm^{-3} (measured by Alouette 1, as cited by Angerami and Carpenter, 1966), assuming a density decrease as L^{-4} or L^{-3} out to $L=4$, as suggested by whistler results (Angerami and Carpenter, 1966), and assuming for simplicity that the propagation path lies in the equatorial

plane, the integrated density between 1000 km and $L=4$ is

$$10^4 \text{cm}^{-3} \times 6.4 \times 10^8 \text{cm} \times 10^4 \text{cm}^2 \text{m}^{-2} \int_1^4 \frac{dL}{L^n}$$

where $n = 3$ or 4 , giving values $3.2 \times 10^{17} \text{m}^{-2}$ or $2.1 \times 10^{17} \text{m}^{-2}$, quite comparable to values quoted by Yoh et al. The lunar radar technique thus probably can be a valuable method of studying the high density region within the whistler knee; whether it can also provide significant information about the density beyond the knee is questionable.

Satellite observations - general remarks. - Aside from the few, rather specialized, ground-based techniques just described, the only way to observe electrons in the magnetosphere has been to send a detector there on a satellite. Since 1957, a variety of particle detectors have been flown on a variety of satellites. Restricting oneself to satellites of interest in connection with the present work, however, a rough classification is possible. On the basis of their orbits, these satellites fall into two groups. In the first group are satellites (such as Explorers 10, 12, 14, 18 and 21, as well as OGO-A) in highly eccentric orbits with long apogee distances; their apogees are at relatively low latitudes (within $\pm 30^\circ$, say) and thus their primary use is for studying the radial distribution of electrons in the equatorial region of the magnetosphere. Any one orbit samples all radial distances (between perigee and apogee) within a longitude sector; a number of orbits covering a significant fraction of a year scans a large range of longitudes (as measured from the earth-sun line). since the magnetosphere is fixed relative to the earth-sun line and thus rotates

(relative to an inertial reference frame) around the ecliptic pole once a year while the orbit is fixed in inertial space (aside from secular perturbations, which are small for these orbits). Figure 4 shows, projected on the solar magnetic plane*, the regions scanned by the principal satellites that have provided magnetospheric electron surveys.

The second group consists of satellites (for example, Injun 3, Alouette 1 and 1963-38C) in low altitude (typically around 1000 km), very high inclination (near 90°), usually nearly circular orbits. Although on a magnetospheric distance scale these satellites are barely off the ground, they go to very high latitudes which are connected by magnetic field lines to the distant equatorial regions scanned by satellites of the first group. These low-altitude, high-latitude observations thus should reflect the structure found in the equatorial region and help to trace its relation to auroral and geomagnetic phenomena.

An unusual group of satellites that do not fit the above classification are the Vela Hotel nuclear test detection satellites, in nearly circular orbits at about 17 R_e and at a relatively high inclination (near 60°).

The most widely used electron detector has been the Geiger tube; others include magnetic spectrometers, scintillation counters, and solid-state detectors. None of these detectors, as used, has had appreciable response to electrons of energy below about 30 keV; the usual threshold has been 40 keV. The current view of electron distribution in the magnetosphere has been derived largely from measurements on electrons in the

* See Appendix E for description of relevant coordinate systems

40-300 kev range, except for charged particle trap measurements of electrons above 200 ev from three soviet space probes (each of which, however, made only one pass through the magnetosphere) and the Explorer 12 measurements with a CdS energy flux detector that was sensitive to electrons from 200 ev to 500 kev (but with no means of energy selection). The distribution of low energy (a few kev or less) electrons has been explored only recently, with curved-plate electrostatic analyzers on the Vela satellites and with a Faraday cup on OGO-A which is the subject of this thesis.

Satellite observations - radial surveys. - It is well-known that near the earth there is a region filled with energetic particles trapped on magnetic lines of force - the Van Allen radiation belts (for reviews and historical accounts, see e.g. O'Brien, 1962-63, Farley, 1963, or White, 1966). The so-called "inner belt" consists primarily of protons; peak fluxes occur at L values between 2 and 4, depending on the energy. The "outer belt", which is of concern here, consists primarily of electrons: the fluxes show large time variations, but typical fluxes of electrons above 40 kev are of the order of $10^7 - 10^8 \text{ cm}^{-2} \text{ sec}^{-1}$, a broad maximum occurring at L values around 5 or 6. The extent of this trapping region near the equatorial plane has been investigated with detectors on Explorer 12 (Freeman et al., 1963; Freeman, 1964), Explorer 14 (Frank and Van Allen, 1964; Frank, 1965; Serlemitsos, 1965, 1966), Explorer 18 (Anderson et al., 1965; Anderson, 1965) and Electron - 2 (summarized by Vernov et al., 1966). In the subsolar region there is generally a fairly sharp termination of energetic particle fluxes at distances near 10 Re, occurring at or near the

magnetosphere boundary (as checked in a number of cases by comparison with simultaneous magnetic field measurements). At all angles from the earth-sun line there is found a generally not very sharp but nevertheless clearly identifiable boundary, at a distance of roughly 8 Re in the geomagnetic equatorial plane, enclosing a region called the "hard core" of electrons by Frank (1965) or the Van Allen trapping zone by Anderson (1965); within it fluxes of electrons above 40 keV are of the order of $10^7 \text{ cm}^{-2}\text{sec}^{-1}$, the particle distribution in space is at least to some extent governed by the geomagnetic field (i.e. its gross features are at least roughly symmetric about the geomagnetic equator and aligned with L shells), and time variations are relatively small compared to those outside. Between this "hard core" and the magnetosphere boundary and extending from near the subsolar point to somewhat beyond the dawn and dusk meridians lies a region characterized by fluxes ($E > 40 \text{ keV}$, always) of the order of $10^5 - 10^6 \text{ cm}^{-2}\text{sec}^{-1}$, large temporal fluctuations, and an energy spectrum softer (i.e. containing fewer high-energy electrons) than within the trapping zone; "the radiation is agitated and very soft" is the description given by Anderson (1965). This region is often called the skirt, a name apparently first used by Frank et al., (1963). Over the sunlit hemisphere the skirt extends in latitude up to the highest latitudes reached by Explorers 14 and 18, about 30° south geomagnetic latitude. In longitude it extends back to about $110^\circ - 120^\circ$ from the earth-sun line; whether it extends in front right up to the subsolar point, or whether instead the trapping zone touches the magnetosphere boundary there, is at present not clear (Anderson, 1965, has identified skirt-type electrons as close as 23° from the sun-earth line).

The distribution of $E > 40$ kev electrons in the night side of the magnetosphere is somewhat more complicated. The first extensive survey of this region was done with Explorer 14 (apogee distance 16 Re); the results, as described by Frank (1965), indicated that (a) there is a tail of electron fluxes beyond about 10 Re (and out to beyond the satellite apogee) over the night side of the earth, lying more or less in the ecliptic plane (definitely not in the geomagnetic equatorial plane; the observations were made at a time close to the winter solstice, when the relative inclination of the two planes is at a maximum), and (b) electrons (outside the trapping zone) on the flanks of the night side of the magnetosphere (i.e. between this tail and the dawn-dusk meridian) are confined to a relatively narrow range of latitudes, in contrast to the sunlit skirt region. Anderson (1965), using data from Explorer 18, (apogee distance 31 Re), confirmed result (b) and gave the name cusp to the latitudinally confined region of electrons on the night side. He distinguished the cusp from the skirt (placing the boundary between them at about 120° from the earth-sun line) not only by their extent in latitude but also by the type of time variations within them, the cusp being characterized by fast increases in flux followed by slow decreases, as distinct from the more or less random fluctuations within the skirt. According to Anderson's observations the cusp is not drawn out into a tail but has a sharp termination at a distance varying between 10 and 15 Re. Beyond this boundary there are no steady electron fluxes observed on Explorer 18; instead, there occur so-called electron patches or islands, isolated

electron fluxes up to 10^6 or even 10^7 $\text{cm}^{-2}\text{sec}^{-1}$ that appear rapidly (rise time of minutes) and decay slowly (decay time up to a few hours), then often disappear again rapidly. The fast rise - slow decay behavior is observed on both inbound and outbound passes, showing that the "islands" are caused by actual time variations of electron flux, and are not fixed spatial features with gradients producing apparent time variations due to satellite motion (hence the name "islands", although widely used, is rather inappropriate). Similar observations have been reported by Serlemitsos (1965, 1966) and Konradi (1966), using data from Explorer 14 (and can be recognized, with the benefit of hindsight, in some of Frank's published data), and by Vela experimenters (Montgomery et al., 1965; Singer et al. 1966). The "islands" generally occur within about $6R_E$ of the solar magnetospheric equatorial plane; Frank's electron tail may perhaps be identified with the average position of the "islands", since at the solstices the mean position of the solar magnetospheric equator coincides with the ecliptic. Such a spatial distribution is in agreement with the suggestion of Ness (1965) that the $E > 40$ keV electrons are the high energy tail of a plasma that balances magnetic pressure in regions of weak or zero field associated with the neutral sheet, a suggestion supported by detection of the low-energy ($E \lesssim 1$ keV) electron component of the plasma with detectors on Vela satellites (Bame et al., 1966a,b) and the observation of frequent correlation between occurrence of "islands" and depression of magnetic field strength (Anderson and Ness, 1966). Both Anderson and Serlemitsos find that the occurrence frequency of "islands" decreases with increasing radial distance, but according to a statistical

analysis of Explorer 18 data by Murayama (1966) the occurrence frequency is independent of radial distance and depends on height above the neutral sheet (or the solar magnetospheric Z coordinate), the coupling of the two distances through the satellite orbit producing the apparent radial variation.

The neutral sheet is almost certainly a permanent feature of the magnetospheric tail, and hence the plasma sheet associated with it must also be permanent. The transient nature of $E > 40$ kev electron fluxes can then be explained in at least two ways: (a) the permanent plasma sheet has an electron spectrum soft enough so that 40 kev electrons are undetectable except when occasional "heating" (i.e. acceleration) occurs, or (b) the plasma sheet always contains detectable 40 kev electrons but the observed variations arise from motions of the sheet, or from changes in its thickness as suggested by Axford (1966) (this is rather plausible since most satellite orbits more or less graze the sheet).

Whether there is an actual sharp termination to the cusp region as inferred by Anderson or whether instead the cusp joins on smoothly to the tail plasma sheet and the observed termination results from the satellite orbit (as sketched in Fig. 5) is not conclusively settled by observations available to date. Anderson and Ness (1966) find that the cusp is associated with a depression of magnetic field strength and its observed termination (i.e. decrease of electron fluxes) coincides with abrupt increase in field strength. They infer that the field lines inside the cusp are closed so that particles can be trapped between mirror points; the cusp boundary coincides with the first open line of

force, and the field decrease inside the cusp is caused by the diamagnetic effects of trapped particles within it. No drawing of the envisaged model is given in their paper, and it is not clear what the proposed field and particle configuration near the cusp-neutral sheet interface is. Fig. 6 shows a plausible model, consistent with the observations of Anderson and Ness, in which the cusp joins smoothly to the plasma tail associated with the neutral sheet.

The foregoing results were obtained largely from measurements of omnidirectional electron fluxes, any angular distributions being ignored or averaged out. Angular distributions of electrons near 100 keV energy were observed on Explorer 14, as reported by Serlemitsos (1965, 1966), who finds three types of behavior in the night side of the magnetosphere: (a) inside about $8R_E$ more electrons move at right angles to the magnetic field than along it, i.e. the angular distribution is peaked at right angles to the field, a well-known behavior in the case of the stably trapped particles of the Van Allen belts; (b) outside $8R_E$ and out to distances as large as $13R_E$ during magnetically quiet periods the distribution peaks along the field; during magnetically disturbed periods the outer boundary of this type of anisotropy (which Serlemitsos identifies as the boundary of the trapped particle region) moves closer to the earth, and isotropic, highly variable fluxes are found outside of it; (c) near 8 to 9 R_E , at the transition between (a) and (b), the angular distribution is nearly isotropic. The distances given strongly suggest that the region of anisotropy of type (a) should be identified with the "hard core" trapping zone, and that of anisotropy of type (b)

should be identified with the cusp (as has been done by Anderson and Ness, 1966).

To recapitulate, from the extensive observations now available of electrons with energies above 40 kev a reasonably definite, if somewhat schematic, picture of their spatial distribution within the equatorial region of the magnetosphere can be drawn. The classical Van Allen trapping region, in which the energetic particle distribution is governed by the dipole field, extends to about 8 Re. Between it and the magnetosphere boundary lie regions of weaker, softer, and more variable electron fluxes: the skirt region, over the sunlit hemisphere, extends over a wide range of latitudes; the cusp region, over the dark hemisphere, is confined to a narrow range of latitudes, roughly near the solar magnetospheric equatorial plane. The cusp apparently terminates at distances of 12-15 Re in the antisolar direction; beyond it lies a region of highly variable or even transient electron fluxes (the "islands") related to the magnetic neutral sheet found in the magnetospheric tail. The precise connection between the cusp, the neutral sheet, and the "islands" remains obscure, as does the nature of the boundary between the cusp and the skirt.

Observations of lower energy electrons, of more direct relevance to the present work, have been very meager indeed compared to the 40 kev work. Fluxes of electrons with energies above 200 ev were measured by Gringauz and coworkers, using Faraday cups with retarding D.C. potentials flown aboard Luniks 1 and 2, in 1959 (Gringauz et al., 1960a,b); the two space probes each crossed the magnetosphere once, Lunik 1 at an angle of about 80° to the earth-sun line on the dawn side, Lunik 2 at about 130°

on the dusk side, both remaining relatively close to the geomagnetic equator (the directions relative to the earth-sun line, not given in the original papers, were later published by Gringauz, 1964). In each flight electrons were detected within one interval of radial distances, just outside the Van Allen belts; in the case of Lunik 2, they were detected between geocentric distances of 61,400 km and 81,400 km (9.6 and 12.7 Re), well inside the magnetosphere (solar plasma was not encountered until a distance of 39 Re); typical fluxes were $\sim 2 \times 10^8 \text{ cm}^{-2}\text{sec}^{-1}$. These observations indicate a well-defined band of low energy electrons lying outside the Van Allen belts, which was named by Gringauz the "third" or "outermost radiation belt" (Gringauz and Rytov, 1960), though what precisely this term was meant to imply has since been disputed (Gringauz, 1964; Van Allen, 1964). A similar detector was carried on the Mars 1 space probe in 1962, which went away from the earth at high geomagnetic latitudes and near the late evening and midnight meridians (Gringauz et al., 1964; Gringauz, 1964); the belt of low energy electrons was again detected, this time at distances between 12,900 and 20,400 km (2.2 and 3.2 Re) corresponding, at the high latitudes, to roughly the same L value as the Lunik 2 observations; the inner boundary coincided with the termination of the outer belt as determined from simultaneous 50 keV electron observations. The flux of low energy electrons was essentially the same as that found by Lunik 2, $\sim 4 \times 10^8 \text{ cm}^{-2}\text{sec}^{-1}$, in spite of the somewhat lower threshold (80 eV instead of 200 eV) of the detector, indicating that most of the electrons had energies above 200 eV if the spectrum had not changed much between 1959 and 1962.

A similar sharply bounded region of electrons, with energies above 100 ev and flux $\sim 10^8 \text{cm}^{-2} \text{sec}^{-1}$, beginning at 8 Re and extending out to the magnetosphere boundary and beyond it to the shock, was found at an angle of 25° from the sun-earth line by Serbu (1965), using data from one orbit of Explorer 18.

The other observations, prior to the summer of 1964, that provided some information on low energy electrons were made aboard Explorer 12 (Freeman et al., 1963; Freeman, 1964). The detector consisted of a CdS crystal that measured the total energy flux due to electrons between 200 ev and 500 kev and protons between 1 kev and 10 Mev (the energy flux was actually weighted by an energy-dependent efficiency function that increased by a factor of 10 over the energy range quoted); the proton contribution was determined with a similar detector from which electrons were excluded by a magnet. Some information on the electron energy spectrum could be obtained by comparing the CdS results with those of two magnetic spectrometers on the same satellite measuring electrons in 40-50 kev and 80-100 kev energy ranges. With this set of detectors Freeman found a band of soft electrons on the dawn side of the magnetosphere at angles from the earth-sun line greater than about 120° ; how far back this band extends could not be determined because of "the untimely death of the satellite". The energy fluxes quoted by Freeman are of the order of tens of $\text{ergs cm}^{-2} \text{sec}^{-1} \text{ster}^{-1}$, corresponding to fluxes of $10^9 \text{cm}^{-2} \text{sec}^{-1} \text{ster}^{-1}$ if the electrons are predominantly of 10 kev energy; these numbers must be viewed with some caution because, as will appear in the discussion of transition region observations, the effective solid angle of the

CdS detector apparently is known no better than within an order of magnitude.

Freeman identifies this band of low energy electrons with that observed by the soviet probes, although there appear to be at least two possible discrepancies: (a) no radial terminations of the soft electron flux are reported by Freeman; his one published pass through this region shows no significant change of flux between 20,000 and 70,000 km radial distance; (b) Freeman's soft electron band is only found farther than about 120° from the earth-sun line, whereas the Lunik 1 observations were at about 80° ^{*} (and, it may now be added, the Explorer 18 observations of Serbu were at 25°). The second point suggests a major question about Freeman's analysis. The conclusion that the electrons on the night side are very soft was drawn primarily from the large decrease of the flux measured by the 40 kev magnetic spectrometer; there is no evidence presented for a coincident increase in the flux measured by the CdS detector, and indeed no significant such increase is apparent from the published data. It is thus entirely possible that Freeman's soft electron belt is simply a region of reduced high energy electron fluxes, which could be quite distinct from the regions of enhanced low energy electron fluxes reported by Gringauz (it should be kept in mind that although the energy ranges of the two detectors are similar, the CdS detector gives much more weight to high energy particles than the ion trap and thus is much less sensitive to low energy particles). Indeed, the boundary of the soft

* See Gringauz, 1964.

electron belt given by Freeman and his observation that low 40 keV electron fluxes occur during outbound passes when the satellite, as is apparent from his plots, is at (southerly) geomagnetic latitudes near 20° or higher are in striking agreement with the properties of the cusp region as subsequently discovered by Frank and Anderson.

In summary, prior to the launchings of Vela 2 and OGO-A in late 1964 there were definite but scattered pieces of evidence for existence of low energy electrons within the magnetosphere beyond the radiation belts, but no systematic surveys (in contrast to $E > 40$ keV electron studies). Such a survey is one of the major objectives of this work.

Satellite Observations at High Latitudes, Low Altitudes. —

Magnetic field lines that leave the earth at high latitudes extend out to large distances in the equatorial region of the magnetosphere. Given the ease with which charged particles and magnetic disturbances can propagate along the field lines, the structure and the activity of the distant magnetosphere should be reflected in the high latitude regions of the earth. This connection is today thought to be the principal reason for the variety and complexity of high latitude phenomena, of which the most spectacular is the aurora but which also include, to name just a few, magnetic disturbances (bays), short period magnetic fluctuations, very low frequency radio emission, galactic radio noise absorption, charged particle precipitation, etc. Here I will briefly discuss only two aspects of high latitude studies that are of most direct relevance to the present work: the boundary of the outer radiation zone and satellite observations of electron precipitation.

Although the fluxes of energetic ($E > 40$ kev) trapped electrons of the outer radiation zone show large temporal variations at heights of ~ 10000 km, on any one satellite pass there usually is found a well-defined latitude above which the trapped electron flux is below a detectable level and which is therefore identified as the boundary of the outer zone (see, e.g. McDiarmid and Burrows, 1964, Frank et al., 1964, Williams and Palmer, 1965). A useful spatial coordinate for describing magnetically related phenomena at high latitudes is the invariant latitude Λ , related to the L parameter;* for a dipole field, Λ is just the usual magnetic latitude. In a magnetosphere undistorted by the solar wind any trapped radiation boundary would occur at a constant Λ (or, in other words, the boundary would coincide with an L shell), independently of local time. The actual boundary, however, shows a striking dependence on local time: the boundary is found at highest latitudes on the noon meridian and at lowest latitudes on the midnight meridian, varying monotonically in between. Measuring electrons above 40 kev, Frank et al. (1964) find the boundary at $\Lambda \approx 77^\circ$ at noon and at $\Lambda \approx 69^\circ$ at midnight. At the same energies McDiarmid and Burrows (1964) obtain as the corresponding numbers 76° and 71° ; the two measurements must be considered to be in good agreement, especially in view of the fact that somewhat different criteria were used by the two groups to define the precise boundary. Measuring electrons above 280 kev Williams and Palmer (1965), on the other hand, obtained values ranging from 70.4° at noon and 66.1° at midnight to 73.1° at noon and 70.3° at

* See Appendix E

midnight; the midnight values are in agreement with 40 kev results, but the noon values are (probably significantly) higher. The boundary generally moves to lower latitudes during magnetic disturbances (Maehlum and O'Brien, 1963; Ness and Williams, 1966; Williams and Ness, 1966; a similar effect has been noted at higher altitudes by Rosen, 1965). The position of the boundary is slightly above the conventional auroral zone; its variation with local time and with magnetic activity is similar to corresponding variation of the auroral zone (see, e.g. Davis, 1965; Sugiura and Heppner, 1965). By considering the boundary as the shell formed by electrons mirroring near 1000 km height and drifting, with conservation of the first two adiabatic invariants, in a model magnetic field that includes distortion of the earth's dipole field both by compression of the magnetosphere and by fields due to the tail neutral sheet, Williams and Mead (1965) were able to account semi-quantitatively for all these properties, as well as for the correlation between decrease of boundary latitude and increase of magnetic field strength in the magnetospheric tail during magnetic storms found by Ness and Williams (1966; also Williams and Ness, 1966).

In addition to trapped electrons, one observes precipitated electrons, that is, electrons whose pitch angles are small enough so that their mirror points lie in the atmosphere and hence they are absorbed by the atmosphere before they can mirror.* These precipitated electrons are today thought to be the principal cause of aurora and related phenomena, an idea

* Very recently a comprehensive review of electron precipitation has been published by Brown, 1966.

confirmed by a strong correlation between occurrence of particle precipitation and auroral light emission observed by instruments on Injun 3 (O'Brien and Taylor, 1964). Average fluxes of precipitated electrons $E > 40$ kev reach $\sim 4 \times 10^4 \text{ cm}^{-2} \text{ sec}^{-1}$, compared to $\sim 6 \times 10^5 \text{ cm}^{-2} \text{ sec}^{-1}$ trapped fluxes at comparable latitudes both measured on Injun 3 (Frank et al., 1964); events in which precipitated flux becomes nearly equal to the trapped flux have been reported by O'Brien (1964). There is a latitude boundary above which precipitated $E > 40$ kev electrons are not generally observed, which coincides approximately with the trapped radiation boundary, showing the same local time dependence (McDiarmid and Burrows, 1964; Frank et al., 1964).

At latitudes above the radiation zone boundary occasional short bursts of $E > 40$ kev electrons have been observed by Alouette 1 detectors, described by McDiarmid and Burrows (1965), who call them the "high latitude spikes"* of energetic electrons. Fluxes range from 10^4 to $10^9 \text{ cm}^{-2} \text{ sec}^{-1} \text{ ster}^{-1}$. The events occur predominantly on the night side, between local times 15h and 7h (all but 4 events out of 38 reported occur between 19h and 5h), and within a well-defined latitude range, between $\Lambda = 67^\circ$ and $\Lambda = 83^\circ$ (30 events out of 38 between $\Lambda = 70^\circ$ and $\Lambda = 78^\circ$); the probability of their occurrence increases with increasing geomagnetic agitation as measured by the K_p index. Similar observations at lower energies have been reported by Fritz and Gurnett (1965), using data from an electron multiplier flown on Injun 3 that measured the flux of

* Not to be confused with transition region spikes, to be discussed later.

electrons above 10 kev. They observed about 600 events with fluxes greater than $2.5 \times 10^7 \text{cm}^{-2} \text{sec}^{-1} \text{ster}^{-1}$, reaching up to $10^9 \text{cm}^{-2} \text{sec}^{-1} \text{ster}^{-1}$; the events are confined to local times between 16h and 8h and invariant latitudes between 58° and 76° (with few events below $\Lambda = 67^\circ$) and their occurrence frequency increases with increasing Kp. Some spectral information could be obtained by comparing data from the electron multiplier with that from Geiger tubes measuring electrons above 40 kev on the same satellite. Fritz and Gurnett give spectral parameters for two events, for which they obtain exponents $\gamma = +6.8$ and $+7.3$ if a power law spectrum is assumed, or e-folding energies $E_0 = 3.4$ kev and 3.1 kev, respectively, if an exponential spectrum is assumed; by contrast, in the outer radiation zone during the same passes they obtain $\gamma < 2.8$ or $E_0 > 15$ kev in the first case and $\gamma = 2.2$ or $E_0 = 22$ kev in the second. The $E > 40$ kev "spikes" found in Alouette 1 data and the $E > 10$ kev "spikes" found in Injun 3 data thus have very similar geographic distributions and a similar dependence on geomagnetic activity; whether they are the same events is not entirely clear, especially as the fluxes found by Fritz and Gurnett when extrapolated to 40 kev seem considerably lower than those found by McDiarmid and Burrows. All these authors, and others, have speculated that these events might be related to the tail electron "islands" described earlier and/or to the low energy electron belt of Gringauz and Freeman, but no definite theory has yet been formulated.

Precipitation of still lower energy electrons into the auroral zone has been observed by Sharp et al. (1964, 1965), who used plastic scintillator detectors responding to electrons of energy down to 2 kev

in one flight and 180 kev in another. They observed typical downward energy fluxes carried by $E > 2$ kev electrons of the order of several ergs $\text{cm}^{-2}\text{sec}^{-1}$ (but as high as $100 \text{ ergs cm}^{-2}\text{sec}^{-1}$ on one occasion) and found that most of the energy was generally carried by electrons below 10 kev. In one case (in which, however, the visual aurora observed was not typical) they compared the measured energy flux above 2 kev, $5 \text{ ergs cm}^{-2}\text{sec}^{-1}$, with the total energy influx as determined from the luminosity profile of the visible aurora (measured at the same time from the ground), $200 \text{ ergs cm}^{-2}\text{sec}^{-1}$, concluding that (at least in this case) the bulk of the particle energy producing the aurora was carried by electrons of energy below 2 kev (Sharp et al., 1964; see also Evans and Belon, 1963).

To conclude this very cursory review of some aspects of high latitude studies, a number of observations suggest that an important role in high latitude phenomena is played by low energy electrons, especially those near the boundary of the outer radiation zone and outside it.

C. Electron Observations In The Transition Region

No steady fluxes of electrons of energy above 40 kev have been detected in the transition region; as discussed in an earlier section, abrupt termination of 40 kev electron fluxes is a well-established characteristic of the magnetosphere boundary, at least over the sunlit hemisphere. Transient fluxes of these electrons, referred to as "spikes", generally lasting several minutes and reaching flux values of $10^4 - 10^6 \text{ cm}^{-2}\text{sec}^{-1}$, have been observed with detectors on Explorer 14 by Frank and Van Allen (1964) and on Explorer 18 by Anderson et al. (1965) and Fan et al. (1966). The spikes are occasionally found as far as several earth radii ahead of the shock front, in the interplanetary medium, especially during magnetic disturbances. Assuming a power law spectrum for the electrons above 30 kev in the spikes and using measurements from two detectors (a Geiger tube and a solid state counter) aboard Explorer 18 Fan et al. obtained exponents between 2.5 and 4.0 for spikes occurring at angles less than 45° from the sun-earth line and between 3.0 and 4.5 at angles greater than 80° . They also found that spikes closest to the magnetosphere boundary (which have the highest fluxes, as had already been pointed out by Anderson et al.) tend to have the softest spectra (i.e. the highest exponents).

Several explanations of these spikes have been proposed. Anderson et al. suggest that they are electrons escaping from the magnetosphere, on the grounds that the spike intensity decreases with increasing distance

from the magnetosphere boundary. Fan et al. reject this hypothesis as inconsistent with the observed lack of correlation between the intensities and spectra of electrons in the spikes and in the magnetosphere and suggest that electrons in the spikes are accelerated near the shock front. A theory of the spikes along these lines has been proposed by Jokipii and Davis (1964; also Jokipii, 1966a) who suggest that electrons are accelerated in front of the shock by the classical Fermi process as they bounce back and forth between the shock and an approaching magnetic irregularity in the interplanetary medium; Jokipii (1966b) also accounts for the observed spectral changes in terms of an energy-dependent diffusion process, the highest energy electrons diffusing away most rapidly as the spike is convected by the plasma flow through the transition region away from the subsolar region. Another theory has been proposed by Shen and Chang (1966), in which electrons are accelerated inside the transition region by large amplitude hydromagnetic waves. Yet another theory, invoking electron acceleration by ion acoustic waves in the transition region, has been proposed by Scarf and coworkers (Scarf et al., 1965; Fredricks et al., 1965).

As in the case of the magnetosphere, study of low energy electrons has lagged behind study of 40 kev electrons. Serbu (1965) and Serbu and Maier (1966), using data from the Explorer 18 retarding potential analyser, report densities of 2 ev electrons of the order of 50 cm^{-3} and no change in this 2 ev component across the magnetosphere boundary; for reasons mentioned in an earlier section, however, this result is open to question. Serbu and Maier also find a "high energy" electron component

in the transition region, having energies higher than 15 ev and a total flux $\sim 10^9 \text{cm}^{-2} \text{sec}^{-1}$. Freeman (1964), using the CdS total energy detector aboard Explorer 12 described earlier, found energy fluxes of tens of $\text{ergs cm}^{-2} \text{sec}^{-1}$ in the transition region, usually about a factor of 2 higher than the energy flux inside the magnetosphere on the same pass. On 13 orbits he also found a sharp decrease of energy flux at larger distances which he interpreted as the shock front (judging from his 4 published plots, the energy flux outside the shock is slightly lower than or comparable to that in the magnetosphere); the positions of these shock crossings are in fair agreement with the shock boundary as subsequently mapped by Explorer 18. The only published discussion of electron energy spectra in the transition region based on Explorer 12 results is that of Freeman et al. (1963); it refers to a single pass and its conclusions were assumed in later papers (Freeman, 1964) to be valid generally. As this discussion has formed the observational basis for three years of theoretical speculation on transition region electrons, a detailed critique of its remarkable argument is given in Appendix F. Freeman et al. conclude that the average electron energy is near 2.6 kev; however, as described in Appendix F, an inconsistency between results of their various detectors was avoided and the 2.6 kev figure obtained only by a procedure that amounts to an ad hoc increase of the CdS detector solid angle value by a factor of about 4 or 5.

On general theoretical grounds it is to be expected that electrons will be heated at the shock along with the protons. The amount of heating and hence the expected average electron energy in the transition region,

however, depends on the details of the randomizing process that must be active at the shock. The most common assumption has been that this process is due to a two-stream instability caused by relative motion of protons and electrons; detailed calculations (e.g. Parker, 1958b; Kellogg, 1964) then lead to the conclusion that electrons will acquire a significant fraction, up to $1/2$, of the energy carried by solar wind protons, giving mean electron energies of the order of hundreds of eV. The previously mentioned results of Freeman et al. have often been cited as observational support for this deduction. The supposition that transition region electrons have energies comparable to those of solar wind protons has been made the basis of far-reaching theories (e.g. Bernstein et al., 1964; Scarf et al., 1965) and has been well on its way to acquiring "it is well known that..." status. The results of the present work, as well as of Vela 2 and 3 observations, for the first time allow a direct observational test of this hot electron hypothesis.

III. THE EXPERIMENT

The description of the experiment given in this chapter is brief and intended to provide only the information needed to understand the results. A more detailed description will be found in Appendices A, B, and C.

The flight. - OGO-A (official designation 1964-54A), the first satellite in NASA's Orbiting Geophysical Observatory series, was launched from Cape Kennedy at 01:23:10UT and injected into orbit at 02:17UT on September 5, 1964. Some parameters of the (initial) orbit are:

geocentric distance of apogee $24.4 R_e$

height of perigee 280.5 km

eccentricity 0.918

period 3839.4 minutes (8/3 days)

solar ecliptic latitude at apogee 35°

initial sun-earth-satellite (or sun-earth-probe, abbreviated SEP) angle at apogee 135° and decreasing

initial solar ecliptic longitude at apogee 150° and decreasing

inclination of orbital plane to the ecliptic 62°

speed at perigee 10.7 km/sec

speed at apogee 0.46 km/sec

The orbit is shown in relation to the ecliptic plane and the sun in Fig.8, and projected on the solar ecliptic (S.E.) coordinate XY and XZ planes

(for the first two revolutions*) in Fig. 9. Looking from the sun: in the early orbits the satellite, as it moves away from the earth, goes up (above the ecliptic), to the right (the dusk side of the earth), and to the back (toward the antisolar direction); the sense of revolution is clockwise in the S.E. Y-Z plane looking from the sun, and counterclockwise in the S.E. X-Y plane looking from the north ecliptic pole. Later orbits as seen in S.E. coordinates are obtained from these, of course, by clockwise rotation about the S.E. Z axis. The data discussed in this work were obtained during October through December 1964; at this time apogee was always on the dusk side of the earth and at SEP angles from 135° to 54° or S.E. longitudes 150° to 44° .

Another important aspect of the orbit is its relation to the earth's magnetic dipole orientation. Fig. 10 is a polar plot of radial distance vs. geomagnetic latitude (i.e. the orbit projected onto a magnetic meridian by rotation about the dipole) for three consecutive orbits; because three orbits corresponds to very nearly an integral number of days (8) every third orbit is approximately the same in this projection. The main feature to be noted is that in all inbound passes the satellite is relatively close to the geomagnetic equator. Projections of the orbit in more complicated coordinate systems will be discussed later where appropriate.

OGO-A was planned to be completely stabilized; however, the attitude control system failed soon after launch and the satellite was

* In accordance with common usage I shall refer to revolutions as "orbits"; thus first orbit, second orbit, etc.

left spinning with a period of nearly 12 sec about an axis pointing approximately to right ascension 44° , declination -10° ; or, if referred to the ecliptic plane, pointing 23° below the ecliptic and 38° from the vernal equinox (as shown in Fig. 8). Throughout the period under consideration the spin axis is pointing to a direction well within the antisolar hemisphere; it does not come within 90° of the sun until late in January 1965 and comes closest to the sun around May 1.

OGO-A carries 20 experiments (for a complete list, as well as a general description of the satellite, see IG Bulletin No. 92, 1965). Among those of particular relevance to the present work are the companion MIT experiment to measure plasma protons, the flux gate magnetometer (J.P. Heppner), the search coil magnetometer (R.E. Holzer and E.J. Smith), experiments to observe high energy (>40 kev) electrons with Geiger tubes (J.A. Van Allen), magnetic spectrometer (J.R. Wincker and R.L. Arnoldy) and scintillation counter (A. Konradi), an electrostatic analyser plasma probe (J. Wolfe), experiments to observe very low energy (0-100 ev) ions and electrons with spherical (R.C. Sagalyn) and planar (E.C. Whipple) traps, a positive ion mass spectrometer (H.A. Taylor, Jr.), and a very-low-frequency noise detecting antenna (R.A. Helliwell). The experiments can be operated from September through December and from March through June; at other times the spin axis-sun angle is such that the solar cells do not produce enough power for the experiments. With this limitation, the satellite has been operating from soon after launch and still is. The present work is restricted to data between September and December 1964 because (a) the data from March to June 1965 proved to

be unusable, as will be discussed later, and (b) later data were not made available soon enough to be included.

Apparatus. - The detector (very similar to the positive ion detectors extensively used by the M.I.T. group, described in e.g. Bonetti et al., 1963, or Lyon, 1966) is shown schematically in Fig. 11. It consists of a cylindrical metal cup open at one end with a collector plate at the other end and 5 planar grids. A periodic voltage (ideally a square wave with upper and lower voltages $-V_2$ and $-V_1$, $V_2 > V_1$) is applied to grid G3, called the modulator grid. Charged particles are variously affected, depending on their charge, energy, and direction of motion. Let E = particle energy, Θ = angle between direction of incidence and cup axis, e = magnitude of particle charge; the following cases occur:

(1) Negative particles for which

$$E \cos^2 \Theta < eV_1$$

are repelled by the electric field of the modulator grid and never reach the collector.

(2) Negative particles for which

$$eV_1 < E \cos^2 \Theta < eV_2$$

reach the collector during one half of the modulation cycle (when the modulator potential is $-V_1$) but not during the other half, producing an A.C. current to the collector at the same frequency as the modulating potential and 180° out of phase with it (when the modulating potential goes from $-V_1$ to $-V_2$, it algebraically decreases; at the same time the number of negative particles reaching the collector also decreases, i.e. the current to the collector increases if the usual sign convention is

used); the amplitude of the current is proportional to the flux of particles in the stated range.

(3) Negative particles for which

$$eV_2 < E \cos^2 \theta$$

and positive particles for which $E \cos^2 \theta / e > 150$ volts (the positive potential on the collector, discussed later) reach the collector at all times, producing, to first approximation, only a D.C. current to the collector. Positive particles for which $E \cos^2 \theta / e < 150$ volts never reach the collector.

Grid G1 and the walls of the cup are "grounded" (i.e. electrically connected to the skin of the satellite), forming a closed equipotential surface around the detector. Grid G4 (the shield grid), also grounded, prevents direct capacitive coupling between the modulator and the collector. Grids G2 and G5 are grounded and serve no particular purpose in the present detector. The collector plate is maintained at a D.C. potential of +150 volts in order to prevent the escape of secondary electrons produced as the incident particles impinge on the collector.

The quantity measured is the A.C. component at the modulator frequency (in this case 2.461 kc/s) of the current to the collector. A block diagram of the electronics is shown in Fig. 11. The collector plate is capacitor coupled to a linear preamplifier, whose output is passed first through a narrow band filter which removes all but the fundamental component at the desired frequency, and then through a non-linear compression amplifier with an approximately logarithmic characteristic, 3 decades of input current corresponding to a 0.5 to 5.1 volt output

range. The synchronous detector (which can be thought of as an integrator preceded by a switch that is closed during one half of the modulator cycle and open during the other half) then removes any A.C. component that is 90° out of phase with the modulator and smoothes the remaining signal (by integrating over about 5 cycles, or 20 milliseconds), producing a nearly D.C. output that is positive if the original A.C. signal was 180° out of phase with the modulator (as it should be if the detector is functioning normally) and negative if it was in phase. The emitter follower circuit acts as a link to the spacecraft telemetry system; since the latter can accept only positive signals, any negative signal is blocked and a zero is presented in its place to the telemetry. The smallest detectable collector current is about 2×10^{-11} amps. With zero A.C. current to the collector the output of the system is about 0.5 volts; thus a steady zero output unambiguously indicates that, for some reason, the A.C. current to the collector is of the wrong phase. Additional details about the apparatus, calibration procedures, etc. are given in Appendix A.

The actual wave form of the modulating potential is not exactly square, but has nearly rectangular "spikes" added at the beginning of each half-cycle, as shown in Fig. 12. The modulation must be described by four voltages, $V_1 < V_2 < V_3 < V_4$, instead of two. Positive particles and negative particles in the ranges $E \cos^2 \theta < eV_1$ and $E \cos^2 \theta > eV_4$ produce no significant effect, as before. The remaining negative particles are detected but the fluxes of particles within each of the three ranges

$$(1) \quad eV_1 < E \cos^2 \Theta < eV_2$$

$$(2) \quad eV_2 < E \cos^2 \Theta < eV_3$$

$$(3) \quad eV_3 < E \cos^2 \Theta < eV_4$$

are weighted unequally, as discussed in Appendix A; the "main window" (2) is weighted most heavily and the "side lobes" (1) and (3) are weighted by a factor of about 0.3 to 0.4 relative to (2), but (1) is weighted negatively, because of phase considerations. In other words, if $F(eV, eV')$ is the flux of negative particles within the range

$$eV < E \cos^2 \Theta < eV'$$

that can reach the collector, then the measured current is proportional to

$$-a_l F(eV_1, eV_2) + F(eV_2, eV_3) + a_u F(eV_3, eV_4)$$

where a_l , a_u are constants depending on the modulator wave form.

One can define a function $W_k(E)$ describing an "energy window" of the detector

$$\begin{aligned} W_k(E) &= 0 & E < eV_1 \\ &= -a_l & eV_1 < E < eV_2 \\ &= 1 & eV_2 < E < eV_3 \\ &= a_u & eV_3 < E < eV_4 \\ &= 0 & eV_4 < E \end{aligned}$$

(where W_k refers to the k^{th} set of modulation voltages) which will later prove useful for a precise discussion of the meaning of the measurement.

There are 4 sets of modulation voltages (referred to , for brevity, as "energy channels" or "energy windows"). The parameters $V_1, V_2, V_3, V_4, a_l,$ and a_u of each channel are given in Table I and the functions $W_k(E)$ are shown in Fig. 13; note that on a logarithmic energy scale the 4 channels

are roughly of equal width and equally spaced. The timing of the measurements is shown in Fig. 14. The currents in the 4 channels are measured in sequence, from the highest energy channel to the lowest; the complete set of 4 measurements takes 2.3 seconds and is repeated every 9.2 seconds.

There are some additional complications, besides the non-square modulation. They are discussed in Appendix A and only the conclusions are given here. Effects due to varying curvature of the particle trajectories are not important. Secondary electrons emitted from the shield grid contribute to the current at the collector; the A.C. component of this contribution, however, is proportional to the modulated incident electron flux and effectively multiplies it by a factor λ (which I shall call the effective secondary electron yield) that can be estimated, from published data on secondary electron emission, to be between 1.5 and 2.5. Other complications are the detector response to sunlight and to protons. The response to sunlight is presumably caused by photoelectrons emitted from various surfaces within the detector, though the mechanism by which they are modulated is not yet completely understood; in practice the effect is found to be rather severe, and useful data can be obtained only when the sun is not within the field of view of the detector. The response to protons occurs by means of energy-dependent secondary electron emission from the modulator grid; the A.C. current produced is of the wrong phase (in the sense discussed earlier) and is approximately proportional to the modulation potential. The effect corresponds to detection of at most one percent of the total incident proton flux and thus is important only when the total proton flux exceeds by two orders of magnitude the electron flux

within a given energy window, a situation that only occurs (as will be shown in a later chapter) within the high density, low temperature region delimited by the whistler knee, i.e. within 4-5 Re distance. That the detector is responding predominantly to protons can be recognized, when it occurs, by a continuous zero output (since the proton signal has the wrong phase). Protons of energy above 150 ev can be detected by another mechanism, the variable bending of their trajectories in the modulating electric fields, but this effect can be estimated from the direct proton measurements simultaneously carried out on this satellite and shown to be at or below the electron detector noise level in the transition region and much smaller elsewhere.

The detector is mounted on the main body of the satellite. The direction of normal incidence is within a few degrees (2° to 7° , not known precisely yet) of the satellite spin axis. The angular response function $G(\theta)$, giving the fraction of particles incident at an angle θ to the cup axis that are detected, can be calculated from the geometry (with due regard to secondary electron effects), as discussed in Appendix A, and is shown in Fig. 15; a simple analytical approximation that has a maximum deviation of 4% is

$$\begin{aligned} G(\theta) &= 1.408 \cos^2 \theta - 0.451 & 0 \leq \theta < 55^{\circ}30 \\ &= 0 & \theta > 55^{\circ}30 \end{aligned}$$

The angular field of view of the detector thus is a cone of half-angle 55° , the weight given to the flux of particles incident at an angle decreasing from 1 at $\theta = 0$ to 0.5 at $\theta = 35^{\circ}$ to zero at $\theta = 55^{\circ}$; the axis of the cone nearly coincides with the spin axis. Referring to the

earlier discussion of the spin axis orientation, during the period September through December the detector points well away from the sun (and also, it may be noted, away from the solar plasma flow) and there are no photoelectron problems. During March through June, on the other hand, the detector faces the sun and the data are largely useless.

For later use it is convenient to express the measurements in terms of the electron velocity distribution function. Let $f(\vec{v})d\vec{v}$ be the number of electrons per unit volume, at the position of the satellite and at the time of a measurement, whose velocity vectors lie within a volume $d\vec{v}$ of the point \vec{v} in velocity space; the integral $\int d\vec{v}f(\vec{v})$ gives the total density of electrons at the point stated. Then the current i_k in the k^{th} channel is

$$i_k = eA\lambda \int d\vec{v} v \cos\theta G(\theta) W_k\left(\frac{1}{2}mv^2 \cos^2\theta\right) f(\vec{v})$$

where θ = angle between \vec{v} and the cup axis, $A = 18.3 \text{ cm}^2$ = effective area of detector (allowing for the transparency of the various grids), and λ , $G(\theta)$, and W_k have been defined previously. The basic data of the experiment are a set of 4 such numbers i_k , $k = 1,2,3,4$, every 9.2 seconds; the object of the analysis is to obtain what information one can about the function $f(\vec{v})$ and its spatial and temporal variations.

Data acquisition and processing. — OGO-A has 4 telemetry modes: data can be transmitted in real time (i.e. as it is produced) at one of three rates, 1, 8, or 64 kilobits per second; or it can be stored on an onboard tape recorder (at the rate of 1 kbit/sec) and played back and transmitted later. The orientation of the satellite directional antenna is such that real-time transmission is possible only during the outbound

portion of the orbit; during the inbound portion data must be stored on the tape recorder and played back near perigee. The choice of bit rate for the real-time transmission is governed by two competing factors: for most experiments the higher bit rates provide more information; on the other hand, the relative number of errors increases sharply at the higher bit rates and increases with satellite altitude at all bit rates. As a compromise, a telemetry schedule was worked out which is roughly as follows: 64 kbit transmission from perigee out to about 30,000 km altitude; 8 kbit from there to about 120,000 km, alternating with 1 kb above about 80,000; 1 kbit from there to apogee; data storage (at 1 kbit) from apogee on. On any particular orbit there are deviations from this schedule and gaps, depending on availability of tracking stations at suitable locations.

The present experiment functions only when the telemetry is in a 1 kbit mode, either real time or data storage. Thus there are no data available on the outbound part of the orbit from perigee to about 14-15 Re, pieces (typically an hour or two, with gaps of comparable duration) from there to about 20 Re, and more or less continuous coverage with occasional gaps from there on; the data for the last 4 or 6 Re are not useful because of the positive ion effect mentioned earlier. Fig. 16 shows the data coverage for various orbits.

The data are digitized on the satellite and transmitted in the form of 9-bit integers. Initial processing, including determination of the time at which a measurement was made, is done at Goddard Space Flight Center; the data for the 20 experiments are then put on separate magnetic tapes and

sent to the respective experimenters. The processing done at M.I.T. is described in Appendix C. Briefly, the electron and proton data are separated; the data are sorted by energy windows, using the special marker signals generated by the detector electronics; the data are arranged in correct time sequence; the fluxes in the 4 energy windows are plotted as functions of time, with the position of the satellite in space* indicated on three additional independent coordinate axes. Most of the results in this thesis were obtained from examination of these summary plots; for a closer study of the energy spectra, 2-minute averages at selected times were plotted as a function of the energy window.

* All orbit calculations are done at the Goddard Space Flight Center.

IV. RESULTS

A. The Transition Region

The properties of electrons in the transition region, as determined in this experiment, can be summarized in a few sentences:

(1) The omnidirectional flux of electrons with energies above 200 ev varies between 10^8 and 10^{10} $\text{cm}^{-2}\text{sec}^{-1}$. The flux generally fluctuates in a more or less random way, with periods of flux enhanced by a factor of 3 or so lasting from a few minutes to a few hours. Large, long-lasting increases occur in association with magnetic storms.

(2) In the range 125 to 1000 ev the differential flux is a sharply decreasing function of energy, typically varying roughly as E^{-4} or E^{-5} . The observed electrons thus must be a non-Maxwellian tail of a distribution peaked well below 125 ev.

(3) There is some, generally inconclusive, evidence for occasional flattening or even possibly a second peak in the spectrum somewhere in the vicinity of or above 1 kev, especially in data from orbit 27 inbound, during one of the most intense magnetic storms that occurred within the period studied.

(4) In the undisturbed solar wind the electron flux is usually below, or only slightly above, the noise level of the instrument, corresponding to a flux above 200 ev $\lesssim 8 \times 10^7$ $\text{cm}^{-2}\text{sec}^{-1}$. The change

from this to the strong fluxes characteristic of the transition region usually is sudden (within the 9 second resolution of the measurements) and occurs at the shock crossing as determined from simultaneous proton and (in the few cases so far where comparison has been made) magnetic field observations.* In a few notable cases, however, all during a magnetic storm, strong electron fluxes are found out to some distance outside the shock.

(5) The change from transition region to magnetosphere electron behavior, discussed in a later section, usually is also relatively sudden and occurs, in the cases where comparison has been possible, at the magnetopause as determined from proton and/or magnetic field data.

All these properties were inferred from observations during October, November, and December 1964, at angles from sun-earth line between 60° and 115° on the dusk side of the earth, close to the geomagnetic equatorial plane but considerably above the ecliptic plane.

To illustrate some of these points, figures 17 and 18 show two highly contrasted passes. Orbit 23 inbound (Fig.17) is a typical quiet time pass. The transition region here extends down to 16.4 Re (at which point the satellite enters the magnetosphere); inside it, the current in the 4th (lowest energy) channel fluctuates around 10^{-10} amps, occasionally (as, for example, between 22 and 20 Re) dropping nearly to the noise level. On the other hand, orbit 22 inbound (Fig.18), occurring only 3 days earlier

* I am grateful to Drs. J.P.Heppner and M. Sugiura of Goddard Space Flight Center for access to some of their magnetic field data before publication.

but during a moderate magnetic storm that had begun with a sudden commencement at 03:20U.T. on November 1, has a markedly different character. The seven shock crossings identified from proton data are indicated in the figure (here and in most other figures, the electron data have been smoothed by taking a 2 minute sliding average to eliminate some instrumental fluctuations, as discussed in Appendix A, and hence the change at a shock crossing appears more gradual than it actually is); the magnetosphere boundary crossing occurs somewhere in the data gap between 19.3 and 18.1 Re. Within the transition region, the most obvious difference from the preceding figure is the much larger current in all channels, at times exceeding 10^{-9} amps in the 4th channel. Another example of storm-time transition region electrons, showing currents reaching 3×10^{-9} amps and once as high as 9×10^{-9} amps, is given in Fig. 19 (note the expanded time scale and the reduced smoothing, using a 36 second sliding average); this is a portion of orbit 27 inbound (November 15), which will be mentioned again later on. Similar enhancements of electron current by a factor from 3 to 10 and more above quiet-time values occur during all the other magnetic storms for which transition region data are available: the sudden commencement storms of October 26 and November 8, and the disturbed period October 18 to 20.*

While the electron intensity thus changes from orbit to orbit, the electron energy spectrum, as indicated by the ratios of currents in the various channels, is much less variable. Figures 17, 18, and 19 all show

* A list of sudden commencements and a plot of K_p indices for this period are given by Lincoln, 1965a,b.

that within the transition region the current in channel 4 (responding primarily to electrons between 170 and 315 ev) is significantly larger than that in channel 3 (primarily 240 to 500 ev), typically by a factor of 3 or so; the current in channel 3 in turn exceeds that in channel 2 whenever the over-all intensity is high enough so that the latter is above the noise level. This behavior, the decrease of current with increasing channel energy, at least in the range 150 to about 600 ev corresponding to channels 4,3, and 2 (the behavior of channel 1, about 700 to 1760 ev, is somewhat more complicated and will be discussed later), is found in all the available transition region data; there has not yet been one case in which the current in channel 3 was equal to or greater than that in channel 4, within the transition region. Note in particular from Fig. 19 that this behavior persists even during the most intense enhancements of total current that occur during magnetic storms.

The general character of the energy spectrum is even more apparent from a plot of current vs. channel energy at a given time. Such plots are given for 33 times, scattered throughout the period under study, in Fig. 20; the selection of these times was somewhat biased toward periods of higher intensity (since I chose mostly cases where significant currents were found in at least 3 channels) but otherwise was intended to provide a reasonably representative sample of spectra observed in the transition region. The abscissa in these plots is log of the voltage V_2 of each channel*; the ordinate is log of the measured current, which is

* See Chapter III, section B.

proportional to the electron flux averaged (with a certain weight function) over the energy range of the channel, as described earlier. From these plots it is clear that (a) the measured current decreases with increasing channel energy, as already mentioned; (b) the decrease goes, roughly speaking, as a power law of the energy with a rather steep exponent, about -3 to -6 (except for a few "flat" cases such as numbers 27 and 33 in Fig. 20); (c) this general character of the energy spectrum does not change much even while the over-all intensity varies by more than an order of magnitude. The "flat" cases, where the exponent is of the order of -0.7, are isolated events each lasting a few minutes; the total number of such events found in the data for the period studied is three, two of them during the November 15 magnetic storm and the third during a rather quiet pass on December 12.

Thus, with the exception of a few uncommon occurrences and, of course, within the spatial and temporal limits of the present study, the transition region electron spectrum in roughly the 150-600 ev energy range has a well-defined and relatively unchanging character: the flux of electrons at a given energy decreases with increasing energy; the decrease, although fairly sharp, is not as fast as an exponential and at least qualitatively behaves like a power law. In other words, the spectrum in this energy range can be described as a non-Maxwellian high-energy "tail" of a distribution whose peak lies somewhere below 150 ev, below the range of the instrument. The data are definitely inconsistent with any distribution that peaks near a few hundred ev; electrons in the transition region seem to be colder than had been

theoretically anticipated.

Electrons in the energy range near 1 to 2 kev can be studied with the present instrument only when the over-all intensity is high enough so that a significant current can be measured in channel 1. A number of such cases is included in Fig. 20. In some of them the channel 1 current falls on a smooth extrapolation of the lower energy points (for instance, numbers 13, 22, 25, or 27 in Fig. 20); in others it is comparable to (numbers 11, 26) or even larger than (number 24) the current in channel 2; nearly all the latter cases occur during the November 15 magnetic storm and can be seen clearly in Fig. 19. Such behavior would indicate a "knee" or "hump" in the spectrum somewhere near or above 1 kev.

To obtain more precise information about the electron velocity distribution function $f(\vec{v})$ it is necessary to start from the relation given earlier between the distribution function and the measured current in the k^{th} channel

$$i_k = eA \lambda \int d\vec{v} v \cos \theta G(\theta) W_k \left(\frac{1}{2}mv^2 \cos^2 \theta \right) f(v) \quad (1)$$

In principle, this defines an integral equation for $f(\vec{v})$ in terms of i_k , provided one knows i_k for a sufficient number of energy windows and detector orientations. In practice, with only four energy windows and one orientation, it is necessary to assume a reasonable (and reasonably simple) functional form for $f(\vec{v})$ containing a few parameters, calculate the expected currents in the four channels as functions of the parameters, and try to find a set of parameters that will reproduce the measured currents; in other words, one tries to find a model distribution function that will fit the observations and hopes that, at least within the energy

range of the observations, this model will have some resemblance to reality.

The first assumption I will make is that the electron distribution is isotropic, i.e. $f(\vec{v})$ depends only on the speed v (a natural assumption for an experiment in which the detector points in a fixed direction!). An approximate isotropy of electron fluxes (within a factor of 2 or so) has in fact been observed with detectors on Explorer 18 (Moreno et al., 1966) and Vela (Asbridge et al., 1966) and would be expected because of the turbulence of transition region magnetic fields and the consequent lack of a permanent preferred orientation. With this assumption, writing the integral in equation (1) in a spherical coordinate system with the z axis along the Faraday cup normal and carrying out the ϕ integration

$$i_k = 2\pi e A \lambda \int_0^{\frac{\pi}{2}} \sin\theta d\theta \cos\theta G(\theta) \int_0^{\infty} v^3 dv W_k \left(\frac{1}{2}mv^2 \cos^2\theta \right) f(v) \quad (2)$$

It is convenient to express i_k in terms of the omnidirectional integral flux above energy E

$$J(E) = 4\pi \int_{\frac{2E}{m}}^{\infty} v^3 dv f(v) \quad (3)$$

then, differentiating (3)

$$v^3 dv f(v) = \frac{-dJ}{dE} \frac{dE}{4\pi} \quad (4)$$

inserting into (2) and integrating by parts, assuming that $J(E) W_k(E \cos^2\theta)$ vanishes at both $E = 0$ and $E = \infty$

$$i_k = \frac{eA\lambda}{2} \int_0^{\frac{\pi}{2}} \sin\theta d\theta \cos\theta G(\theta) \int_0^{\infty} dE J(E) W_k'(E \cos^2\theta) \cos^4\theta \quad (5)$$

where $W'(x) \equiv \frac{d}{dx} W(x)$. Making the substitutions $x = \sec^2\theta$ and $v = E \cos^2\theta$ one obtains

$$i_k = \frac{eA\lambda}{4} \int_1^\infty \frac{dx}{x^2} G(x) \int_0^\infty dV W_k'(V) J(Vx) \quad (6)$$

where for convenience $G(\text{sec}^{-1} \sqrt{x})$ is written simply as $G(x)$. With the step-function form for W_k given earlier, W_k' is a sum of delta functions, so that finally, carrying out the V integration

$$i_k = \frac{eA\lambda}{4} \int_1^\infty \frac{dx}{x^2} G(x) I_k(x) \quad (7)$$

where

$$I_k(x) \equiv -a_l J(eV_1x) + (1 + a_l) J(eV_2x) - (1 - a_u) J(eV_3x) - a_u J(eV_4x) \quad (8)$$

and $V_1, V_2, V_3, V_4, a_l, a_u$ refer, of course, to the k^{th} channel.

To proceed further it is necessary to specify a functional form for $f(v)$. In view of the earlier qualitative discussion, $f(v)$ should go over into something like a power law at high energies; in addition, it should lead to finite values for physically significant quantities such as density or pressure, have few free parameters and be as simple as possible. A model distribution function meeting these requirements, first proposed in this context by Olbert (cf. Moreno et al., 1966; some special cases of it have been used in the literature earlier), is

$$f(v) = \frac{N}{w_0^3} \frac{\Gamma(K+1)}{(\pi K)^{\frac{3}{2}} \Gamma(K - \frac{1}{2})} \frac{1}{(1 + \frac{v^2}{Kw_0^2})^{K+1}} \quad (9)$$

where the parameters are

N the total density of electrons.

w_0 the most probable speed (the position of the peak in the speed distribution $v^2 f(v)$).

K the exponent, at high energies, of the differential flux per unit energy.

As $K \rightarrow \infty$, $f(v)$ approaches a Maxwellian distribution with temperature $kT = \frac{1}{2}mv_0^2$. The function is shown, for several K, in Fig. 21. The corresponding omnidirectional integral flux, obtained by an elementary integration, is

$$J(E) = Nw_0 \left(\frac{K}{\pi}\right)^{\frac{1}{2}} \frac{2\Gamma(K-1)}{\Gamma(K-\frac{1}{2})} \frac{1 + \frac{E}{E_0}}{\left(1 + \frac{E}{KE_0}\right)^K} \quad (10)$$

where $E_0 = \frac{1}{2}mv_0^2$.

Several other quantities of interest are

$$\text{total omnidirectional flux } \phi = J(0) = Nw_0 \left(\frac{K}{\pi}\right)^{\frac{1}{2}} \frac{2\Gamma(K-1)}{\Gamma(K-\frac{1}{2})} \quad (11)$$

$$\text{energy density } U = \int d\vec{v} \frac{1}{2}mv^2 f(\vec{v}) = NE_0 \frac{3}{2} \frac{K}{K-\frac{3}{2}} \quad (12)$$

total omnidirectional energy flux

$$\phi_U = \int d\vec{v} \frac{1}{2}mv^3 f(\vec{v}) = \phi \frac{2K}{K-2} \quad (13)$$

A list of the various K - dependent coefficients is given in Table II. These formulas are collected here primarily for reference and for later use in discussing magnetosphere observations. In the transition region only the high-energy tail of any model distribution can be expected to be significant since only electrons in the tail of the actual distribution are detected; model quantities like K or J(E) for large E will be significant, whereas N and E_0 will not.

The expected currents i_k were calculated, using the form (10) for J(E), by numerically evaluating the integrals (7). The results are

shown in Figs. 22a to 22d; for each channel, the quantity $F(K,x)$ defined by

$$i_k = \frac{eA\lambda}{4} \frac{K-1}{K} \left(\frac{K}{\pi}\right)^{\frac{1}{2}} \frac{2\Gamma(K-1)}{\Gamma(K-\frac{1}{2})} Nw_0 F\left(K, \frac{V_2}{E_0}\right) \quad (14)$$

is plotted as a function of $x = \frac{V_2}{E_0}$ with K as a parameter. F is essentially the current expressed in flux units divided by the total flux, with some additional normalization.

The first question to be investigated using these model calculations is the relation between the measured current in channel 4 and the electron flux. Fig. 23 shows the ratio of the omnidirectional flux above energy E , $J(E)$ as given for some E_0 and K by equation (10), to the current i_4 in channel 4 calculated from equation (7) for the same E_0 and K (the ratio is of course independent of N), plotted vs. the energy E , for several K and a number of values E_0 in the range 10 ev to 100 ev. The curves all come close together (within a factor of 1.5) near $E = 200$ ev; hence i_4 is proportional to the omnidirectional flux of electrons above 200 ev, the constant of proportionality being approximately (within $\pm 30\%$) independent of the distribution function provided its parameters fall in the range cited. The relation is

$$\text{flux } (E > 200\text{ev}) \approx 4 \times 10^8 \text{ cm}^{-2} \text{ sec}^{-1} \frac{i_4}{10^{-10}\text{amps}} \quad (15)$$

With this conversion factor, everything said earlier about the current in channel 4 can be restated in terms of flux above 200 ev; thus, in

particular, the typical quiet time flux fluctuates around $4 \times 10^8 \text{ cm}^{-2}\text{sec}^{-1}$ and peak storm time fluxes reach $1.2 \times 10^{10} \text{ cm}^{-2}\text{sec}^{-1}$ and once $3.6 \times 10^{10} \text{ cm}^{-2}\text{sec}^{-1}$.

A related quantity is the density of electrons

with energies above E,

$$N(E) = 4\pi \int_{(2E/m)^{\frac{1}{2}}}^{\infty} v^2 dv f(v) \quad (16)$$

which can be related to J(E) using equation (4)

$$N(E) = - \int_E^{\infty} dE' \frac{1}{v(E')} \frac{dJ}{dE'} \quad (17)$$

where v(E) is the speed corresponding to energy E; integrating by parts

$$\begin{aligned} N(E) &= \frac{J(E)}{v(E)} - \frac{1}{2} \int_E^{\infty} \frac{dE'}{E'} \frac{J(E')}{v(E')} \\ &= \frac{J(E)}{v(E)} \left[1 - \frac{1}{2} \int_E^{\infty} \frac{dE'}{E'} \left(\frac{E}{E'} \right)^{\frac{1}{2}} \frac{J(E')}{J(E)} \right] \end{aligned} \quad (18)$$

For a steeply falling spectrum the quantity in brackets is close to 1 (for example, it equals $2\alpha / (2\alpha + 1)$ if $J(E) \sim E^{-\alpha}$) and one has, approximately,

$$N(E) \sim \frac{J(E)}{v(E)} \quad (19)$$

The current i_4 thus can be also related to the density of electrons with energies above 200 ev ($v(200\text{ev}) \approx 8.4 \times 10^8 \text{ cm sec}^{-1}$)

$$\text{density } (E > 200\text{ev}) \sim 0.5 \text{ cm}^{-3} \frac{i_4}{10^{-10} \text{ amps}} \quad (20)$$

Densities above 200 ev thus range from around 0.5 cm^{-3} during quiet times to as high as 15 cm^{-3} (and once 45 cm^{-3}) during magnetic storms.

Turning now to the use of model distributions to study the electron energy spectra, I will deal mainly with the cases shown in Fig. 20. It is convenient to form the current ratios i_4/i_3 , i_3/i_2 , and i_2/i_1 , which are independent of the total density N and, within the context of the model, are functions of the two parameters K and E_0 . Fig. 24 is a plot

with $\log (i_3/i_2)$ as abscissa and $\log (i_4/i_3)$ as ordinate; the lines are curves of constant K and curves of constant E_0 calculated from the model; the numbers enclosed in circles or squares indicate points corresponding to measured spectra from Fig. 20 (① indicates spectrum number 1 in Fig. 20, etc.). Fig. 25 is a similar plot with $\log (i_2/i_1)$ and $\log (i_3/i_2)$. Spectra with measurable currents in all four channels, which therefore appear in both Figs. 24 and 25, are shown enclosed in squares; those in which the current in channel 1 was below noise level and which thus appear only in Fig. 24 are shown circled. With only a few exceptions, the circled points in Fig. 24 fall within a region corresponding to distribution functions with exponents K in the range 4.5 to 7 and energies E_0 in the range roughly 10 to 50 ev, that is, well below the energy range of the instrument, in agreement with earlier qualitative deductions. Of the points enclosed in squares, numbers 27 and 33, the "flat" cases mentioned earlier, fall in regions corresponding, within the uncertainty of the measurements, to the same parameters K and E_0 in both Figs. 24 and 25, namely, an exponent $K \sim 2$ and a low E_0 ; thus the "flat" cases indeed correspond to an unusually flat power law distribution. The other squared points, however, tend to deviate in a systematic way from the predictions of the model. In Fig. 24 they tend to be somewhat higher than allowed by the model; in Fig. 25 they fall into two groups, either considerably higher than allowed (this includes, of course, the cases such as number 24 where i_1 exceeds i_2) or somewhat low. The qualitative character of the distribution function indicated by these deviations is sketched for the several cases in Fig. 26. All the deviations suggest that the "hump" in the spectrum so readily apparent during the November 15 storm (see

Fig. 19 and earlier discussion) may exist also at other times, to a lesser extent and sometimes at a lower energy. This must be regarded, however, merely as an interesting suggestion and not an established fact, for at least two reasons: (a) the observational evidence for the "hump" being based entirely on currents in channels 2 and 1 which are almost always close to noise level, is of marginal significance; (b) at these very low current levels there may be some contribution from proton fluxes, as discussed in Appendix A.*

To summarize the whole discussion of energy spectra, the present measurements provide strong evidence that transition region electrons have a non-Maxwellian energy distribution peaked well below 125 ev; only a sharply decreasing, approximately power law distribution is found in the several hundred ev range. The exponent of the differential flux per unit energy ranges roughly between -4 and -7, although there occur isolated, apparently rare at this time, events in which the exponent flattens to about -2. Fluxes of electrons above 200 ev range from 10^8 to a few times 10^{10} $\text{cm}^{-2}\text{sec}^{-1}$, corresponding densities from 0.1 to 40 cm^{-3} , the highest values occurring during magnetic storms. There are occasional indications of a "hump" or a flattening in the spectrum in the vicinity of 1 kev, but these must at present be considered as inconclusive.

The very detailed electron energy spectrum measurements (64 points

* Eventually, but not at present, it will be possible to evaluate the proton contribution, if any, from the simultaneous proton measurements.

between 70 ev and 18 kev) with an electrostatic analyser on Vela 3, recently reported by Asbridge et al. (1966), show, within the transition region, a power law spectrum between about 100 ev and 900 ev, with (differential) exponents in the range -3.5 to -5.5, in substantial agreement with the present work; earlier reports (including the published abstract of the paper of Asbridge et al.) of a peak in the spectrum near 200 ev resulted from failure to take into account the reduced detector efficiency at low energies.

The last question to be discussed is whether the decrease of electron flux from transition region to solar wind values coincides with the shock front as determined from proton measurements. In most of the cases the answer is, within the 40 second resolution of the proton measurements, in the affirmative. An example of this is given in Fig. 27 which shows the unsmoothed electron data for a portion of orbit 33 out-bound; each of the large sharp increases and decreases of electron flux coincides with a shock crossing observed in the proton data. A few dramatic exceptions to this general rule, however, occurred during the November 15 magnetic storm and can be seen in Fig. 19; at 10:17 UT and again at 10:53, as the shock front was driven in past the satellite by the increased pressure of the solar wind causing the storm, strong electron fluxes were observed in the interplanetary medium until they disappeared suddenly at 10:30 and 11:02, respectively. This sharp disappearance some distance upstream from the shock strongly suggests that these electrons are not part of the solar wind itself but are

related to the shock. The electrons observed around 11:45, from 12:45 to 13:30, and again from 14:00 to the shock crossing at 14:47 are probably of the same origin.

B. The Magnetosphere

For reasons already mentioned, nearly all the electron data in the magnetosphere were obtained from inbound passes of the satellite and hence from regions relatively close to the geomagnetic equatorial plane; between geocentric distances 20 and 10 Re on inbound passes, the geomagnetic latitude of the satellite during the period considered ranged from -6° to $+25^{\circ}$. The sun-earth-probe angle during this period, for portions of the inbound orbits between the magnetosphere boundary and about 10 Re distance ranged from 145° to 80° , on the dusk side of the earth. The part of the magnetosphere to which the present study refers is thus the evening sector (about 18h to 22h local time) of the equatorial region. The principal features of the electron distribution found in this experiment are the following:

(1) There exists in this evening sector a band of electrons extending, within the equatorial region, from the magnetosphere boundary inward to a geocentric distance of about 11 Re, characterized by densities of the order of 1 cm^{-3} , mean energies of several hundred ev, and omnidirectional fluxes of the order of $10^9 \text{ cm}^{-2}\text{sec}^{-1}$. The band extends in longitude toward the sun-earth line beyond the limits of the present survey, i.e. to within at least 80° . Toward the anti-solar direction it is found as far as 10 Re behind the dawn-dusk meridian*; the electron distribution beyond that distance cannot be unambiguously determined

* The meridian plane perpendicular to the sun-earth line

because of limited data coverage. This band should probably be identified with the once so-called "outermost radiation belt" of Gringauz.

(2) Within this band, the electron flux, mean energy, and density, although fluctuating in time and varying from one orbit to another, do not show any obvious systematic dependence on geocentric distance or on the angle from the sun-earth line. As to possible dependence on geomagnetic activity, a significant increase in density occurs during the magnetic storm of November 15, but no such increase is apparent during the storms of November 1 and 9; because of the very small number of storms available for study during this period, the question of storm effects must for the present be left open.

(3) Toward the tail region of the magnetosphere, roughly farther than 10 R_e from the dawn-dusk meridian, a region of electrons of considerably lower energies is encountered; as far as can be determined with the present instrument, the density is of the order of 5 to 10 cm^{-3} , the mean energy is of the order of 40 to 80 eV, and the total omnidirectional flux is of the order of 4×10^9 to $10^{10} \text{ cm}^{-2} \text{ sec}^{-1}$. Only a very limited amount of data from this region is so far available and its precise spatial limits cannot be established.

(4) Electrons in both this region and the previously mentioned band have roughly the same and relatively unvarying energy density; assuming equipartition of energy between electrons and (so far undetected) protons, the energy density of the entire plasma corresponds to that of a magnetic field of magnitude 20 to 40 γ , comparable to the observed field. The only significant increases of energy density above this range

that have been found so far occur during the magnetic storm of November 15, when values corresponding to 50-60 γ are reached.

(5) The band of several hundred ev electrons usually has a well-defined boundary on the earthward side, occurring generally at a geocentric distance of 11_{-1}^{+1} Re but sometimes as close as 8 or even 6 Re; most of the close boundary crossings occur at the larger angles from the earth-sun line, but because of the small numbers involved it is not clear whether this is a significant result or just a coincidence. The boundary is defined by a remarkable change in the electron spectrum: as the satellite moves inward, the electron mean energy decreases, while the density increases somewhat; it is possible to follow the energy decrease from 400-500 ev to about 100 ev, (and the corresponding density increase, e.g. from 0.8 to 1.3 cm^{-3}), at which point the measured currents are almost at noise level. The decrease from the typical measured current of a few times 10^{-10} amps outside the boundary to noise level (about 2×10^{-11} amps) inside usually occurs relatively rapidly, while the satellite moves 1 Re or less, although in some cases the low energy electrons can be detected for a distance of several Re inside the onset of the decrease.

(6) At distances closer than about 4-5 Re the output of the detector falls to zero (as distinct from noise level); the effect is believed due to the large fluxes of positive ions acting through the mechanism described in an earlier chapter. The boundary of the high-density plasma region obtained from the onset of this effect is in agreement with whistler and other determinations.

Examples of inbound passes through the magnetosphere are shown in figures 17 (orbit 23), 18 (orbit 22), and 19 (orbit 27); as additional examples, Fig. 28 shows one of the earlier orbits, orbit 15, at relatively large angles from the sun-earth line (note that the magnetopause is encountered at a distance of 23 Re) and Fig. 29 shows the last orbit in 1964 for which complete data coverage through the magnetosphere is available, orbit 35, at an angle of about 80° from the sun-earth line (note the magnetopause crossing at 12.5 Re). All these figures show a region, extending inward from the magnetosphere boundary, in which the largest currents are observed in channels 1 and 2, the high energy channels (in contrast to the transition region, in which the largest current always occurs in channel 4, the lowest energy channel); the current in channel 1 is usually somewhat smaller than that in channel 2, indicating that the differential electron flux has a maximum at an energy somewhere near or within the range of channel 2 (roughly 300 to 1000 ev) and is already decreasing within the range of channel 1. The sharp earthward boundary of this region appears as the rapid decrease of current in all channels, at 10 Re in orbit 15 (Fig.28), 10.8 Re in orbit 23 (Fig. 17), and 10 Re in orbit 35 (Fig. 29). The change of the energy spectrum across the boundary is especially clear in orbit 23; while the satellite moves a distance of 1 Re, the maximum of current shifts from channel 1 through channels 2 and 3 to channel 4; it is apparent that the energy at which the peak electron flux occurs is falling. Similar behavior, although not as marked, can be seen in orbit 15, and is found in most of the cases available. In orbit 35, however,

the decrease of the currents to noise level is so sudden that the details cannot be made out from a plot on this time scale; in orbit 22 (Fig. 18), by contrast, the channel 1 current drops to noise level at 11 Re, but currents in the lower channels persist to 6 Re. In orbit 27 (Fig. 19), finally, strong electron fluxes are found as close as 8 Re.

A very different electron spectrum can be seen in orbit 11 inbound (Fig. 30); the peak current occurs in channel 4, and the spectrum falls with increasing energy in almost transition-region-like fashion, although the ratio of the current in channel 4 to that in channel 3 is somewhat smaller than in the transition region, indicating that the spectrum near 100-200 ev is flatter (and hence presumably the peak of the electron distribution is at a higher energy). During orbit 11 inbound there is a magnetic storm, but a similar spectrum is found at quiet times in a portion of orbit 14 inbound and, for a very brief period only, in orbit 15 inbound (the pulse in channel 4 at 19.6 Re in Fig. 28).

The behavior of the observed signal at distances less than about 5 Re cannot be represented on these plots, which show the input current corresponding to the telemetered voltage, a quantity which has no meaning for voltages smaller than the noise level at zero input. A plot of the telemetered voltage for orbit 23 inbound from 14 Re to perigee is shown in Fig. 31. The previously mentioned boundary at 10.8 Re is clearly visible; inside it, the signals in all four channels stay at their noise levels* until a distance of 5.3 Re when first the signal

* The difference in widths of the four traces is purely an instrumental effect, discussed in Appendix A.

in channel 1 and then in succession those in channels 2, 3 and 4 decrease rapidly to zero. This, according to the discussion in Chapter III B, indicates a wrong phase signal*, such as one produced by strong fluxes of positive ions; the fact that the onset of the decrease is not simultaneous in all channels results from the dependence of the positive ion signal on modulation potential, as explained in Appendix A, and indicates that the positive ion flux increases with decreasing distance. This phenomenon is observed in all orbits, inbound and outbound, for which data are available at the appropriate distances. The value of the L coordinate at the onset of zero in channel 1 ranges from 3.7 to 5.3 (with one far-out case at 6.3), in good agreement with previously reported boundaries of the high density plasma region near the earth (see Carpenter, 1966; Taylor et al., 1965; and the discussion of whistler work in Chapter II B); in the one case so far where comparison has been made, the onset of zero in channel 1 coincides with the "knee" in ion density as determined from simultaneous measurements on OGO-A by Taylor et al. (1965).

Data on the spatial distribution of electrons are summarized in Fig. 32. The coordinates are distance along the sun-earth line (or the solar ecliptic X coordinate, XSE) and distance perpendicular to the sun-earth line ($(YSE^2 + ZSE^2)^{\frac{1}{2}}$), or equivalently the polar coordinates geocentric distance and angle from the sun-earth line; because

* The electron detector on Explorer 21, of the same type as the present one but measuring only the amplitude of the AC signal regardless of the phase, finds a large sharp increase in current at distances of 3-5 Re, in agreement with this interpretation (J. Binsack, private communication, 1966).

of the nature of the orbits, an essentially indistinguishable plot would result in solar magnetospheric X, Y coordinates or in solar-oriented geomagnetic X, Y coordinates. All portions of the orbits inside the magnetosphere from which useful electron data were obtained are shown, different types of lines indicating the various types of electron spectra; the three types of observed boundaries - magnetosphere, several hundred ev electron region, and high density plasma region - are marked.

In Fig. 32 there appears to be a fairly well defined boundary between the "high energy" (several hundred ev, density $\sim 1 \text{ cm}^{-3}$; solid lines in the figure) and "low energy" ($< 100 \text{ ev}$, density $\sim 5 - 10 \text{ cm}^{-3}$; dashed lines) electron regimes, corresponding roughly to the line $XSE = -10 \text{ Re}$. It should be kept in mind, however, that observations on the low energy side of this line are very scarce (fractions of two orbits) and that all of these were at somewhat higher than average magnetic latitudes (10 to 20°); thus the actual shape of this boundary, and in particular whether the high energy regime actually terminates at about $XSE = -10$ or instead is just confined to a thin sheet beyond there so that the orbits lie above it, cannot be settled on the basis of the present observations (a very similar ambiguity, it will be recalled, exists regarding the 40 kev electron cusp region boundary).

The early observations of soft electrons on Lunik 2 (whose orbit passed through part of the region surveyed by OGO-A, as shown in Fig. 4) are in good agreement with the electron distribution here described. The band of electrons with energies above 200 ev detected by Lunik 2 extends from 9.6 Re distance (close to the electron earthward boundary observed at

11± 1Re or closer by OGO-A) to 12.7 Re at a sun-earth-probe angle of approximately 130-140° (or XSE ~ -8 to -10, at approximately the boundary here inferred of the region of low energy electrons, which would probably be undetectable by the Lunik 2 instrument with its 200 ev threshold and limited sensitivity); at the latter point the geomagnetic latitude of Lunik 2 was about 10° south and increasing, so the ambiguity about this boundary mentioned earlier is not clarified.

Turning now to an analysis of the electron energy spectra, the method to be followed has already been described in the section on transition region observations, namely, assuming a specific form for the electron distribution function with a few parameters whose values are chosen to fit the measurements. The form chosen is again that given by equation (9); of the assumptions involved, isotropy of the electrons at these energies has been verified by measurements on Vela (Bame et al., 1966) and on the space probe Pioneer 6 (using a detector very similar to the present one) during its one pass through the magnetosphere near the dusk meridian*; the power law character of the spectrum at high energies has been observed on Vela (Montgomery et al., 1965; Bame et al., 1966). The required formulas have already been presented in the earlier section. Since the peak of the electron spectrum now lies, as is clear from the earlier qualitative discussion, well within the energy range of the detector which therefore is responding to a significant fraction of the

* I am indebted to Prof. A.J. Lazarus and Dr. V. Formisano of M.I.T. for making the Pioneer 6 data available prior to publication.

total number of electrons present (rather than just to the small fraction on the high energy tail, as in the transition region), one can reasonably attempt to estimate quantities referring to the distribution as a whole, such as density, flux, or mean energy; on the other hand, since the high energy tail of the distribution now lies mostly above the range of the detector, it cannot be assumed that the value obtained for a parameter like K will necessarily reflect the exponent of the tail.

A simple graphical method was devised to estimate the parameters N, E₀, and K from the measured currents i_k. Equation (14), which can be rewritten as

$$i_k = e A \lambda C(K) N w_0 F\left(K, \frac{V_2}{E_0}\right) \quad (21)$$

where for brevity

$$C(K) \equiv \frac{1}{4} \frac{K-1}{K} \left(\frac{K}{\pi}\right)^{\frac{1}{2}} \frac{2\Gamma(K-1)}{\Gamma(K-\frac{1}{2})} \quad (22)$$

expresses i_k as a function of three variables Nw₀, E₀, and K. Now for an assumed K and a measured current i_k in a given channel k, equation (21) defines a curve in the Nw₀ - E₀ plane; writing the equation of the curve as

$$\log Nw_0 = \log \left(\frac{i_k}{e A \lambda} \right) + \log F\left(K, \log V_2 - \log E_0\right) - \log C(K) \quad (23)$$

and comparing with a corresponding form of (21)

$$-\log \left(\frac{i_k}{e A \lambda} \right) = -\log Nw_0 - \log F\left(K, -\log E_0 - (-\log V_2)\right) - \log C(K) \quad (24)$$

it is clear, after a little thought, that the curve $\log Nw_0$ vs. $\log E_0$ for fixed i_k and V_2 is the same as the curve $-\log\left(\frac{i_k}{eA\lambda}\right)$ vs $-\log V_2$ for fixed Nw_0 and E_0 , i.e. the curve of Fig. 22 rotated by 180° and suitably normalized. There are four channels and hence four such curves in the $Nw_0 - E_0$ plane, which should all intersect at a common point corresponding to the correct values of Nw_0 and E_0 ; if the curves do not all intersect at the same point for any value of K , the data cannot be fitted by a distribution of the assumed form.

These curves were constructed by first plotting the four measured values i_k as functions of V_2 , then, for each channel, taking the appropriate section of Fig. 22, rotating it by 180° , superposing it on the plot so that the point $X=1$, $F(K,X)=0.1$ (the intersection of the coordinate axes) lay on the measured point, and tracing the curve for the assumed K ; for the curve thus obtained the coordinates V_2 , i_k must be reinterpreted as E_0 , $(0.1 eA\lambda C(K)Nw_0)$. To obtain K with the least amount of trial and error, use was made of the fact, apparent from Fig. 22 that $F(K,X)$ is practically independent of K for $X=\frac{V_2}{E_0} < 1$ and the four curves were constructed in the following sequence: first the curve for channel 3, the relevant portion of which nearly always proved independent of K ; then the curve for channel 2, the intersection of which with 3 was only weakly dependent on K ; the requirement that the curve for channel 1, drawn next, pass through the intersection of 2 and 3 served to select K ; the curve for channel 4, the relevant part of which was of course completely independent of K , served to check the fit (channel 4 was not used at the start because its current was generally the weakest and hence least

accurate. From the intersection point, finally, the values of Nw_0 and E_0 were read off, and from these N can be readily obtained.

Three examples of this process, of varying goodness of fit, are shown in Fig. 33. In a number of cases, exemplified by the leftmost set in Fig. 33, a nearly exact fit was obtained; in others, such as the remaining two in Fig. 33, although the intersections did not all coincide, they were clustered together within a relatively small area, which could be taken as defining a probable region within which the actual parameters Nw_0 and E_0 lay*; the lack of fit in such cases could reasonably be attributed to uncertainties in the measured values. No really bad fits, indicating that the model distribution was entirely inappropriate, were found except in some cases when one of the measured currents was close to noise level and hence unreliable.

59 measured spectra have been analyzed by this method; the results are given in Table IV, which lists the values obtained for the most probable energy E_0 , the density N , the omnidirectional flux ϕ (computed from equation (11)), and the parameter K (where no value of K is given, E_0 is high enough so that the fitting process is independent of K). Where a range of values for E_0 and N is specified, an exact fit could not be obtained but a range of possible values is defined by the various intersections; these ranges also give an indication of the uncertainties in the values of E_0 and N generally. The positions

* The region thus defined is generally rather elongated, so that the parameters N and E_0 cannot be varied independently within the ranges obtained, but the largest N corresponds to the smallest E_0 , and vice versa.

in space at which the analysed spectra were measured are shown in Fig. 34 (in the same projection as Fig. 32), together with a rough indication of the energies found; they are scattered throughout the surveyed region of the magnetosphere and include examples from both the high and the low energy regimes.

The electron spectra obtained by OGO-A on the dusk side of the magnetosphere are significantly different from those obtained on Vela 2 within the neutral sheet on the midnight meridian (Bame et al., 1966); the Vela measurements indicate energies near 1 kev* and densities generally near 0.1 to 0.3 cm^{-3} . On the other hand, the values of K obtained in the present work happen to be in agreement with the exponents of the high-energy power law tail quoted by Montgomery et al. (1965).

A most interesting property of the magnetospheric electron spectra becomes apparent if one plots E_0 vs. N for the 59 cases analyzed, (excluding the few inside the earthward boundary of the several hundred ev electron band) as is done in Fig. 35: the points do not scatter at random but are strongly clustered in a band about a line $NE_0 = \text{constant}$, i.e. the spectra tend to have the same energy density. To illustrate this more clearly, lines of constant energy density are drawn in Fig. 35 and labeled by values of the "equivalent field strength", i.e. the magnetic field strength at which the energy density in the field is

* The "average energy" quoted by Bame et al. appears to be ϕ_v / ϕ (energy flux over particle flux) and thus is related to E_0 , according to equation 13, by "av. E" = $\frac{2K}{K-2} E_0 = 4E_0$ for $K = 4$.

equal to the energy density in the plasma, computed in this case from (cf. equation 12)

$$\frac{B_{eq}^2}{8\pi} = 2 \times \frac{3}{2} \frac{K}{K - \frac{3}{2}} N E_0 \quad (25)$$

where the factor of 2 is included to allow for a proton energy density assumed equal to that of electrons; K has been taken equal to 4.

Leaving out the circled points which refer to measurements during the intense magnetic storm of November 15, nearly all the remaining points fall between curves of equivalent field strength 20 and 40 γ , comparable to the measured field magnitudes (cf. Heppner, 1965). Note that this set of points contains measurements from a sizable region of space over a time interval of two months and includes samples from two distinct energy regimes; yet, while the energy of the electrons varies by about a factor of 20 and the number density by about a factor of 40, the energy density varies by no more than a factor of 4.

Finally, Fig. 36 shows the change of spectral parameters E_0 , N , and ϕ as the satellite crossed the earthward boundary of the several hundred ev electron region on orbit 23. As already inferred from qualitative arguments, there is a sharp drop in E_0 as the satellite moves in through the boundary; in this case the drop seems to be, very crudely speaking, exponential in distance with a factor of 5 decrease per 1 Re; at the same time, the density N of the electrons is increasing slightly. A similar behavior, a sharp drop in mean energy together with a slight increase in density, has been found in the two other cases analysed, orbits 17 and 22 (included in Table IV as the last two points

for each of these orbits). It thus appears that, while the outermost region of the magnetosphere, at least near the geomagnetic equatorial plane on the dusk side, is filled with electrons of several hundred ev energy, as one moves toward the earth and approaches the trapped high energy particle region of the Van Allen belts, the mean energy of the bulk of the electrons decreases (while the density increases but only slightly) at a sharply localized, well defined boundary.

V. CONCLUSION

The most important result of this work in the transition region is the discovery, simultaneously with and independently of the Vela observations, that the electrons in the transition region are comparatively cold, with a non-Maxwellian spectrum that peaks below a hundred ev*. This rules out theories of the shock front which lead to strong heating of electrons, such as those that consider the two-stream instability as the dominant randomization process, and also indicates that the transition region plasma, with electrons that are colder than protons, is quite different from the usual plasma treated by theorists in which, following what is thought to be the case in fusion machines, the electrons are assumed much hotter than the ions. In the magnetosphere, the soft electron band talked about since the early years of space exploration has been firmly established, at least near the geomagnetic equator and on the dusk side of the earth, and its spatial extent delineated. The density and mean energy of these electrons have been measured; the energy density appears to be consistent with at least approximate equipartition of energy between plasma and magnetic field. Perhaps the most surprising result of the observations is the peculiar

* More recently Moreno et al. (1966), from an analysis of Explorer 18 observations, have placed the peak of the electron spectrum, at energies ranging from 20 to 50 ev. The peak of the proton thermal spectrum, by contrast, is usually 100-200 ev.

earthward boundary of this electron band, which is found near the termination of the stably trapped particle region and also near the transition from a dipole-like magnetic field configuration to the distorted, nearly constant - magnitude field characteristic of the outer magnetosphere, although so far the sharp boundary has not been correlated with any comparably sharp feature in magnetic field or high energy electron data*; inside the boundary, i.e. in the trapped radiation, dipole-like field region the plasma electrons have much lower energies than those outside, although comparable or somewhat larger densities. It is not easy to see what maintains such a (relatively sharp) temperature gradient, and most processes one can think of would maintain a gradient in the other direction; the high energy electrons, it should be noted, behave in the opposite way, having higher energies inside the radiation belts. To speculate on one possible candidate, the several hundred ev electrons could be dumped into the atmosphere by a resonant interaction with VLF waves such as that discussed by Kennel and Petschek (1966), with low energy electrons being pulled up from the ionosphere to maintain charge neutrality (which would, of course, require steady state electric fields along the magnetic field); the boundary would then result from the fact that only on closed dipole-like lines the VLF waves can bounce back and forth and be amplified. Other possibilities will no doubt be suggested.

A major task for the future is the detailed comparison of these

* Only a few, very limited comparisons have been made yet, however.

observations with those of other experiments flown on OGO-A, especially the observations of protons, magnetic fields, very low energy (< 100 ev) and high energy (> 40 kev) electrons. To mention only a few of the questions that can be raised: are major changes observed in one of these quantities reflected in the others, and if so in what way? Is there an equipartition of energy between plasma and magnetic field which holds in detail, or are the two energies merely comparable on the average but varying independently? What phenomenon, if any, in low energy electron behavior coincides with the 40 kev spikes? Are the different energy regimes for magnetospheric electrons found in this work related to the spatial distribution of 40 kev electrons? Are there any other peculiar observations at the earthward boundary of the soft electron band? It is to be hoped that the full potential of a large multiple-experiment satellite such as OGO-A will eventually be exploited to gain further insight into the complex and fascinating phenomena of space.

Appendix A. Some details of the apparatus

Energy windows. - Consider a beam of particles incident on the cup with the component of velocity normal to the cup corresponding to energy E

$$\frac{1}{2} m v^2 \cos^2 \theta = E$$

The current produced by these particles has a constant value, proportional to their flux, when $E > eV$ (where V is the magnitude of the modulator potential) and is zero when $E < eV$. The electronics of the detector picks out the $\sin \omega t$ component of this current, where ω is the modulation frequency and $t=0$ at the start of the modulation cycle. Referring to Fig. 12, let τ = length of modulation cycle, τ_u = length of upper "spike" of the modulation wave form, τ_l = length of lower "spike", $f_u = \tau_u / \tau$, $f_l = \tau_l / \tau$; then the current during one modulation cycle produced by the beam is

$$\begin{aligned} i(t) &= 0 & 0 < t < \phi_1 \tau \\ &= i_0 & \phi_1 \tau < t < \phi_2 \tau \\ &= 0 & \phi_2 \tau < t < \tau \end{aligned}$$

where i_0 is the current in the beam and ϕ_1, ϕ_2 depend on the energy, as follows:

$$\begin{aligned} \phi_1 &= 0 & \phi_2 &= f_u & eV_3 < E < eV_4 \\ \phi_1 &= 0 & \phi_2 &= \frac{1}{2} & eV_2 < E < eV_3 \\ \phi_1 &= \frac{1}{2} & \phi_2 &= \frac{1}{2} + f_l & eV_1 < E < eV_2 \end{aligned}$$

($i(t) = 0$, of course, for $E > eV_4$ or $E < eV_1$).

Taking the $\sin \omega t$ component, the measured quantity is

$$a = \frac{1}{\tau} \int_0^{\tau} dt i(t) \sin \frac{2\pi t}{\tau} = \frac{i_0}{2} \int_{\phi_1}^{\phi_2} dx \sin x = \frac{i_0}{2} (\cos \phi_1 - \cos \phi_2)$$

Normalized to unity for $eV_2 < E < eV_3$, this is the function $W(E)$ of

Chapter III B

$$\begin{aligned} W(E) &= \frac{1}{2} (1 - \cos 2\pi f_u) & eV_3 < E < eV_4 \\ &= 1 & eV_2 < E < eV_3 \\ &= -\frac{1}{2} (1 - \cos 2\pi f_l) & eV_1 < E < eV_2 \end{aligned}$$

with the definitions

$$\frac{1}{2} (1 - \cos 2\pi f_u) = \sin^2 \pi f_u \equiv a_u$$

$$\frac{1}{2} (1 - \cos 2\pi f_l) = \sin^2 \pi f_l \equiv a_l$$

The modulator waveforms were observed directly with a high-impedance probe; the fractions f_u and f_l for each channel were measured from oscilloscope photographs of the waveforms and the quantities a_u and a_l calculated from the above equations. The voltages V_1, V_2, V_3, V_4 were measured in the same way.

When there is a distribution of particle energies, the amplitude of the appropriate Fourier component is the sum of the amplitudes due to particles of each energy at the input to the compression amplifier, since the electronics is linear up to that point; neglecting possible small phase shifts due to particles within the "side lobes"

of the energy window, the output of the compression amplifier and synchronous detector is a known function of the amplitude at its input. The latter can thus be determined from the output signal using a calibration curve, described further on; it is the quantity so determined, a linear functional of the particle distribution, that is the "measured current" spoken of in the text.

Calibration. - To determine the effective response of the electronics, a square wave current of the correct frequency and phase was fed into the preamplifier and the output voltage was measured as a function of the amplitude of the input square wave. The resulting curve is an empirically determined relation between the output voltage and the input current to the collector, taking into account both the over-all gain of the system and the non-linear characteristic of the compression amplifier, that was used to convert the telemetered voltages to collector currents. The curve is shown in Fig. 37; the points are the averaged measured values, while the line is the smooth curve adopted for use in the analysis (the few points that deviate significantly from the curve are averages of only a few measurements and are not considered reliable). There is a sharp break in the curve at an input current of about 10^{-10} amps; the very flat curve for currents below that point is uncertain (in particular, instead of the single line drawn from 10^{-10} to noise level there may actually be a completely flat "plateau" just below 10^{-10} followed by a decline to noise level; there are not enough measured points in this region to decide between the two possibilities) and the values obtained for very

small measured currents are somewhat doubtful. The gain of the system was checked in flight by passing through it a standard signal of known amplitude.

A peculiar feature of the electronics, observed in both pre-flight calibration runs and in the flight data, is a systematic variability of the output for a fixed input: if one considers the output of a given channel, which is sampled every 9.216 seconds, on successive samples the output will be alternatively high and low, until after 13 samples the pattern will slip by one, i.e. there will be two successive highs; thus, the sequence is

H L H L H L H L H L H L H H L H L H L H L H L H L H H L H L etc.....

Another channel will exhibit that same pattern but randomly phased with respect to the first. The effect of this variation can be clearly seen in unsmoothed data plots (such as figures 27 and 31) where, because of the high density of points (431.25 data points per inch) it produces a broad trace. The amplitude of the variation is about 0.5 volts; at noise level it decreases with increasing channel energy, resulting in the varying width of the traces in Fig. 31.

The cause of this phenomenon is at present unknown, although it is purely a property of the electronics and has nothing to do with the data since it appears in calibration runs. The 13 sample periodicity has been found to hold accurately, however, and the effect thus can be eliminated by taking a 13-point sliding average in the data for each channel; the calibration curve is applicable to data thus smoothed since a similar average was taken in constructing it. This causes some loss

of time resolution; where large short scale time variations occur, most of the instrumental effect can be eliminated by taking a 4-point sliding average and the rest will generally be insignificant compared to the variations of interest (an example is Fig. 19).

Angular response. - The fraction of electrons incident at a given angle that can strike the collector was calculated by projecting each aperture within the cup along the particle trajectories onto the collector plate and finding the area common to the collector and all the projected apertures. Straight line trajectories were used; the curvature of the trajectories within the relatively narrow electric field regions near the modulator and the collector is significant only at larger angles and produces at most a 10% correction, as shown by extensive calculations on the Explorer 21 cup by J. Binsack (private communication, 1966); compared to other uncertainties, this is not significant. The angle-dependent transparency of the grids was approximately included using a formula valid for a rectangular grid

$$\text{transparency} = t_0 (1 - a (\sec \Theta - 1))$$

with the constants t_0 and a determined from measured mesh sizes and wire diameters of the grids.

Besides striking the collector, electrons can also be detected through the secondaries they produce in striking the shield grid (secondary production from other grids is negligible because of their high transparency, 90-93%, and the consequent small area struck by the incident electrons). The effective area of the shield grid struck by incident electrons was calculated (in the same way as that of the collector),

multiplied by an assumed effective secondary yield, and added to that of the collector to obtain the total response function. The value of the effective secondary yield is the most uncertain quantity in the calculation; for an assumed constant effective yield independent of angle, the shape of the angular response curve turns out, however, to be practically independent of the yield as long as it is not too small (not less than 0.5, say). Published values of the secondary electron yield from electrons incident on metal surfaces (see, e.g., McKay, 1948) indicate, for most metals*, a very broad maximum of about 1.0 to 1.5 secondaries per primary at a primary energy of 400-700 ev and at normal incidence; the yield increases with increasing angle θ between the primary electrons and the normal to the surface, roughly as $\sec \theta$ for angles not close to 90° . In the present case the curved surface of the grid wires produces an averaging over directions of incidence for all angles between the cup normal and the incoming electrons, and thus there is some reason to think that the effective yield of the whole grid is independent of the angle between the cup normal and the incoming electrons. In addition, the slow energy variation of the yield over the energy range of the detector was neglected; thus for calculations a constant effective yield δ for all angles and energies was assumed. The quantity λ used in the text is related to δ by

$$\lambda = 1 + \frac{A_s}{A_c} \delta$$

* The shield grid is made of phosphor bronze, the others of tungsten

where A_s , A_c are the effective areas of the shield wires and the collector, respectively, at normal incidence; numerically

$$\lambda = 1 + 1.76 \delta$$

A value of $\delta = 0.6$ was chosen (reduced from measured yields to allow for re-absorption of secondaries by the grid), giving $\lambda = 2$; this number is uncertain by probably about $\pm 50\%$.

Response to protons. - The two mechanisms by which the detector can respond to protons have been briefly described in the text. An increased modulator potential increases slightly the collection efficiency for protons (of energy greater than 150 ev; only these can reach the collector) by bending their trajectories inward; since an increase of modulator potential produces an increase of proton current, which is equivalent to a decrease of electron current, the A.C. signal produced has the phase expected for the genuine modulated electron current. From the calculations of J. Binsack mentioned earlier, the effect with the modulation voltages here used amount to at most 5% of the incident proton flux. The noise level of the Faraday cup proton detector flown on OGO-A corresponds to a flux of about $8 \times 10^7 \text{cm}^{-2} \text{sec}^{-1}$; the corresponding current produced in the electron detector through the effect under discussion is about 1×10^{-11} amps, below the noise level. No protons are detected in the magnetosphere, hence the effect on electrons is below the noise level; in the solar wind the electron cup is pointing away from the highly directed proton flow and the proton flux into it is thus very small and again insignificant. The angle

between the proton detector axis and the sun varies as the satellite spins, during the period considered, roughly between 0 and 20°. In the transition region much of the time the observed proton current is already at noise level at the larger angle, and the proton flux into the electron detector is therefore even smaller; in several cases, however, the proton current at 20° is as much as 5 times the noise level and the effect in the electron detector could be comparable to its noise level. In summary, the proton current observed by the electron detector through this mechanism is negligible except for a few periods of exceptional intensity in the transition region, when it could be comparable to the weak electron currents in channel 1.

The other mechanism results from secondary electrons produced by protons striking the modulator grid; since the energy with which they strike the grid is their initial energy plus e times the potential of the grid and the secondary electron yield increases with incident proton energy (cf. Medved and Strausser, 1965), an increase in modulator potential produces an increase in electron current; the resulting A.C. signal is thus opposite in phase to the genuine modulated electron current. The effect has been investigated experimentally, using a detector similar to the present one; it was found that the A.C. current produced was roughly proportional to the width of the electron energy window and amounted to about 0.007 times the incident proton flux for a 1 keV wide window. The size of the effect (remembering that it comes from the 7 - 10% of the grid area that is covered by wires) and the energy dependence are in approximate agreement with

published data on secondary electron yields from protons incident on metal surfaces (Medved and Strausser, 1965). The effect is at least 5 times smaller than the preceding one and a fortiori negligible in the solar wind, the transition region, and most of the magnetosphere. It is important only in the region of relatively dense, cold plasma near the earth, where its presence is easily recognizable, as discussed in the text.

Appendix B. Orbital Elements

The conventional orbital elements, referred to the celestial coordinate system, are given below for reference; the more useful (for present purposes) elements referred to the ecliptic plane cited in the text can be derived from these by straightforward coordinate transformations.

Orbital elements of OGO-A, epoch 10/14/64:

Semi-major axis	81225.69 km
Eccentricity	0.90779
Anomalistic period	3839.59498 minutes
Inclination	32.132°
Right ascension of ascending node	164.719°
Argument of perigee	317.201°

Appendix C. Some details of data processing.

As indicated in Fig. 14, a complete sequence of measurements of the present detector consists of 16 data points; the 4 measured currents, 4 housekeeping parameters (reset word, standard signal, temperature, and marker signal), and the same 8 points repeated with the modulator off. The detector continuously cycles through this sequence, driven by periodic index pulses from the spacecraft; there is no synchronization with the subcommutator sequence. Since the telemetry format is organized around the subcommutator sequence and is thus unrelated to the detector measurement sequence, finding the latter is a principal task of the data processing. This is done using the marker signals: a 5 volt signal precedes the channel 1 current in each sequence. The data processing program scans each record of the data tapes for these periodically spaced 5 volt signals, picks up the 4 following numbers as the measured currents, and writes a new data tape whose format is organized around the measurement sequence. This new data tape is then sorted to put the records in correct time sequence. Data plots such as those shown in Fig. 17, 18, and 19 are produced using the sorted data tapes and the orbital information tapes. The latter contain the position of the satellite and assorted other information (sun vector, velocity, magnetic coordinates, etc.), at intervals of one minute; positions of the spatial coordinate axis ticks in the plots are obtained by linear interpolation.

All processing at M.I.T. is done on an IBM 7044 computer operated by the Laboratory for Nuclear Science. Plotting is done using a Calcomp model 565 digital incremental plotter.

Appendix D. Some concepts of geomagnetism.

The field of geomagnetic studies, or even just the part of it of particular relevance to satellite measurements, is very extensive and here I will merely define a couple of its terms that have appeared in the text; for a summary account of the field the reader may consult, for example, the recent review by Sugiura and Heppner (1965).

Magnetic storms, as the name might imply, are prolonged periods of disturbance in the earth's magnetic field. Although the detailed field variations at the earth's surface during a magnetic storm are very complex and differ greatly from one storm to another, there is an underlying pattern that can be recognized in most storms, especially in the behavior of the horizontal component of the field (usually called H) at low and middle latitudes. The idealized typical storm begins with a sudden increase of H, observed simultaneously (within a minute or so) all around the earth, called the sudden commencement. This is followed by a period, typically lasting several hours, during which H remains above its pre-storm value; this is the initial phase of the storm. Then the field decreases to below its pre-storm value; this period, which may last as much as a day or so, is the main phase. Finally the field slowly returns to its quiet-time value during the recovery phase, which often lasts several days. There are also storms which begin gradually, without a sudden commencement. Sometimes a sudden worldwide increase(or decrease) in H is

observed without a storm following; this is a positive (or negative) sudden impulse.

A frequently used rough indicator of the degree of geomagnetic activity is the K_p index. The K index for a given observatory is a quasi-logarithmic measure of the range of measured field variation about its quiet time value during a three-hour period, excluding variations which can be recognized as produced by solar electromagnetic radiation through photoionization in the ionosphere; it is intended as a measure of the effects of "solar corpuscular radiation". The planetary (i.e. worldwide) K index, or K_p , is the average, for each three-hour period of U.T., of the K indices from 12 selected observatories in middle latitudes. The values of K_p range from 0 to 9 and are quantized in units of 1/3, indicated by writing -, 0, or + after the number; thus the possible values are 0o, 0+, 1-, 1o, 1+, 2-, 2o, 2+, etc. As already mentioned, K_p is a quasi-logarithmic measure of field variation; an equivalent linear measure, defined for each value of K_p , is the planetary amplitude or A_p index.

Appendix E. Coordinate systems.

A variety of coordinate systems have been introduced in order to simplify the representation and interpretation of satellite measurements by taking advantage of some special symmetry or geometrical pattern thought to exist in the spatial distribution of the measured quantities. Most of them are earth-centered Cartesian systems with an axis aligned in a special direction, and it is convenient to introduce a general formalism for describing them in order to avoid frequent repetition of cumbersome verbal descriptions. Let \hat{a} and \hat{b} be two unit vectors along directions thought to be significant for the problem discussed; then, provided $\hat{a} \times \hat{b} \neq 0$, a coordinate system can be defined by writing the components (X_1, X_2, X_3) of a vector \vec{r} as

$$\begin{aligned} X_1 &= \vec{r} \cdot \hat{a} \\ X_2 &= \vec{r} \cdot \frac{\hat{a} \times \hat{b}}{(1 - (\hat{a} \cdot \hat{b})^2)^{\frac{1}{2}}} \\ X_3 &= \vec{r} \cdot \frac{\hat{a} \times (\hat{a} \times \hat{b})}{(1 - (\hat{a} \cdot \hat{b})^2)^{\frac{1}{2}}} = \vec{r} \cdot \frac{\hat{a}(\hat{a} \cdot \hat{b}) - \hat{b}}{(1 - (\hat{a} \cdot \hat{b})^2)^{\frac{1}{2}}} \end{aligned}$$

In words, the X_1 axis points along \hat{a} , the X_2 axis along the normal to the plane formed by \hat{a} and \hat{b} , and the X_3 axis completes a right-handed Cartesian coordinate system (the X_3 axis can also be described as along the direction at right angles to \hat{a} and as close as possible to \hat{b}). This coordinate system I will designate as (\hat{a}, \hat{b}) .

If $\hat{a} \cdot \hat{b} \neq 0$, a second coordinate system can be formed from \hat{a} and \hat{b} by interchanging them in the above equations, namely the coordinate system (\hat{b}, \hat{a}) (if $\hat{a} \cdot \hat{b} = 0$, (\hat{a}, \hat{b}) and (\hat{b}, \hat{a}) differ only by the labeling of the axes and are not to be considered distinct).

Among the directions that have been used to define coordinate systems are

- the earth's rotation axis \hat{R}
- the earth's magnetic dipole axis $\hat{\mu}$ (taken as pointing north)
- the direction to the sun \hat{S}
- the direction to the ecliptic pole \hat{E}

The standard celestial coordinates, used e.g. to describe satellite orbits are the set (\hat{R}, \hat{E}) , with the axes (X_1, X_2, X_3) conventionally labeled as (z, x, y) . Geomagnetic coordinates, $(\hat{\mu}, \hat{R})$ with axes labeled $(z, -y, x)$, are convenient for discussing phenomena governed by the earth's magnetic field and either corotating with the earth or having axial symmetry about the dipole axis. For phenomena governed primarily by the geomagnetic field but also having a diurnal variation, i.e., a dependence on angle from the sun-earth line, it is convenient to orient the X axis of geomagnetic coordinates toward the sun rather than along some direction fixed relative to the earth; these are coordinates $(\hat{\mu}, \hat{S})$, with axes labeled $(z, y, -x)$, which have been called in the text solar oriented geomagnetic coordinates and are often called more simply solar magnetic coordinates. In both of these systems the polar coordinates are used more often than the Cartesian.

At larger distances from the earth where the effects of the solar wind become significant, it becomes convenient to orient one axis along the direction of the solar wind flow, which for most purposes can be considered the same as the direction of the sun-earth line. The most widely used of such coordinates have been the solar ecliptic coordinates, (\hat{S}, \hat{E}) with axes labeled (x, y, z) . They are particularly useful for describing satellite orbits, since the precession of the orbit relative to the magnetosphere is especially simple in these coordinates, as already discussed in Chapter III A. More recently the solar magnetospheric coordinates, $(\hat{S}, \hat{\mu})$ with axes labeled (x, y, z) , have come into use; they were introduced by Ness (1965), who found that their $x - y$ plane approximately coincided with the magnetic neutral sheet in the tail of the magnetosphere (see Chapter IIIA).

A coordinate system much more sophisticated than the above simple, geometrically constructed systems are the B,L coordinates introduced by McIlwain (1961) for trapped radiation studies; a point in space is labeled by B, the magnitude of the magnetic field at it, and L, a quantity constructed from a model of the earth's main field (including non-dipole terms) such that points on a given shell on which trapped particles moving under conservation of the three adiabatic invariant remain all have the same L value; the third coordinate is usually the geomagnetic longitude. For a pure dipole field exactly and for the earth's real field approximately the L value of a point is the geocentric distance in the dipole's equatorial

plane to the field line passing through the point. With this interpretation, the L coordinate is often used as a convenient label for a field line and for projecting quantities onto the geomagnetic equatorial plane along the field lines, even in studies unrelated to trapped radiation, such as whistlers. Instead of B and L, an equivalent set R, Λ is occasionally used, defined by the relations valid for a dipole field

$$B = \frac{M}{R^3} \left(1 + 3 \sin^2 \Lambda\right)^{\frac{1}{2}}$$

$$R = R_e L \cos^2 \Lambda$$

where M = earth's dipole moment and $R_e = 1 \text{ Re. } \Lambda$, called the invariant latitude, is often used in place of L for high-latitude, low-altitude work; because of the low altitude, R is taken approximately as R_e and the relation between L and Λ simplifies to

$$L \cos^2 \Lambda = 1$$

Appendix F. Critique of the electron energy calculation of Freeman et al.

Freeman et al. (1963) consider the pass of Explorer 12 through the transition region during the initial phase of the magnetic storm on September 13, 1961. They first show, from lack of detectable signals in the magnetic spectrometers and Geiger tube, that only a small fraction of the particles detected by the CdS crystal could have energies above 30 kev. Then, citing arguments from the Chapman-Ferraro theory of magnetic storms, they equate the particle pressure in the transition region to the stress corresponding to the observed magnetic field discontinuity at the magnetopause, and write

$$NMV^2/2 = 5 \times 10^{-8} \text{ erg cm}^{-3}$$

Then they equate the energy flux of the particles to the value measured by CdS and write

$$NMV^3/8\pi = 50 \text{ ergs cm}^{-2} \text{ sec}^{-1} \text{ ster}^{-1}$$

Dividing the two expressions gives

$$V \sim 1.3 \times 10^{10} \text{ cm sec}^{-1}$$

corresponding to electrons of 56 kev; from this they obtain a density of 0.6 cm^{-3} and a flux of $10^{10} \text{ cm}^{-2} \text{ sec}^{-1}$.

As Freeman et al. recognize, this energy is in flagrant contradiction with their high energy detector results; but they remark that V depends on the CdS reading, its solid angle Ω , and the magnetic field discontinuity, and then, in their words

"Since there are clearly uncertainties by factors of the order of unity in each of the three essential quantities (especially Ω), it is evident that a rms particle velocity as low as

$$V \sim 3 \times 10^9 \text{ cm sec}^{-1}$$

can be tolerated."

This gives an electron energy of 2.6 kev, a density of 10 cm^{-3} , and a flux of $3 \times 10^{10} \text{ cm}^{-2} \text{ sec}^{-1}$, which is considered "consistent with all observational evidence".

Nothing more is said about how the electron energy was reduced from 56 to 2.6 kev. It is clear, however, that since one of the equations is

$$\text{energy flux} \sim NV^3$$

and the value of V was reduced from 1.3×10^{10} to 3×10^9 while N was increased from 0.6 to 10, the essential step in the change is a reduction in the assumed energy flux by a factor of

$$\left(\frac{1.3 \times 10^{10}}{3 \times 10^9} \right)^3 \times \frac{0.6}{10} \approx 5$$

The energy flux is proportional to the CdS counting rate divided by its solid angle; since no source of an error of a factor of 5 in the counting rate is apparent, it must be concluded that Freeman et al. can obtain a consistent set of results only by increasing the assumed solid angle of the CdS detector by a factor of 5. The ease with which this step is taken does not increase one's confidence in the numbers obtained from this detector.

Table I. Energy Windows Of The Detector

Channel	1	2	3	4
V_1 (ev)	549	317	181	126
V_2	695	410	240	168
V_3	1653	942	501	315
V_4	1757	1015	552	352
a_u	0.30	0.37	0.45	0.37
a_l	0.19	0.30	0.37	0.30

Table II. Numerical Coefficients For Various Quantities
Related To The Model Distribution Function

K	ϕ / Nw_0	U/NE ₀	ϕ_U / E_0
2	1.80	6	-
2.5	1.59	3.75	10
3	1.47	3	6
3.5	1.40	2.6375	4.67
4	1.36	2.4	4
4.5	1.33	2.25	3.6
5	1.30	2.14	3.33
5.5	1.28	2.0625	3.14
6	1.27	2	3
6.5	1.25	1.95	2.88
∞	1.13	1.5	2

Table III. Positions And Times For Spectra In Fig. 20

Spectrum number	Orbit	Date 1964	U.T.	Distance (RE)	SEP angle (degrees)
1	17 out	10/18	1630	22.8	100
2	"	10/19	0030	24.2	104
3	18 out	10/20	2025	16.1	88
4	"	"	2315	18.4	91
5	"	10/21	0203	21.0	95
6	18 in	"	1820	24.3	104
7	20 out	10/26	0215	14.2	82
8	"	"	0530	17.0	86
9	"	"	1830	23.4	95
10	22 out	11/01	0305	23.4	92
11	22 in	"	1530	23.8	98
12	"	"	1610	23.7	98
13	"	"	1705	23.5	99
14	"	"	1909	23.0	100
15	"	"	2045	22.5	101
16	23 in	11/04	0300	24.3	93
17	24 out	11/05	1925	15.2	77
18	25 in	11/09	1230	24.1	90
19	"	"	1400	24.0	91

Table III. (Continued)

Spectrum number	Orbit	Date 1964	U.T.	Distance (RE)	SEP angle (degrees)
20	26 out	11/11	1530	22.4	82
21	"	11/12	0125	24.2	86
22	26 in	"	0230	24.3	87
23	27 in	11/15	1028	19.9	92
24	"	"	1048	19.8	93
25	"	"	1450	16.9	96
26	"	"	1525	16.5	96
27	"	"	1700	15.1	98
28	28 out	11/16	1355	17.3	73
29	"	"	1442	17.9	73
30	28 in	11/17	1055	24.2	83
31	"	"	1537	23.7	85
32	37 in	12/12	0314	19.4	69
33	"	"	0330	19.3	69

Table IV. Electron Spectra In The Magnetosphere

Orbit (inbound)	Date 1964	U.T.	E_0 ev	N cm^{-3}	ϕ $10^9 \text{cm}^{-2} \text{sec}^{-1}$	K
10	10/01	1612	300-350	2.3	3.6	3
11	10/03	1123	300-350	0.9	1.1	6
		1525	250-270	1.5	2.4	3
		1823	60-80	7-4	3-4	3
		1832	30-42	20-10	5-8	5.5
		1843	70-80	8-6	4-5	2.5
		1905	25-45	35-12	7-14	3.5
		1945	40-50	13-8	4-5	6
		2208	70	20-25	17	7
15	10/14	0715	440	0.74	1.2	4
		1100	295	1.1	1.4	4
		1115	68	5.2	3.3	4
		1200	220-240	2.1	2.1	6
		1620	400-600	0.8	1.2-1.5	4
		1800	280	0.9	1.2	3.5
		1845	210-220	1.9	2.4	5
		2012	280-300	1.3	1.7	4
		2055	280-300	1.1	1.5	4
16	10/17	0320	310	1.0	1.4	5
		0410	310	1.3	2.1	4

Table IV. (Continued)

Orbit (inbound)	Date 1964	U.T.	E_0 ev	N cm^{-3}	ϕ $10^9 \text{cm}^{-2} \text{sec}^{-1}$	K
16	10/17	0539	140-160	2.1-1.9	1.6	6
		0546	190-210	1.9-1.7	1.6	6.5
		0910	370	1.6	2.3	5.5
		1115	540-710	0.9-0.8	3.0	-
		1221	370-480	1.0-0.8	1.4	(4)
		1255	460-600	0.8	1.4	-
		1420	600-700	1.0-0.9	1.8	-
		1535	440-480	1.2	2.5	3
17	10/20	0100	170	3.4	1.3	5
		0640	350-420	0.8	1.4	3
		0650	150-190	1.1	1.3	4
		0745	70-110	2.6-1.6	1.1-1.4	6
21	10/30	2005	410	0.8	1.2	4.5
22	11/2	0820	405	0.9	1.7	3
		0845	440-540	1.5-1.4	2.2	6
		1000	480	1.0	1.5	6
		1110	340-380	1.4	1.7	5
		1147	500-580	0.5	0.8	6
		1235	320	0.7	1.2	3
		1420	160-190	1.3-1.1	1.0	6
		1525	100-140	2.0-1.7	1.4	6

Table IV. (Continued)

Orbit (inbound)	Date 1964	U.T.	E_0 ev	N cm^{-3}	ϕ $10^9 \text{cm}^{-2} \text{sec}^{-1}$	K
23	11/4	2337	74-80	6.8	3.7	4
		2353	150-210	2.8-2.5	2.3-2.8	6
	11/5	0005	210-350	2.1-1.6	1.3-1.7	6
		0030	235	1.7	1.8	6
		0250	310-350	0.7	1.1	3
		0350	580-740	0.9-0.8	1.7	-
		0400	400-500	0.9-0.8	1.2-1.4	5
		0420	410-480	0.7	1.4	3
24	11/7	1900	260	1.7	2.1	4
25	11/10	0805	350-430	0.6-0.5	1.0	3
27	11/15	1818	265	4.4	6.6	3
		1827	280-350	3.5	5.9	3
		1957	410	2.0	3.6	3
		2220	210	7.0	7.4	5
		2236	170-240	8-7	6.4-7.0	6.5
29	11/10	0420	320-400	1.3	2.4	3
30	11/23	2020	290	0.7	1.1	3
35	12/7	0428	280	3.4	4.3	4

REFERENCES

- Anderson, K.A., H.K.Harris, and R.J. Paoli, Energetic electron fluxes in and beyond the earth's outer magnetosphere, J. Geophys. Res. 70, 1039 (1965).
- Anderson, K.A., Energetic electron fluxes in the tail of the geomagnetic field, J. Geophys. Res. 70, 4741 (1965).
- Anderson, K.A., and N.F. Ness, Correlation of magnetic fields and energetic electrons on the IMP 1 satellite, J. Geophys. Res. 71, 3705 (1966).
- Angerami, J.J., and D.L. Carpenter, Whistler studies of the plasmopause in the magnetosphere, 2, Electron density and total tube electron content near the knee in magnetospheric ionization, J. Geophys. Res. 71, 711 (1966).
- Asbridge, J.R., S.J. Bame, H.E. Felthouser, and I.B. Strong, Electrons in the transition region between the bow shock and the magnetosphere, paper presented at the 47th annual meeting of the A.G.U., April 1966.
- Axford, W.I., and C.O. Hines, A unifying theory of high-latitude geophysical phenomena and geomagnetic storms, Canadian J. Phys. 39, 1433 (1961).
- Axford, W.I., The interaction between the solar wind and the earth's magnetosphere, J. Geophys. Res. 67, 3791 (1962).
- Axford, W.I., H.F. Petschek, and G.L. Siscoe, Tail of the magnetosphere, J. Geophys. Res. 70, 1231 (1965).

Axford, W.I., Magnetic storm effects associated with the tail of the magnetosphere, to be published in Proceedings of the ESRO conference on the Magnetosphere held in Stockholm, November 1965; also Cornell - Sydney University Astronomy Center report CSUAC 32 (1966).

Bame, S.J., J.R. Asbridge, H.E. Felthouser, R.A. Olson, and I.B. Strong, Electrons in the plasma sheet of the earth's magnetic tail, Phys. Rev. Letters 16, 138 (1966a).

Bame, S.J., J.R. Asbridge, H.E. Felthouser, E.W. Hones, Jr., and I.B. Strong, Characteristics of the electrons in the plasma sheet of the magnetospheric tail, paper presented at 47th annual meeting of the A.G.U., April 1966b.

Beard, D.B., The solar wind geomagnetic field boundary, Rev. Geophys. 2, 335 (1964).

Bernstein, W., R.W. Fredricks, and F.L. Scarf, A model for a broad disordered transition between the solar wind and the magnetosphere, J. Geophys. Res. 69, 1201 (1964).

Biermann, L., Kometenschweife und solare Korpuscular strahlung, Z. Astrophys. 29, 274 (1951).

Block, L.P., On the distribution of electric fields in the magnetosphere, J. Geophys. Res. 71, 855 (1966).

Bonetti, A., H.S. Bridge, A.J. Lazarus, B. Rossi, and F. Scherb, Explorer 10 Plasma Measurements, J. Geophys. Res. 68, 4017 (1963).

- Bridge, H.S., A.Egidi, A. Lazarus, E.Lyon, and L. Jacobson,
Preliminary results of Plasma Measurements on IMP-A, Space
Research V, King-Hele et al, ed. (North-Holland Publ.Co.,
Amsterdam) p. 969, 1965.
- Bridge, H.S., A. Lazarus, and J. Davis, Preliminary Results from the
Pioneer 6 MIT Plasma Experiment, paper presented at 47th annual
meeting of the A.G.U., April 1966.
- Brown, R.R., Electron precipitation in the auroral zone, Space Sci.
Rev. 5, 311 (1966).
- Cahill, L.J. and P.G. Amazeen, The boundary of the geomagnetic field,
J. Geophys. Res. 68, 1835 (1963).
- Cahill, L.J. and V.L. Patel, The boundary of the geomagnetic field,
August to November, 1961, Univ. of New Hampshire rept. UNH-
64-11, 1966.
- Carpenter, D.L., and R.L. Smith, Whistler measurements of electron
density in the magnetosphere, Rev. Geophys. 2, 415 (1964).
- Carpenter, D.L., Whistler studies of the plasmopause in the magnetosphere,
1, Temporal variations in the position of the knee and some
evidence on plasma motions near the knee, J. Geophys. Res.
71, 693 (1966).
- Chapman, S., and V.C.A. Ferraro, A new theory on magnetic storms,
Terrestrial Magnetism and Atmospheric Elec., 36, 77, 171 (1931);
37, 147, 421 (1932); 38, 79 (1933).
- Coleman, P.J.Jr., Irregularities in the Interplanetary Magnetic Field,
Ph.D. thesis, U.C.L.A. 1966.

- Davis, T.N., The aurora, in Introduction to Space Science, W.Hess ed.
(Gordon and Breach, N.Y.,1965) p. 205.
- Dessler, A.J., Length of magnetospheric tail, J. Geophys. Res. 69,
3913 (1964).
- Dessler, A.J., and R.D. Juday, Configuration of auroral radiation in
space, Planet. Space Sci., 13, 63 (1965).
- Dessler, A.J., and F.C. Michel, Plasma in the geomagnetic tail, J. Geophys.
Res. 71, 1421 (1966).
- Dessler, A.J., Discussion of letter by J.A. 'Van Allen, Further
remarks on the absence of a very extended magnetic tail',
J. Geophys. Res. 71, 2408 (1966).
- Dungey, J.W., Interplanetary magnetic field and the auroral zones,
Phys. Rev. Letters, 6, 47 (1961).
- Dungey, J.W., The length of the magnetospheric tail, J. Geophys.
Res. 70, 1753 (1965).
- Eshleman and others, The interplanetary electron number density from
preliminary analysis of the Pioneer 6 radio propagation exper-
iment, J. Geophys. Res. 71, 3325 (1966).
- Evans, J.E., and A.E. Belon, Preliminary results from coordinated
measurements of auroras, I G Bulletin 77 (Trans. A.G.U. 44,
1073) 1963.
- Fan, C.Y., G. Gloeckler and J.A. Simpson, Acceleration of electrons
near the earth's bow shock and beyond, J. Geophys. Res. 71,
1837 (1966).

- Farley, T.A., The growth of our knowledge of the earth's outer radiation belt, Rev. Geophys. 1, 3 (1963).
- Frank, L.A., J.A. Van Allen, and E. Macagno, Charged-particle observations in the earth's outer magnetosphere, J. Geophys. Res. 68, 3543 (1963).
- Frank, L.A., J.A. Van Allen, and J.D. Craven, Large diurnal variations of geomagnetically trapped and of precipitated electrons observed at low altitudes, J. Geophys. Res. 69, 3155 (1964).
- Frank, L.A., and J.A. Van Allen, Measurements of energetic electrons in the vicinity of the sunward magnetospheric boundary with Explorer 14, J. Geophys. Res. 69, 4923 (1964).
- Frank, L.A., A survey of electrons > 40 kev beyond 5 earth radii with Explorer 14, J. Geophys. Res. 70, 1593 (1965).
- Fredricks, R.W., F.L. Scarf, and W. Bernstein, Numerical estimates of superthermal electron production by ion acoustic waves in the transition region, J. Geophys. Res. 70, 21 (1965).
- Freeman, J.W., J.A. Van Allen, and L.J. Cahill, Explorer 12 observations of the magnetospheric boundary and the associated solar plasma on September 13, 1961, J. Geophys. Res. 68, 2121 (1963).
- Freeman, J.W., The morphology of the electron distribution in the outer radiation zone and near the magnetospheric boundary as observed by Explorer 12, J. Geophys. Res. 69, 1691 (1964).
- Fritz, T.A., and D.A. Gurnett, Diurnal and latitudinal effects observed for 10-kev electrons at low satellite altitudes, J. Geophys. Res. 70, 2485 (1965).
- Gold, T., Motions in the magnetosphere of the earth, J. Geophys. Res. 64, 1219 (1959).

- Gringauz, K.I., V.V. Bezrukikh, V.D. Ozerov, and R.E. Rybchinskii,
A study of the interplanetary ionized gas, high energy electrons,
and corpuscular radiation from the sun by means of the three-
electrode trap for charged particles on the second soviet cosmic
rocket, Dokl. Akad. Nauk SSSR 131, 1301 (1960a)(English trans-
lation: Soviet Phys., Dokl. 5, 361, 1961).
- Gringauz, K.I., V.G. Kurt, V.I. Moroz, and I.S. Shklovskii, Results of
observations of charge particles observed out to $R = 100,000$ km
with the aid of charged-particle traps on soviet space rockets,
Astron. Zh. 37, 716 (1960b) (English translation: Soviet Astron.
A.J., 4, 680, 1961).
- Gringauz, K.I. and S.M. Rytov, Relationship between the results of
measurements by charged particle traps on the soviet cosmic
rockets and magnetic field measurements on the American satellite
Explorer 6 and rocket Pioneer 5, Dokl, Akad. Nauk SSSR 135, 48
(1960) (English translation: Soviet Phys., Dokl. 5, 1225, 1961).
- Gringauz, K.I., Remarks on papers by J.W. Freeman, J.A. Van Allen, and
L.J. Cahill, 'Explorer 12 observations of the Magnetospheric
Boundary and the Associated Solar Plasma on September 13, 1961',
and by L.A. Frank, J.A. Van Allen, and E. Macagno, 'Charged-
Particle Observations in the Earth's Outer Magnetosphere',
J. Geophys. Res. 69, 1007 (1964).
- Gringauz, K.I., V.V. Bezrukikh, L.S. Musatov, R.E. Rybchinsky, and S.M.
Sheronova, Measurements made in the earth's magnetosphere by means
of charged particle traps aboard the Mars 1 probe, Space Res. IV,

- P.Muller ed. (North-Holland Publ. Co., Amsterdam) p.621, 1964.
- Helliwell, R.A., Whistlers and Related Ionospheric Phenomena (Stanford University Press, Stanford, California) 1965.
- Heppner, J.P., N.F. Ness, C.S. Scarce, and T.L. Skillman, Explorer 10 magnetic field measurements, J. Geophys. Res. 68, 1 (1963).
- Heppner, J.P., Recent measurements of the magnetic field in the outer magnetosphere and boundary regions, paper presented at ESRO colloquium on Auroral and Associated Magnetospheric Phenomena at Very High Latitudes, Stockholm, Swede, November 1965; Goddard Space Flight Center report X-612-65-490 (1965).
- Holzer, R.E., M.G.McLeod, and E.J.Smith, Preliminary results from the Ogo 1 search coil magnetometer: boundary positions and magnetic noise spectra, J. Geophys. Res. 71, 1481 (1966).
- Howard, H.T., V.R. Eshleman, G.H. Barry, and R.B. Fenwick, Radar measurements of the cislunar electron content, J. Geophys. Res. 70, 4357 (1965).
- I G Bulletin No. 92, OGO-I, First US Orbiting Geophysical Observatory, Trans. A.G.U. 46, 326 (1965).
- Jokipii, J.R. and L. Davis, Acceleration of electrons near the earth's bow shock, phys. Rev. Letters 13, 739 (1964).
- Jokipii, J.R. A model of Fermi acceleration at shock fronts with an application to the earth's bow shock, Astrophys. J. 143, (1966a).
- Jokipii, J.R., Diffusion and convection of energetic electrons behind the earth's bow shock, J. Geophys. Res. 71, 3173 (1966b).
- Kellogg, P.J., Flow of plasma around the earth, J. Geophys. Res. 67, 3805 (1962).

- Kellogg, P.J., Structure of the shock wave around the earth, paper presented at Midwest Cosmic Ray Colloquium, Denver, Colorado, April 3-4, 1964.
- Kennel, C.F., and H.E. Petschek, Limit on stably trapped particle fluxes, J. Geophys. Res. 71, 1 (1966).
- Konradi, A., Electron and proton fluxes in the tail of the magnetosphere, J. Geophys. Res. 71, 2317 (1966).
- Levy, R.H., H.E. Petschek, and G.L. Siscoe, Aerodynamic aspects of magnetospheric flow, A.I.A.A. Journal 2, 2065 (1964).
- Liemohn, H.B., Partial electron velocity spectrums from cyclotron absorption of whistler power, J. Geophys. Res. 70, 4817 (1965).
- Lincoln, J.V., Geomagnetic and solar data, J. Geophys. Res. 70, 2239 (1965a); 70, 4963 (1965b).
- Lindemann, F.A., Note on the theory of magnetic storms, Phil. Mag. 38, 669 (1919).
- Lyon, E.F., A study of the Interplanetary Plasma, Ph.D. thesis, M.I.T. (1966).
- McDiarmid, I.B., and J.R. Burrows, High-latitude boundary of the outer radiation zone at 1000 km, Can. J. Phys. 42, 616, 1964.
- McDiarmid, I.B., and J.R. Burrows, Electron fluxes at 1000 kilometers associated with the tail of the magnetosphere, J. Geophys. Res. 70, 3031 (1965).
- McIlwain, C.E., Coordinates for mapping the distribution of magnetically trapped particles, J. Geophys. Res. 66, 3681 (1961).
- McKay, K.G., Secondary electron emission, Adv. Electr. 1, 65 (1948).
- Maehlum, B., and B.J. O'Brien, Study of energetic electrons and their relationship to auroral absorption of radio waves, J. Geophys. Res. 68, 997 (1963).

- Mead, G.D., and D.B. Beard, The shape of the geomagnetic field solar wind boundary, *J. Geophys. Res.* 69, 1169 (1964).
- Medved, D.B., and Y.E. Strausser, Kinetic ejection of electrons from solids, *Adv. Electr. and Electron Phys.* 21, 101 (1965).
- Michel, F.C., and A.J. Dessler, Physical significance of inhomogeneities in polar cap absorption events, *J. Geophys. Res.* 70, 4305 (1965).
- Midgley, J.E. and L. Davis, Jr., Calculation by a moment technique of the perturbation of the geomagnetic field by the solar wind, *J. Geophys. Res.* 68, 5111 (1963).
- Montgomery, M.D., S. Singer, J.P. Conner, and E.E. Stogsdill, Spatial distribution, energy spectra, and time variations of energetic electrons ($E > 50$ keV) at 17.7 earth radii, *Phys. Rev. Letters* 14, 209 (1965).
- Moreno, G., S. Olbert, and G.L. Pai, to be published (1966).
- Muldrew, D.B., F-layer ionization troughs deduced from Alouette data, *J. Geophys. Res.* 70, 2635 (1965).
- Murayama, T., Spatial distribution of high-energy electrons in the geomagnetic tail, paper presented at 47th annual meeting of the A.G.U., April 1966.
- Ness, N.F., C.S. Scarce, and J.B. Seek, Initial results of the Imp 1 magnetic field experiment, *J. Geophys. Res.* 69, 3531 (1964).
- Ness, N.F. The earth's magnetic tail, *J. Geophys. Res.* 70, 2989 (1965).
- Ness, N.F., and D.J. Williams, Correlated magnetic tail and radiation belt observations, *J. Geophys. Res.* 71, 322 (1966).

- Ness, N.F., C.S. Scarce, and J.B. Seek, The Imp 3 magnetic field experiment, paper presented at 47th annual meeting of the A.G.U., April 1966.
- Neugebauer, M., and C.W. Snyder, Mariner - 2 Observations of the solar wind I. Average Properties, submitted to J. Geophys. Res. 1966.
- O'Brien, B.J., Review of studies of trapped radiation with satellite borne apparatus, Space Sci. Rev. 1, 415 (1962-63).
- O'Brien, B.J., High-latitude geophysical studies with satellite Injun 3-3. Precipitation of electrons into the atmosphere, J. Geophys. Res. 69, 13 (1964).
- O'Brien, B.J., and H. Taylor, High-latitude geophysical studies with satellite Injun 3 - 4. Auroras and their excitation, J. Geophys. Res. 69, 45 (1964).
- Parker, E.N., Dynamics of the interplanetary gas and magnetic fields, Ap. J. 128, 664 (1958a).
- Parker, E.N., Suprathermal particles. III. Electrons, Phys. Rev. 112, 1429 (1958b).
- Parker, E.N., Interplanetary Dynamical Processes (Interscience Publishers, N.Y.) 1963.
- Rosen, A., The radiation belt boundary near solar cycle maximum as determined from the trapping of energetic electrons, J. Geophys. Res. 70, 4793 (1965).
- Scarf, F.L., W. Bernstein, and R.W. Fredricks, Electron acceleration and plasma instabilities in the transition region, J. Geophys. Res. 70, 9 (1965).

- Serbu, G.P., Results from the IMP I retarding potential analyzer, Space Research V, King-Hele et al., ed. (North-Holland Publishing Company, Amsterdam) p. 564 (1965).
- Serbu, G.P., and E.J.R. Maier, Low-energy electrons measured on IMP 2, J. Geophys. Res. 71, 3755 (1966).
- Serlemitsos, P., Low energy electrons in the magnetosphere, Ph. D. thesis, University of Maryland; also Godard Space Flight Center Rept. X-611-65-378 (1965).
- Serlemitsos, P., Low-energy electrons in the dark magnetosphere, J. Geophys. Res. 71, 61 (1966).
- Sharp, G.W., Midlatitude trough in the night ionosphere, J. Geophys. Res. 71, 1345 (1966).
- Sharp, R.D., J.E. Evans, W.L. Imhof, R.G. Johnson, J.B. Reagan, and R.V. Smith, Satellite measurements of low-energy electrons in the northern auroral zone, J. Geophys. Res. 69, 2721 (1964).
- Sharp, R.D., J.B. Reagan, S.R. Salisbury, and L.F. Smith, Direct measurement of auroral electrons of low energies, J. Geophys. Res. 70, 2119 (1965).
- Shen, C.S., and C.C. Chang, Fermi acceleration of charged particles in transition region beyond magnetosphere, J. Geophys. Res. 71, 241 (1966).
- Singer, S., J.P. Conner, and E.E. Stogsdill, The spatial distribution of energetic electrons near the dawn meridian at 17 earth radii, paper presented at 47th annual meeting of the A.G.U., April 1966.

- Slutz, R.J., and J.R. Winkelman, Shape of the magnetospheric boundary under solar wind pressure, *J. Geophys. Res.* 69, 4933 (1964).
- Snyder, C.W., M. Neugebauer, and U.R. Rao, The solar wind velocity and its correlation with cosmic ray variations and with solar and geomagnetic activity *J. Geophys. Res.* 68, 6361 (1963).
- Spreiter, J.R. and W.P. Jones, On the effect of a weak interplanetary field on the interaction between the solar wind and the geomagnetic field, *J. Geophys. Res.* 68, 3555 (1963).
- Spreiter, J.R., A.L. Summers, and A.Y. Alksne, Hydromagnetic flow around the magnetosphere, *Planet. Space Sci.* 14, 223 (1966).
- Strong, I.B., J.R. Asbridge, S.J. Bame, H.H. Heckman, and A.J. Hundhauser, Measurements of Proton Temperatures in the Solar Wind, *Phys. Rev. Let.* 16, 631 (1966).
- Sugiura, M., and J.P. Heppner, The earth's magnetic field, in Introduction to Space Science, W. Hess ed. (Gordon and Breach, N.Y., 1965) p.5.
- Taylor, H.A., Jr., H.C. Brinton, and C.R. Smith, Positive ion composition in the magnetoionosphere obtained from the Ogo-A satellite, *J. Geophys. Res.* 70, 5769 (1965).
- Van Allen, J.A., Remarks on accompanying letter by K.I. Gringauz, *J. Geophys. Res.* 69, 1011 (1964).
- Van Allen, J.A., Further remarks on the absence of a very extended magnetospheric tail, *J. Geophys. Res.* 71, 2406 (1966).
- Vernov, S.N., E.V. Gortchatov, S.N. Kuznetsov, Yu. I. Logatchev, E.N. Sosnovets, B.A. Tverskoy, and A.E. Chudakov, Earth's radiation belt, preprint, 1966.

- White, R.S., The earth's radiation belts, preprint, April 1966.
- Wilcox, J.M., and N.F. Ness, Quasi-Stationary Corotating Structure in the Interplanetary Medium, J. Geophys. Res. 70, 5793 (1965).
- Williams, D.J., and W.F. Palmer, Distortions in the radiation cavity as measured by an 1100-kilometer polar orbiting satellite, J. Geophys. Res. 70, 557 (1965).
- Williams, D.J., and G.D. Mead, Nightside magnetosphere configuration as obtained from trapped electrons at 1100 kilometers, J. Geophys. Res. 70, 3017 (1965).
- Williams, D.J., and N.F. Ness, Simultaneous trapped electron and magnetic tail field observations, Goddard Space Flight Center rept. X-611-66-264 (1966).
- Wolfe, J.H., R.W. Silva, and M.A. Myers, Observations of the Solar Wind during the Flight of Imp 1, J. Geophys. Res. 71, 1319 (1966).
- Yoh, P., H.T. Howard, B.B. Lusigran, and V.R. Eshleman, Lunar radar measurements of the earth's magnetospheric wake, J. Geophys. Res. 71, 189 (1966).

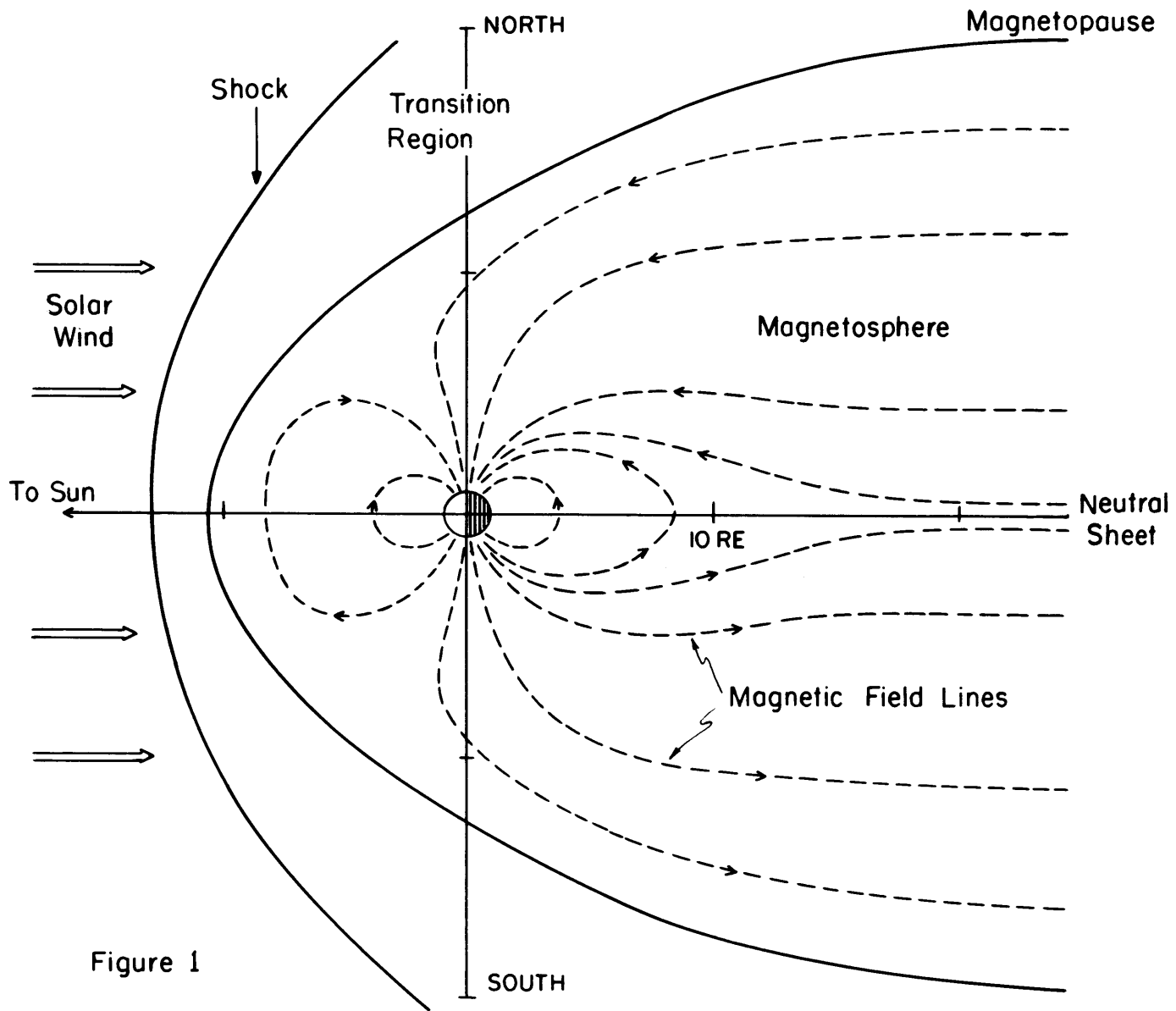


Figure 1

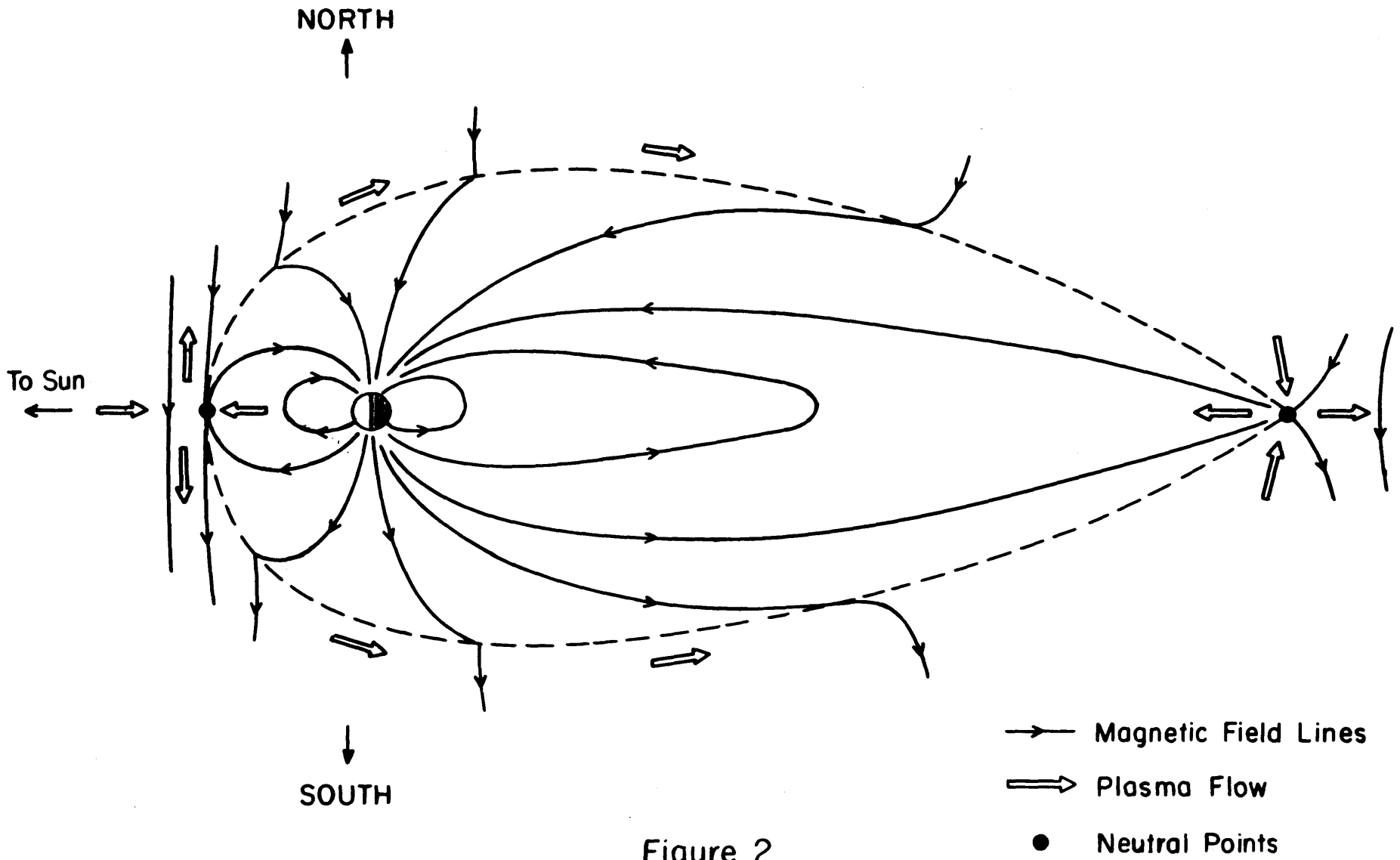


Figure 2

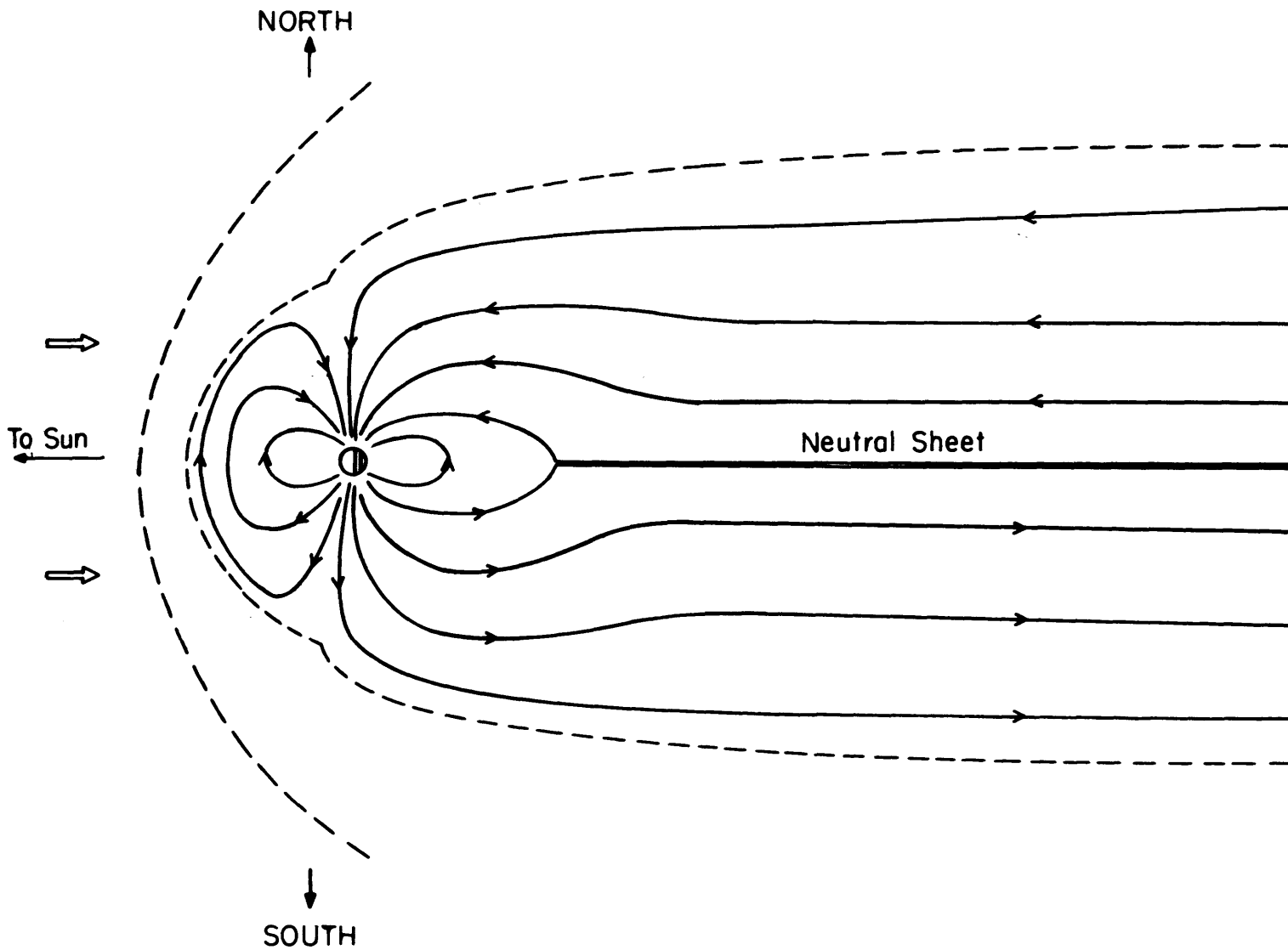


Figure 3

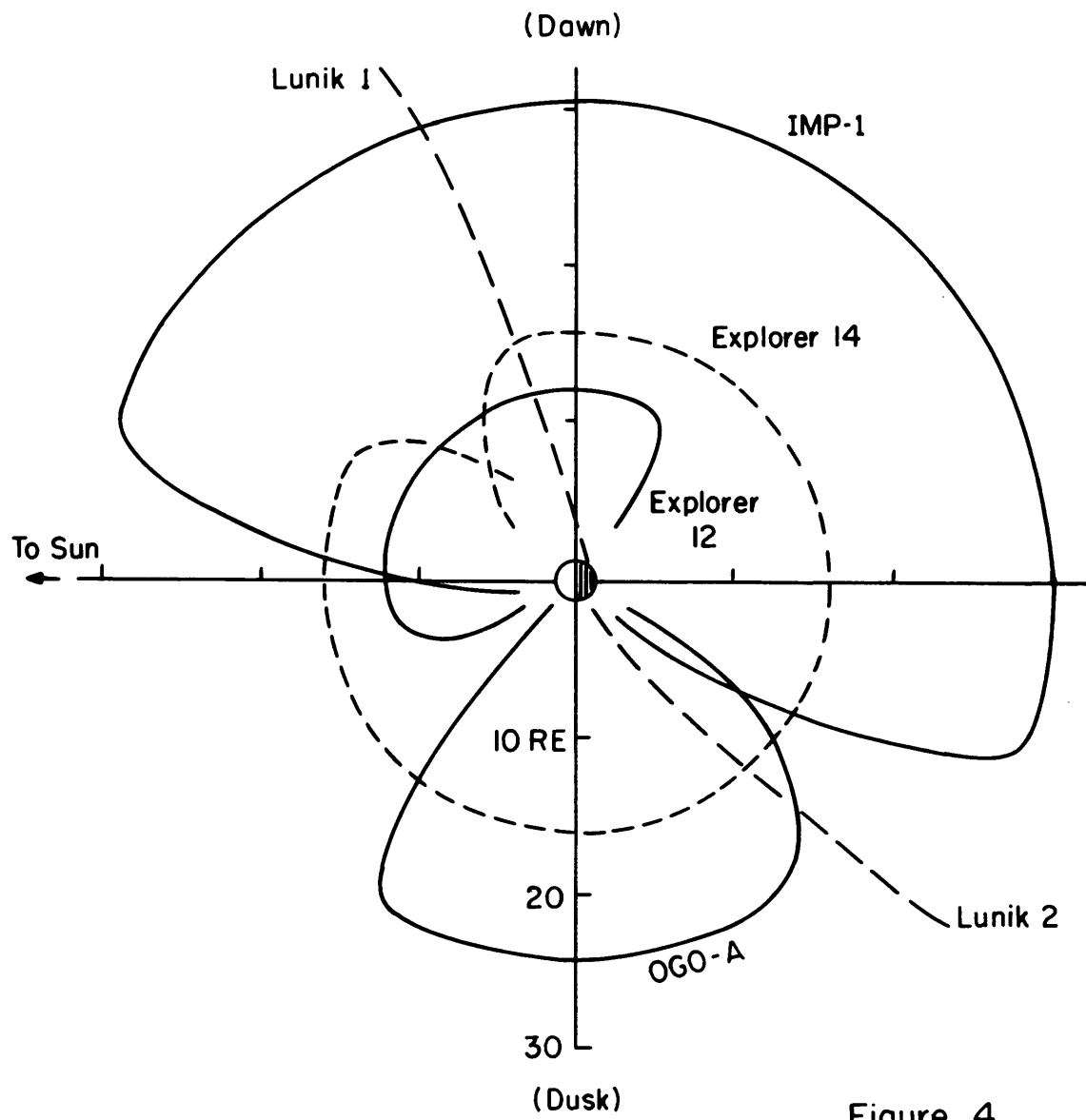


Figure 4

- 133 -

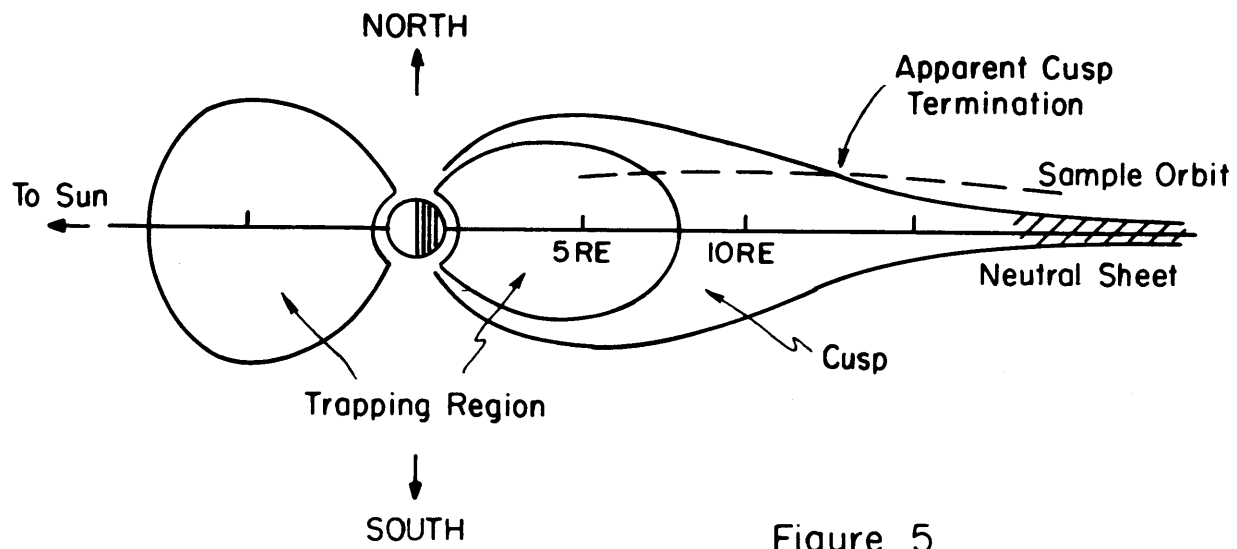
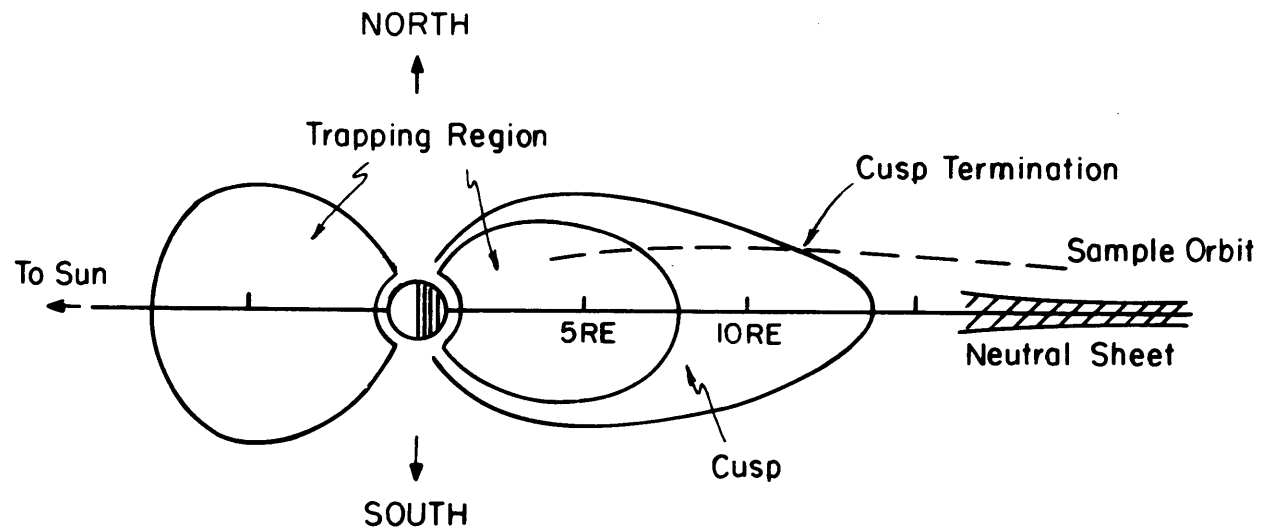


Figure 5

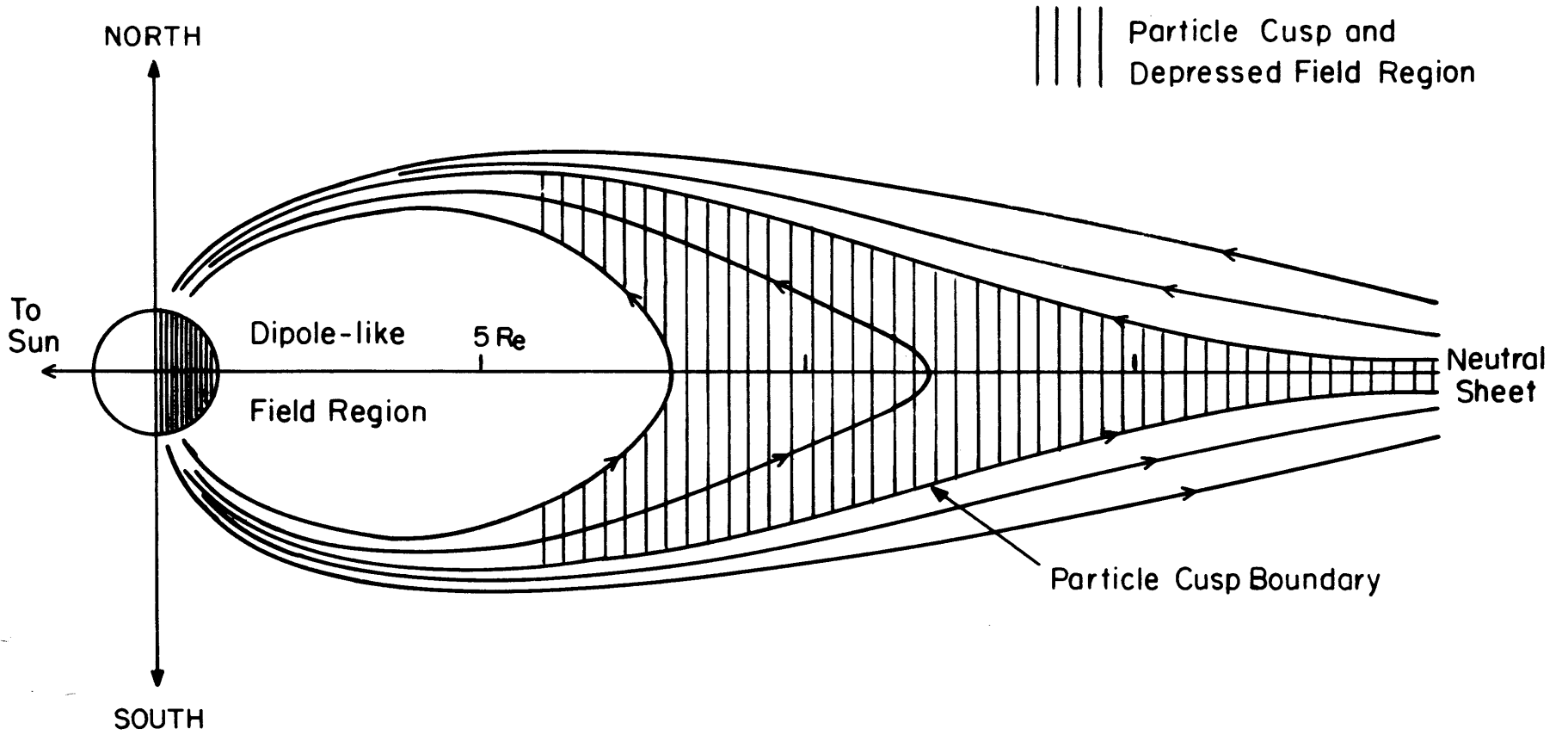


Figure 6

-135-

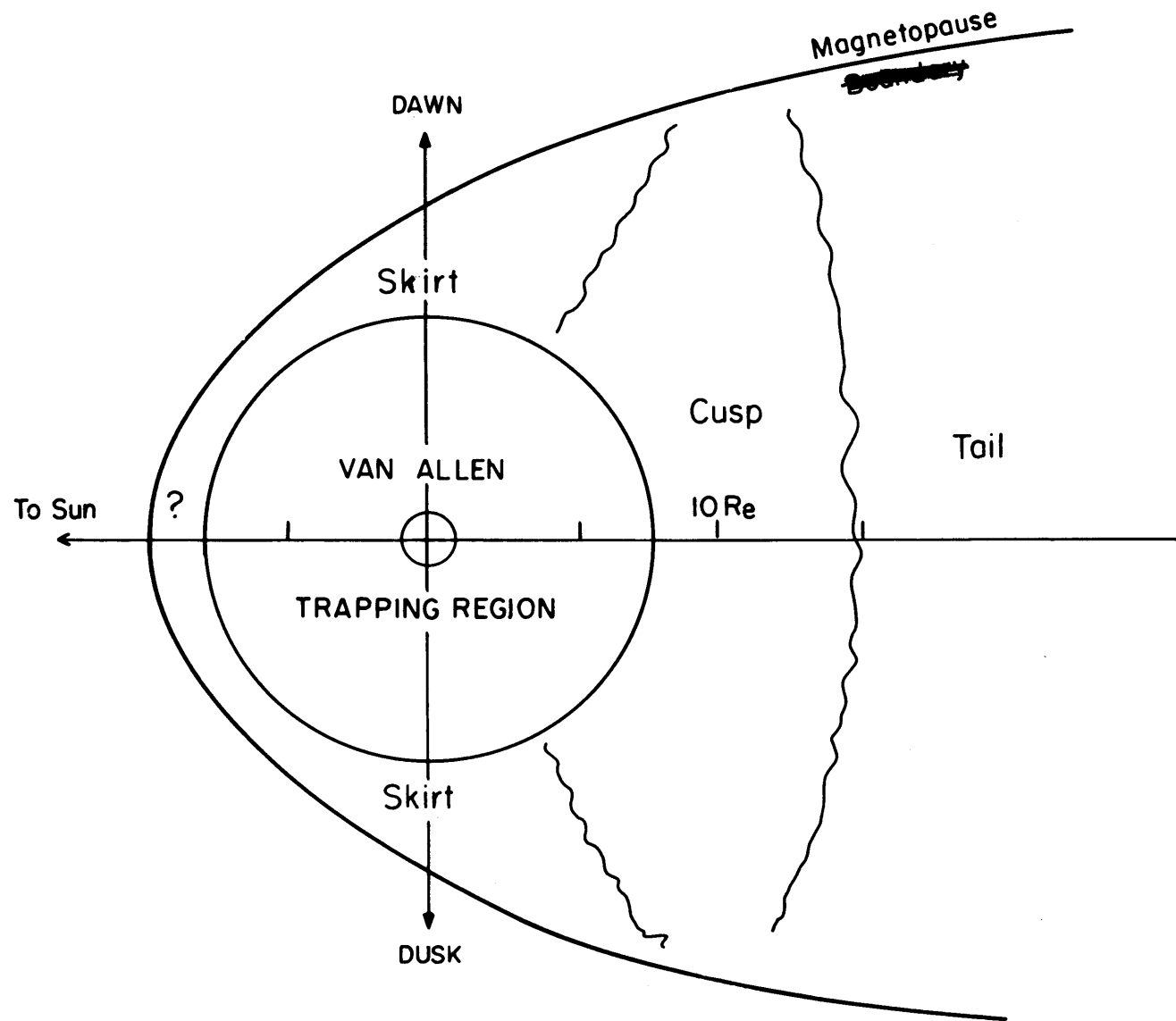


Figure 7

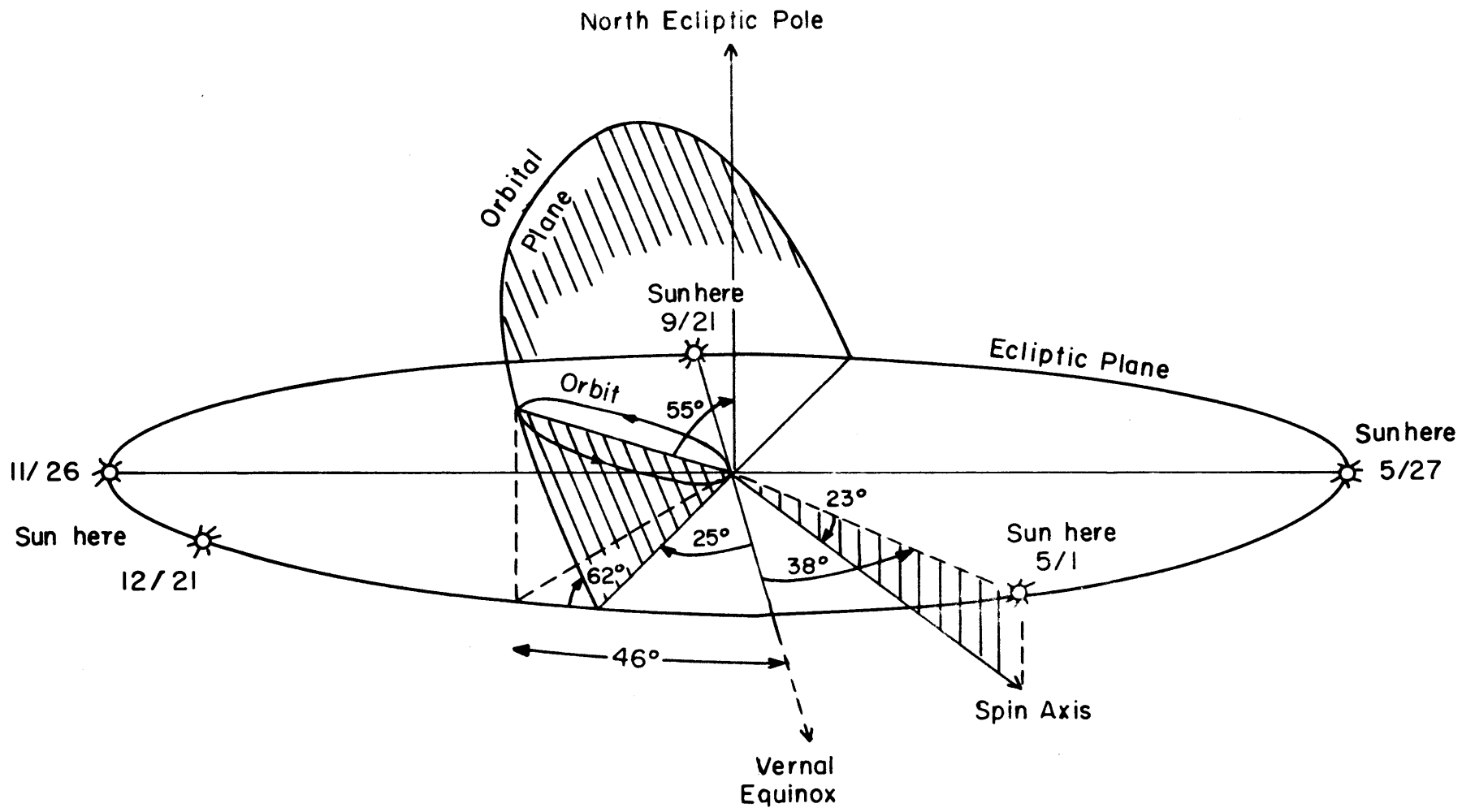


Figure 8

- 137 -

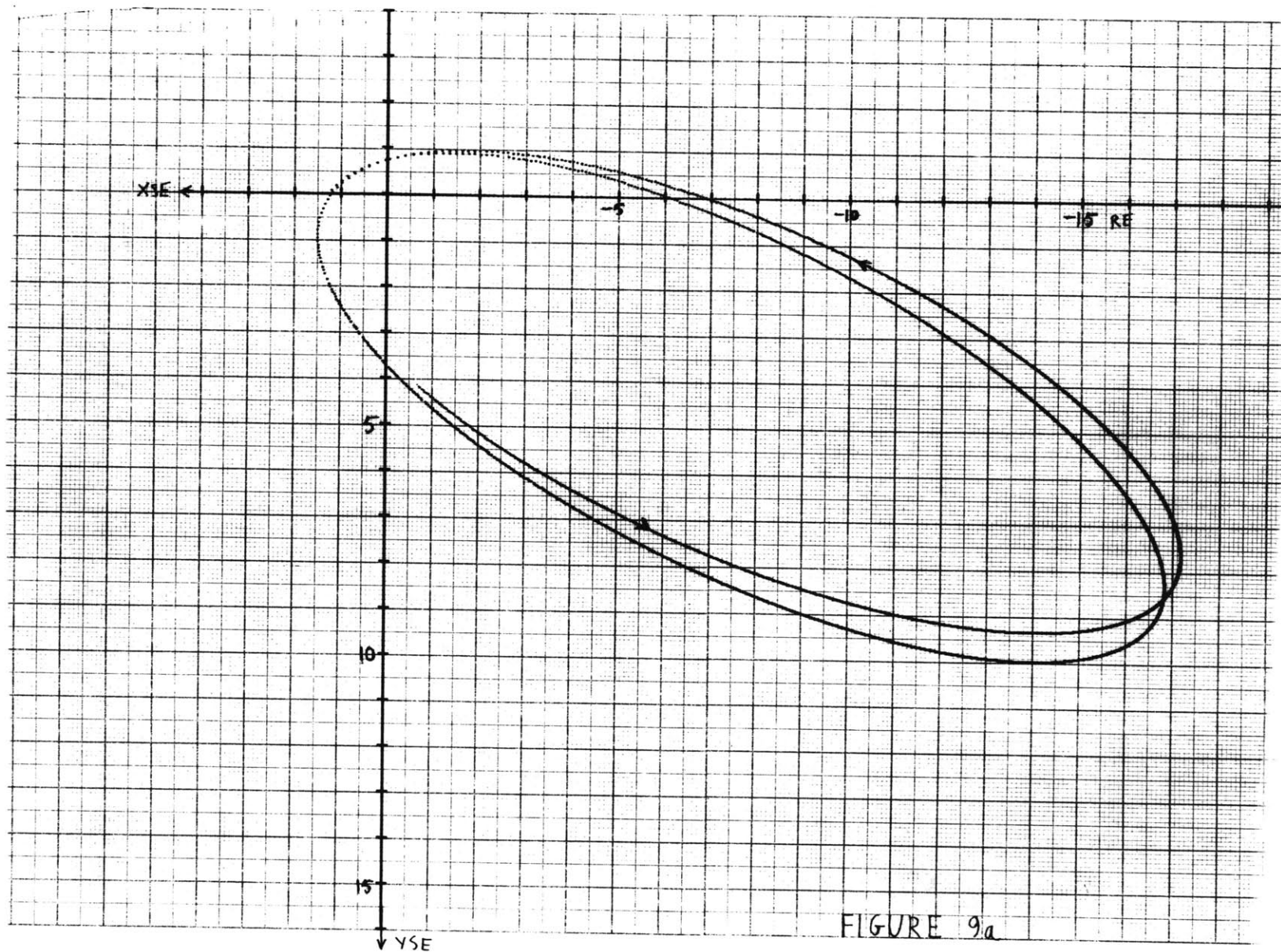


FIGURE 9a

- 138 -

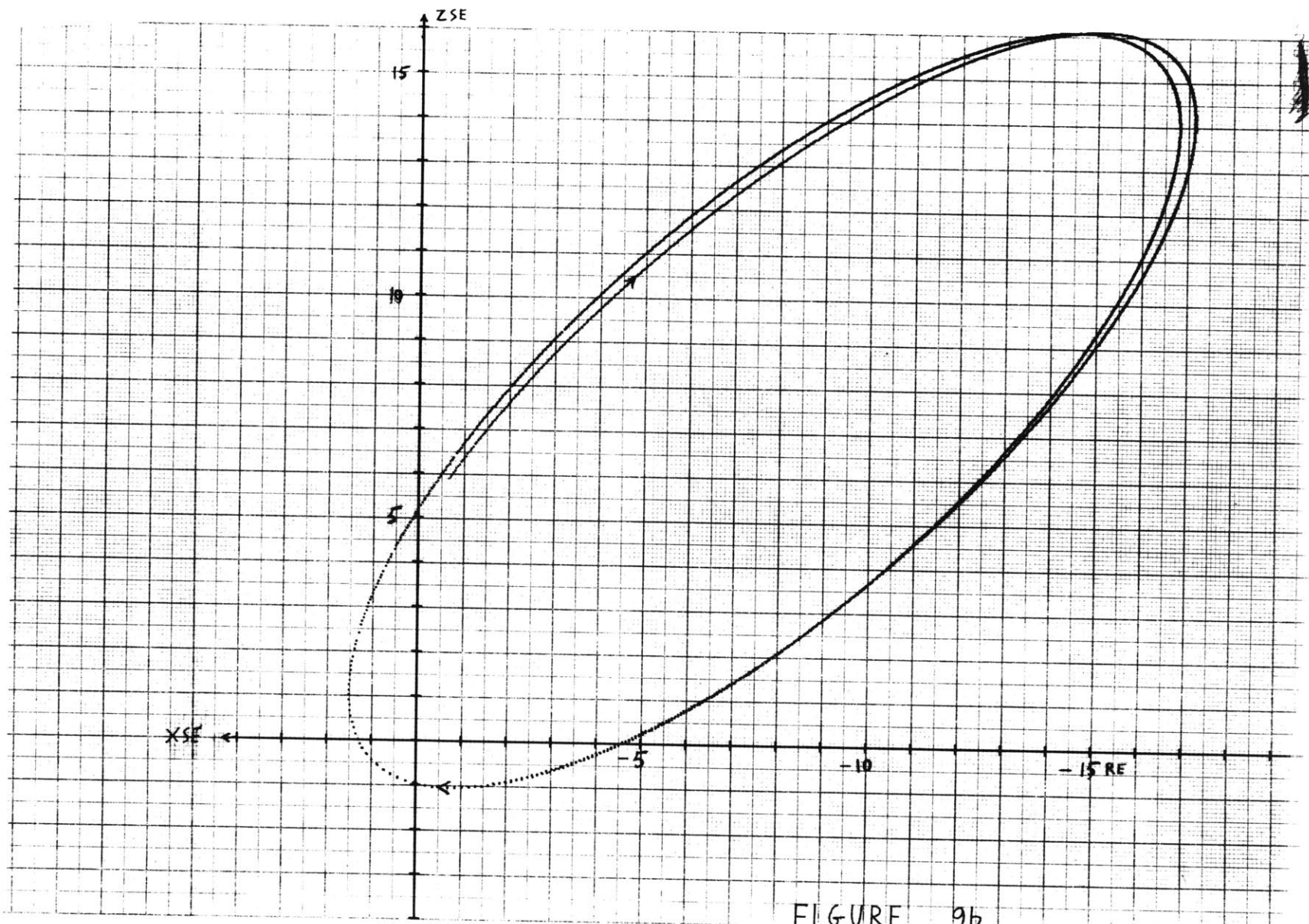


FIGURE 9b

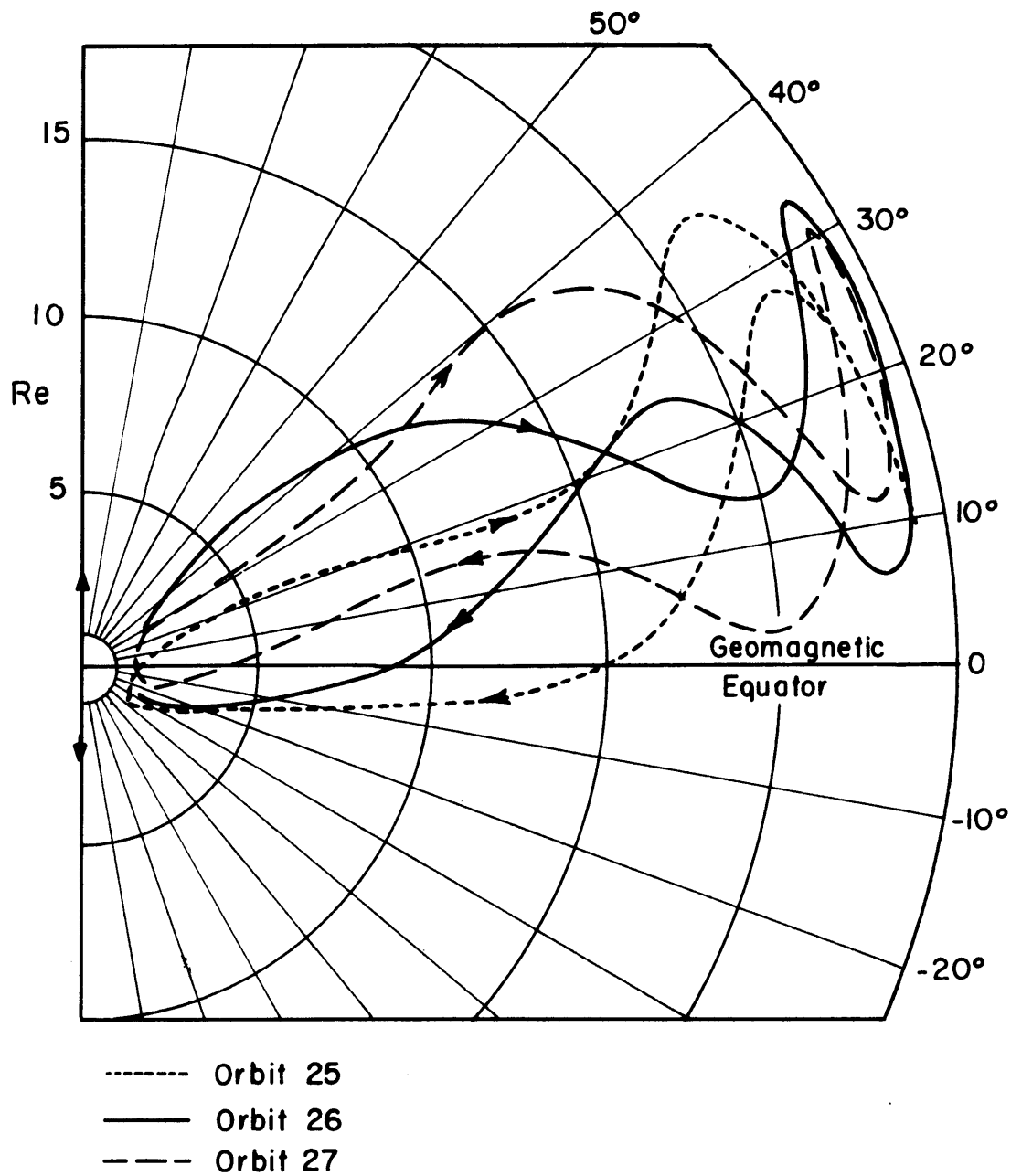


Figure 10

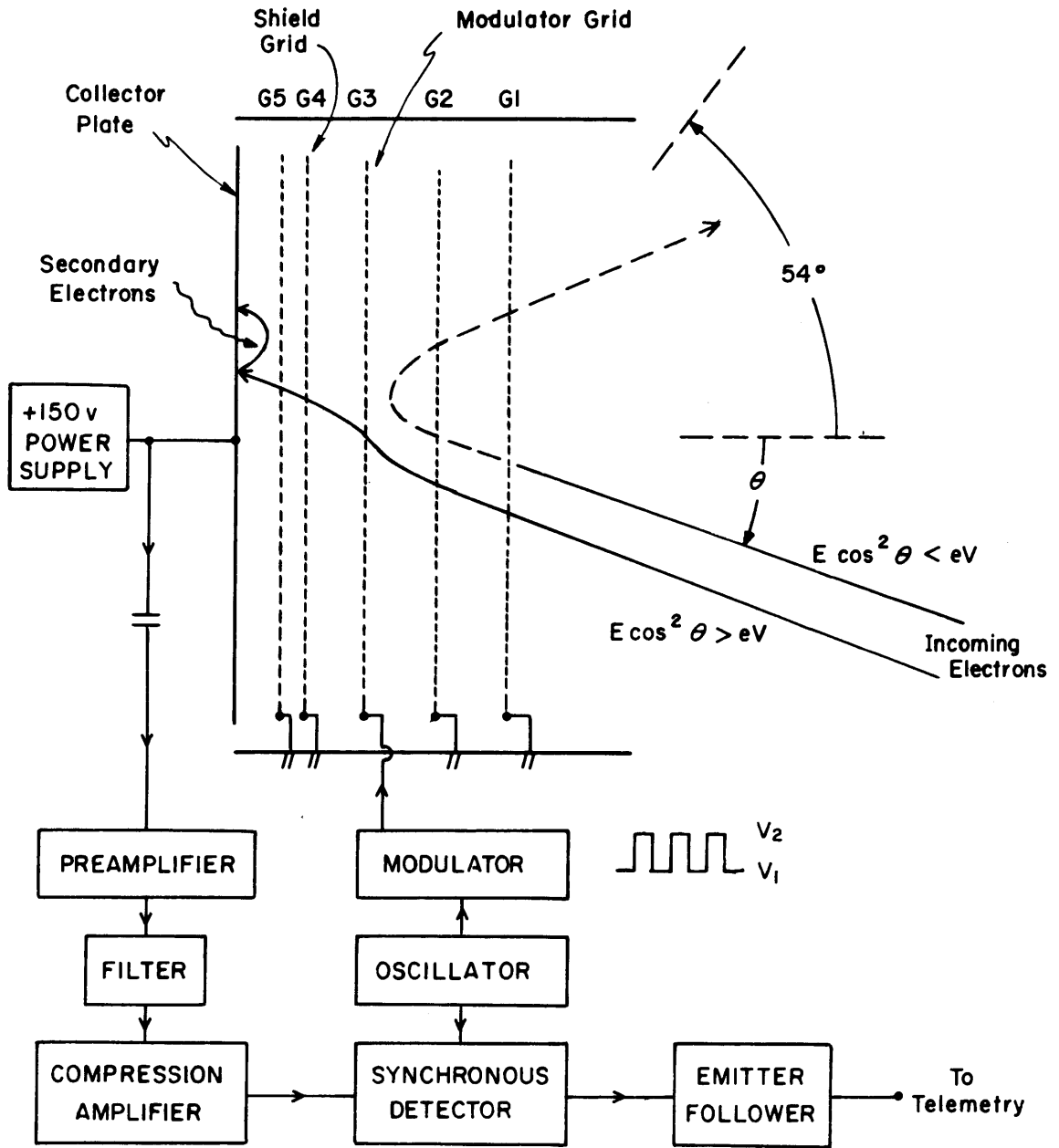


Figure II

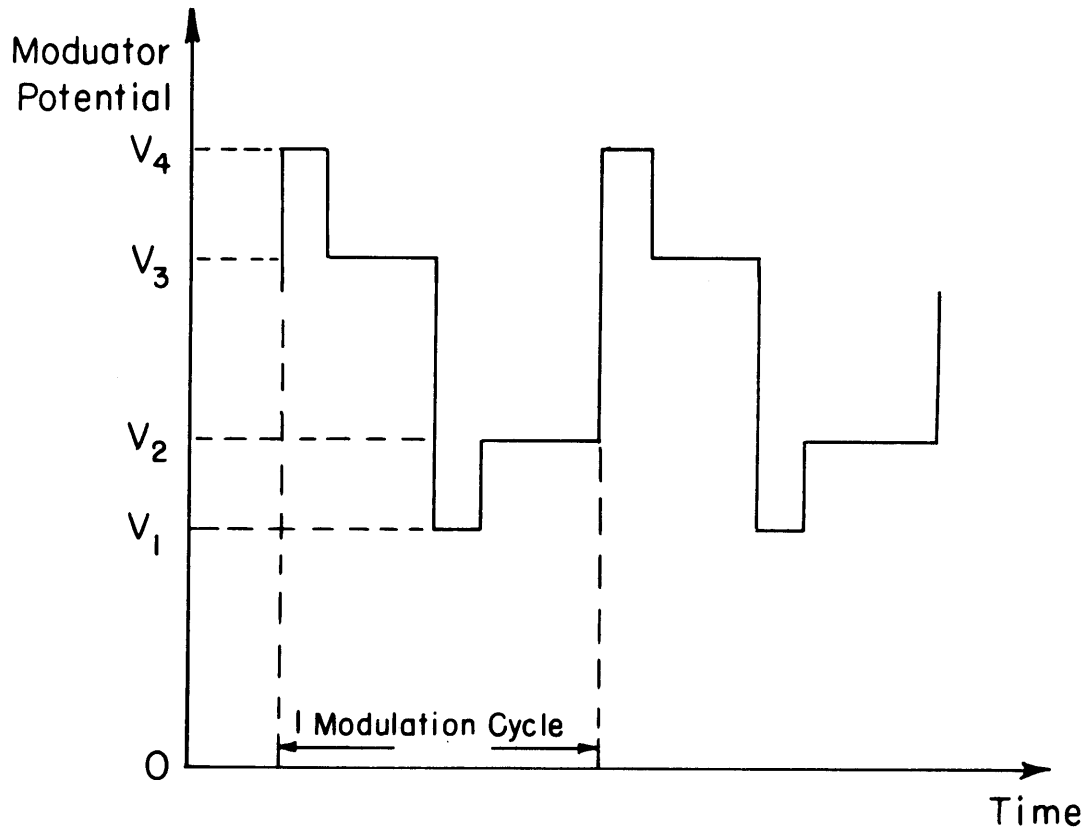


FIGURE 12

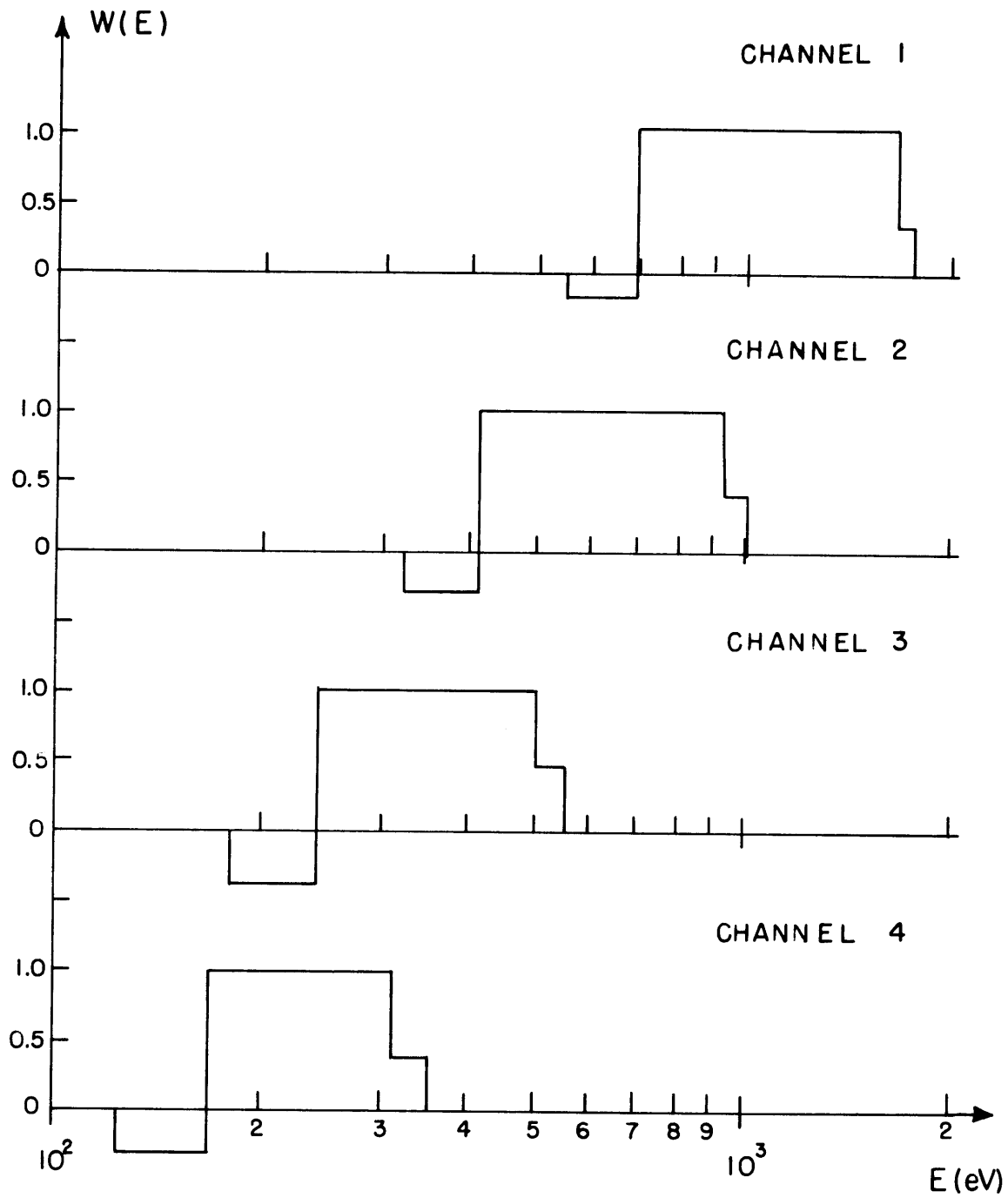


FIGURE 13

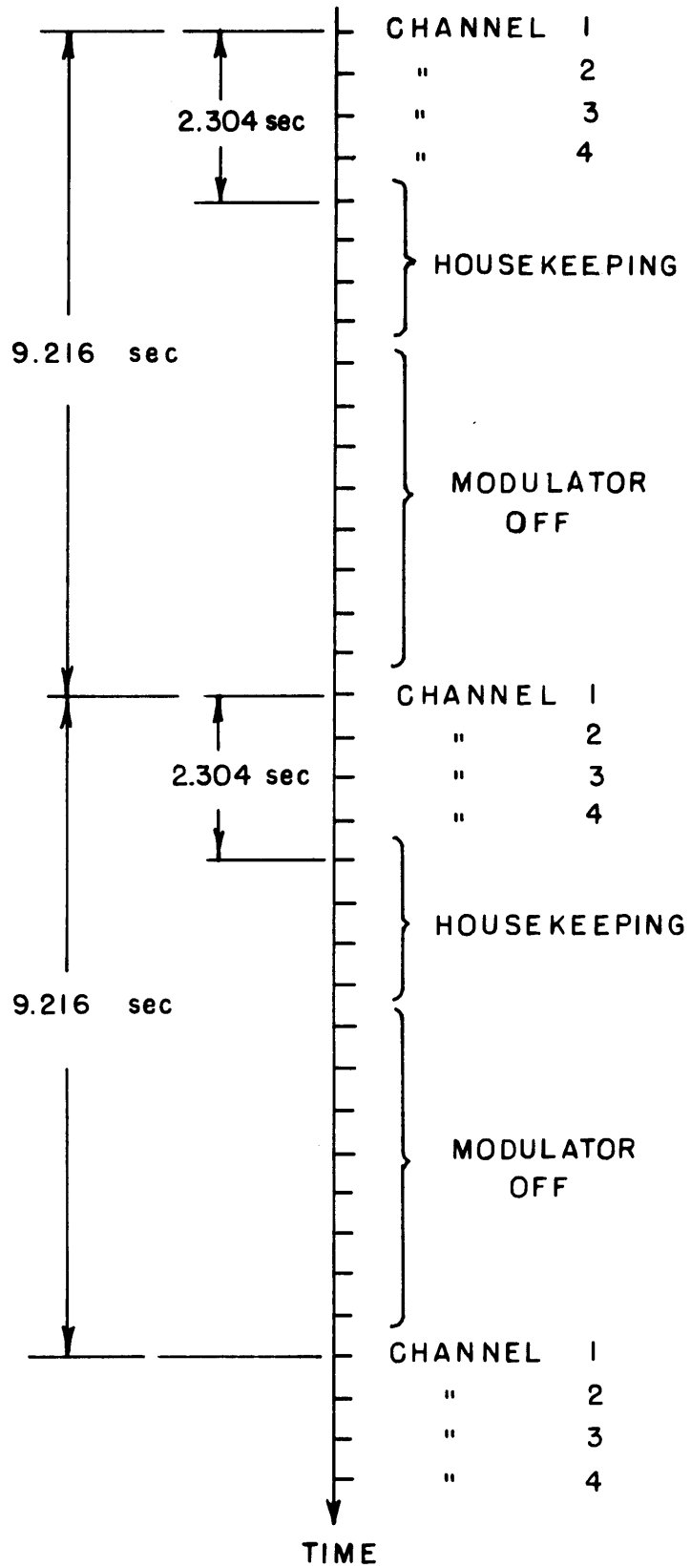
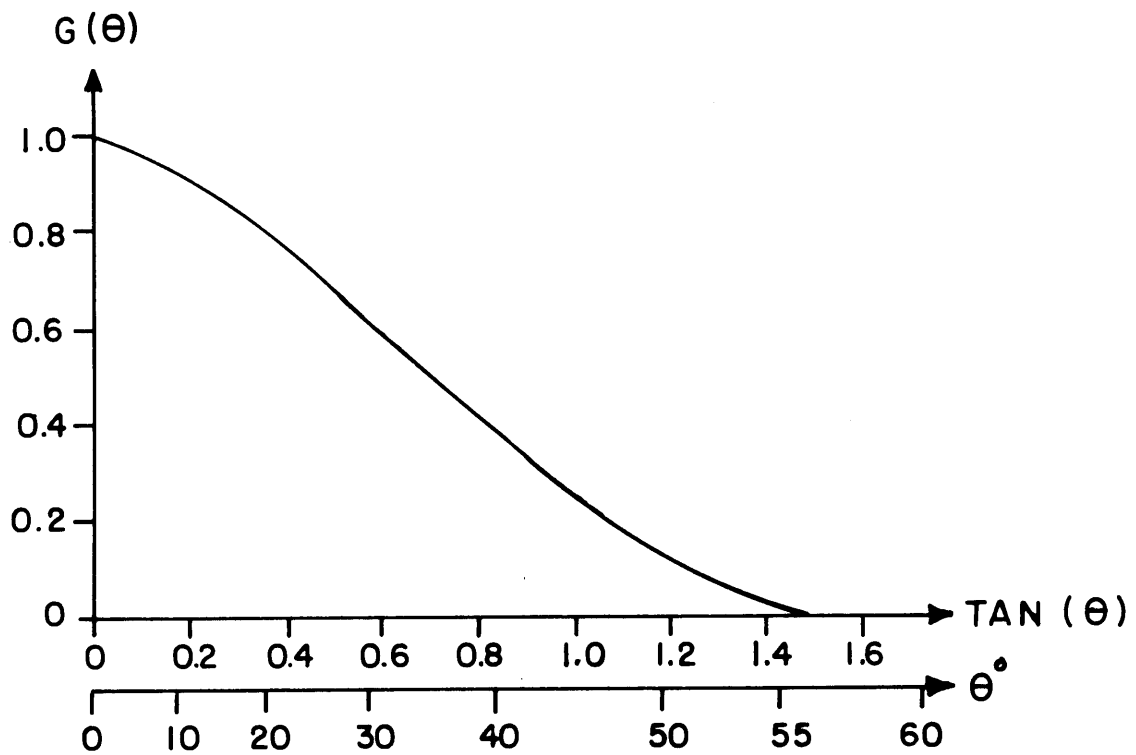


FIGURE 14



ANGULAR RESPONSE FUNCTION

FIGURE 15

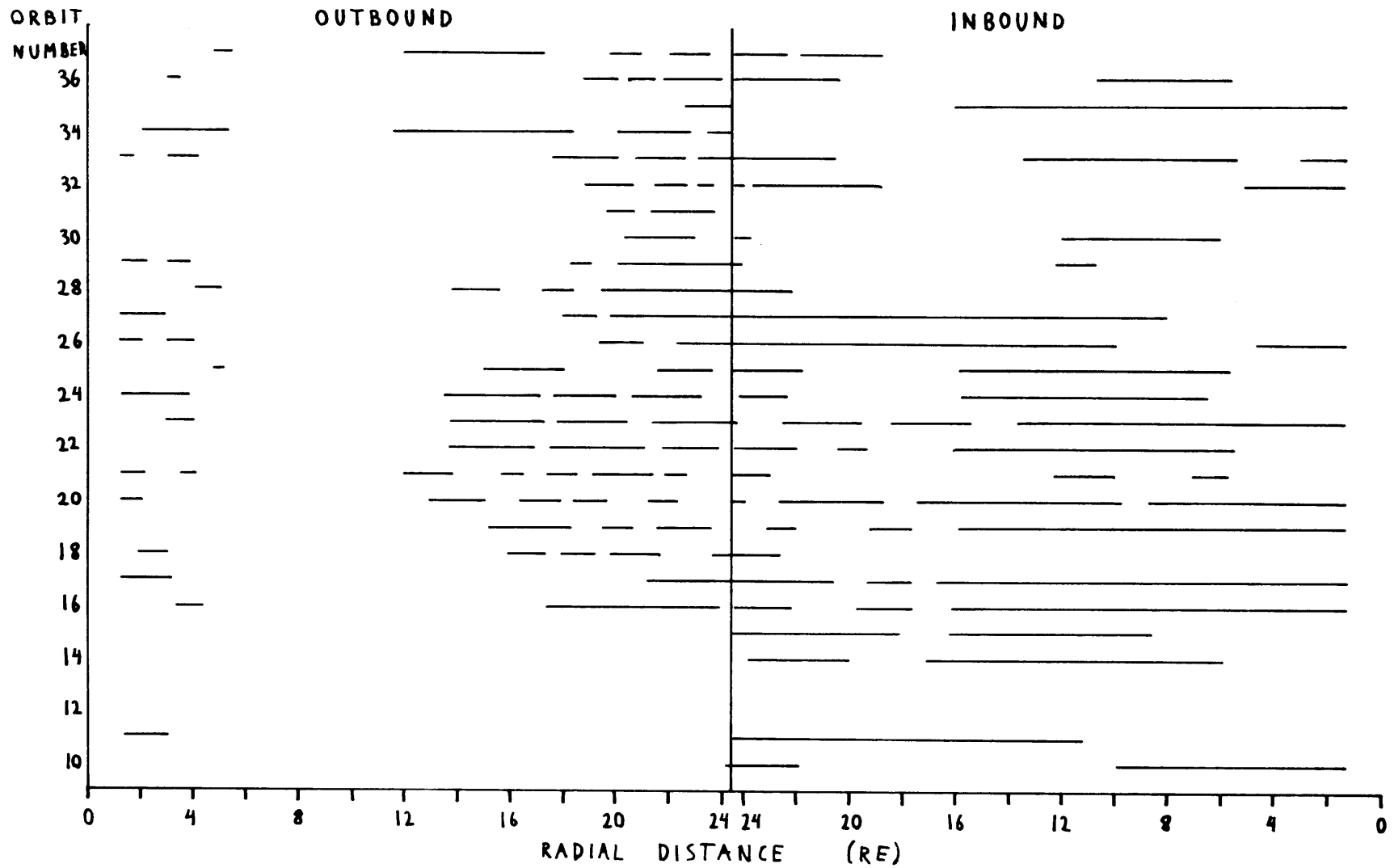
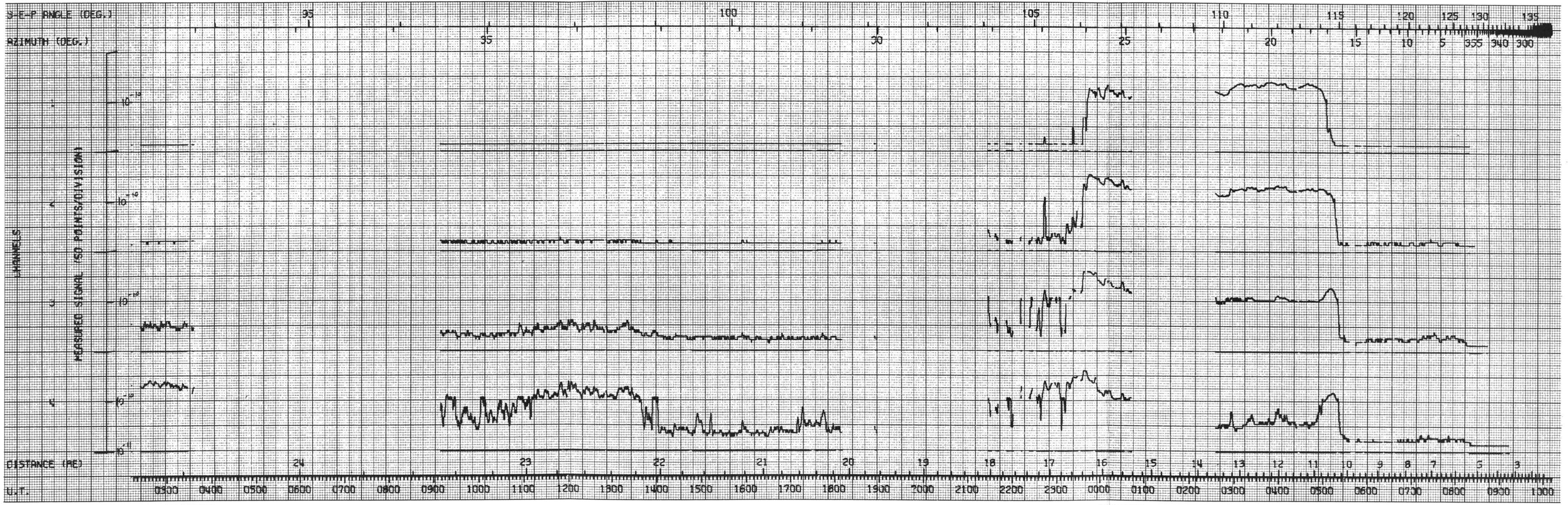


FIGURE 16

- 9/5/ -

ORBIT 23 INBOUND

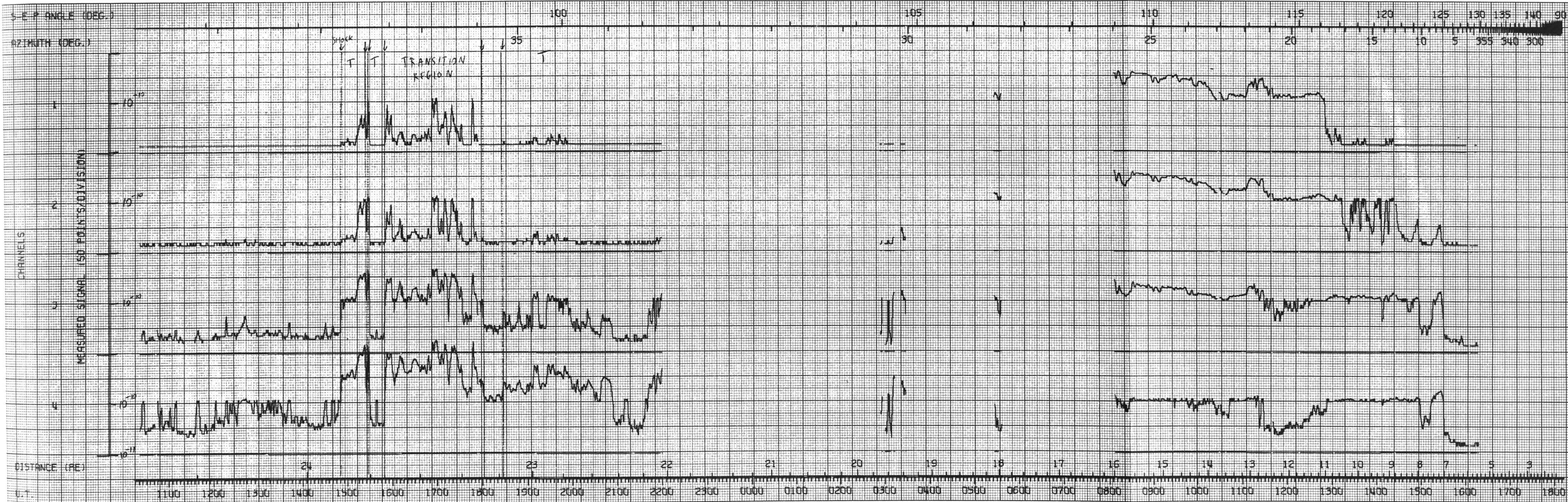


DATE 11/04/64

11/05/64

Fig. 17

ORBIT 22 INBOUND



DATE 11/01/64

11/02/64

Fig. 18

ORBIT 27

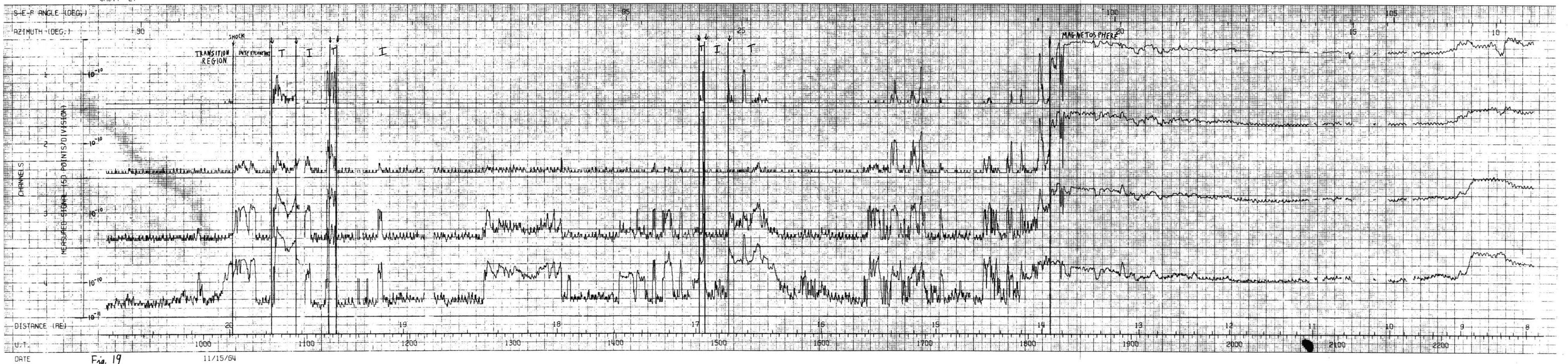


Fig. 19

11/15/64

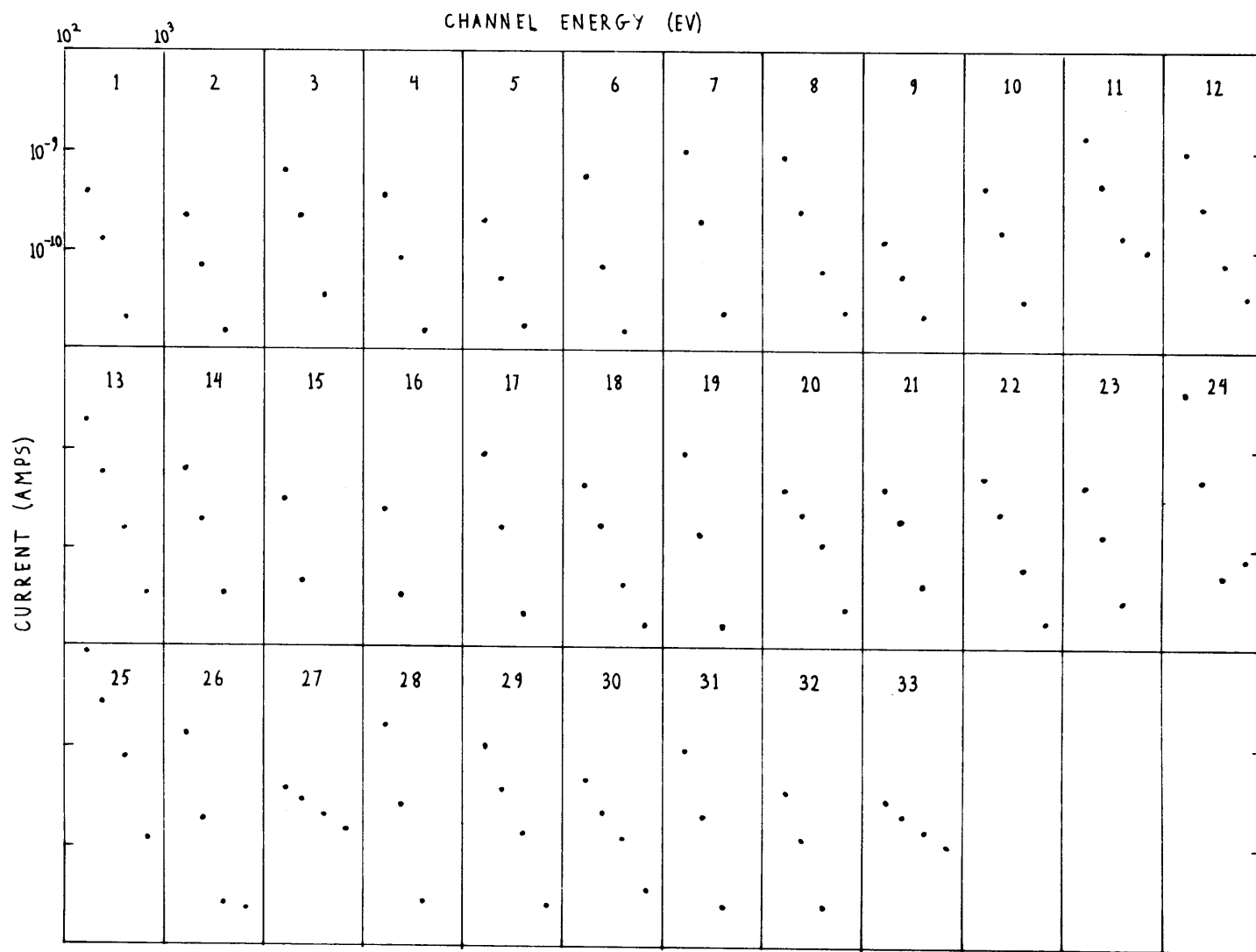
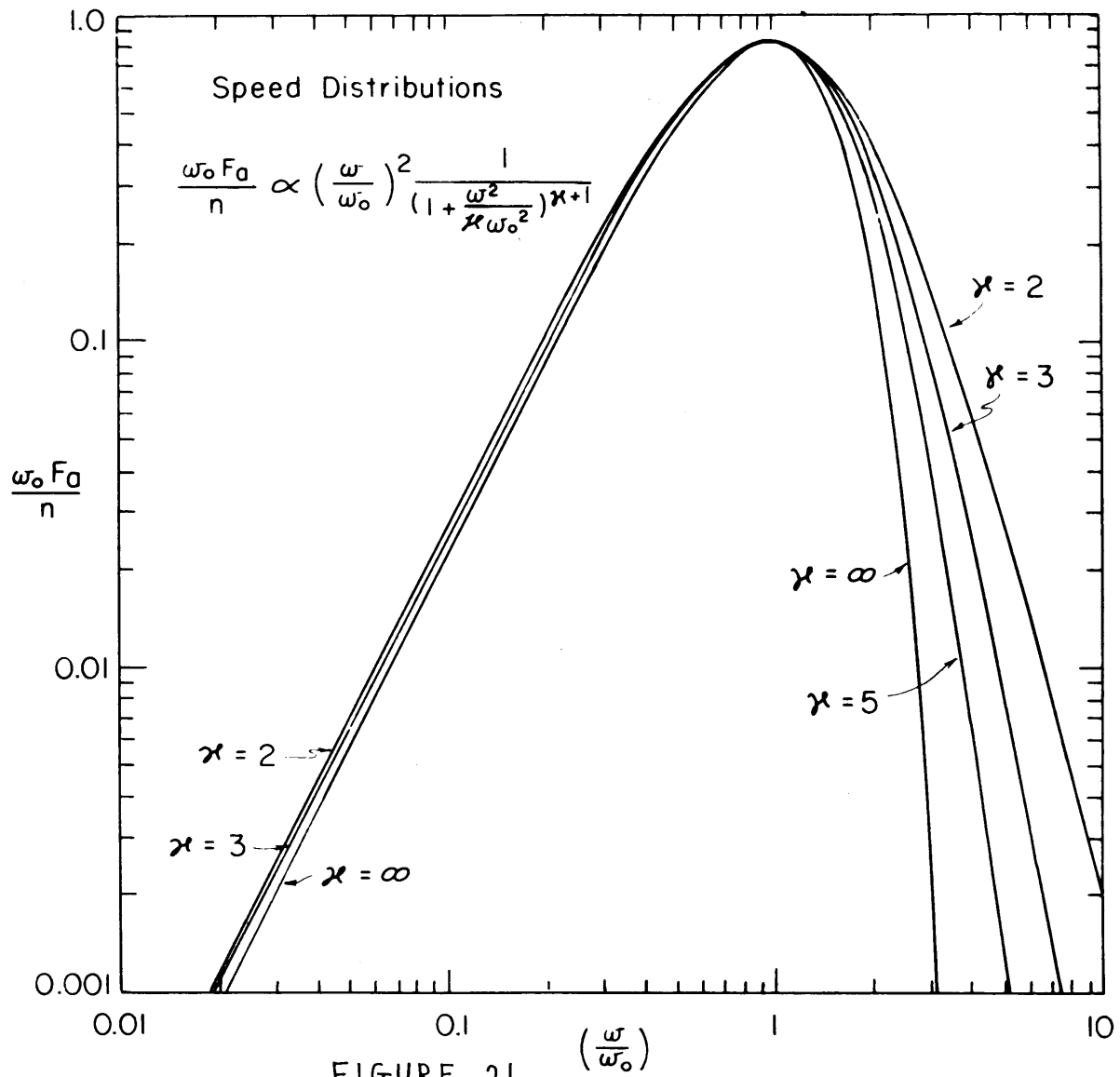


FIGURE 20

-150-



-151-

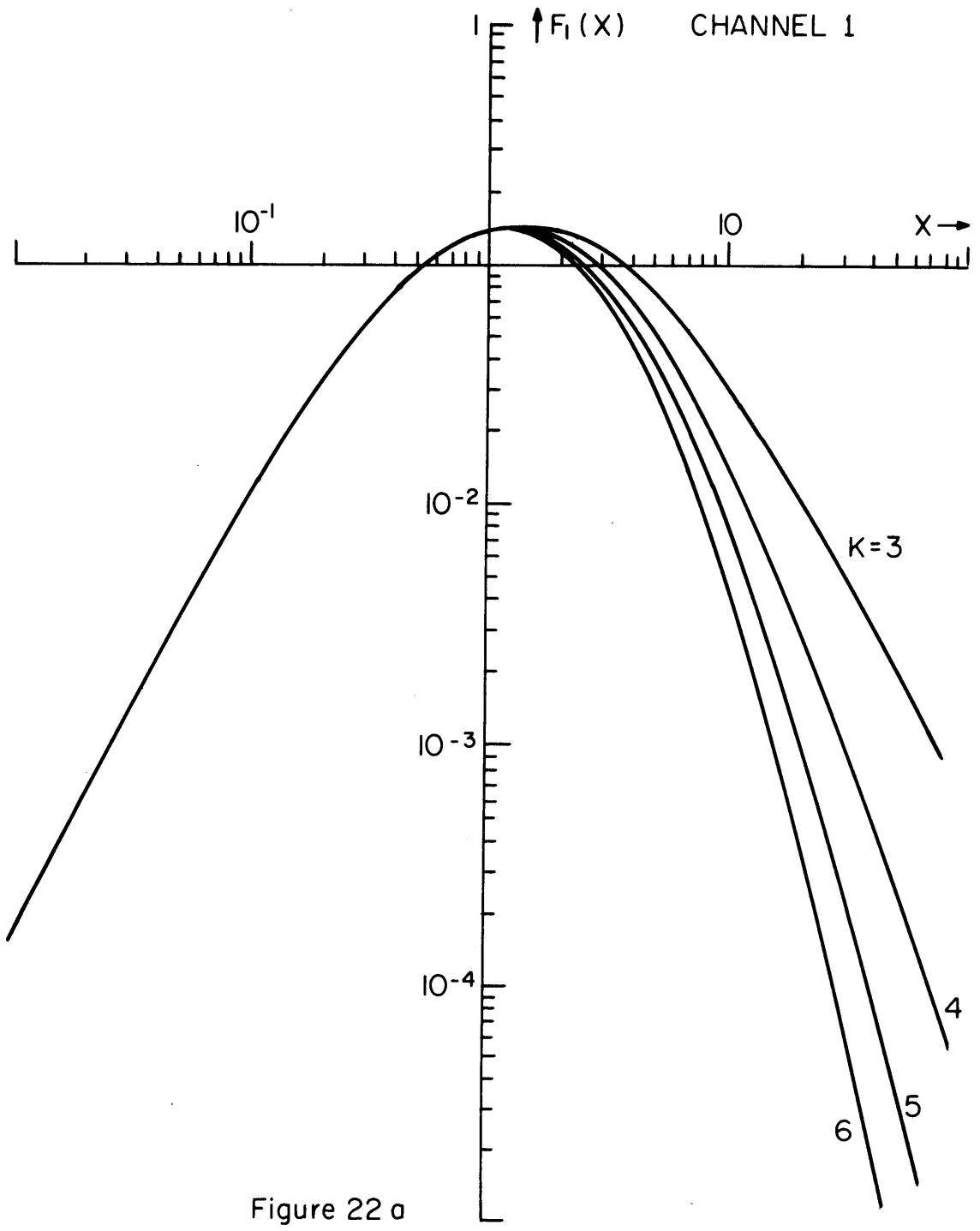


Figure 22 a

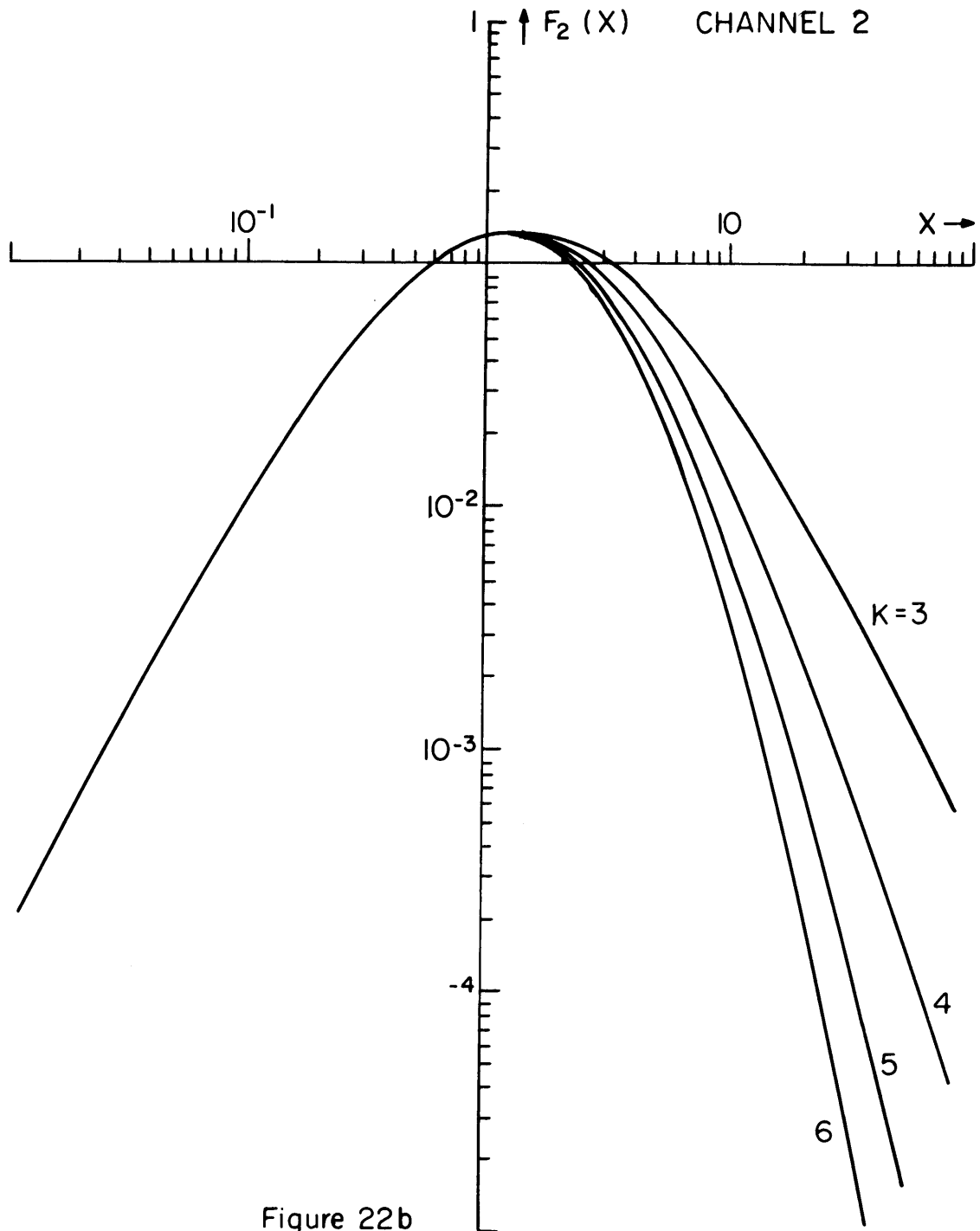


Figure 22b

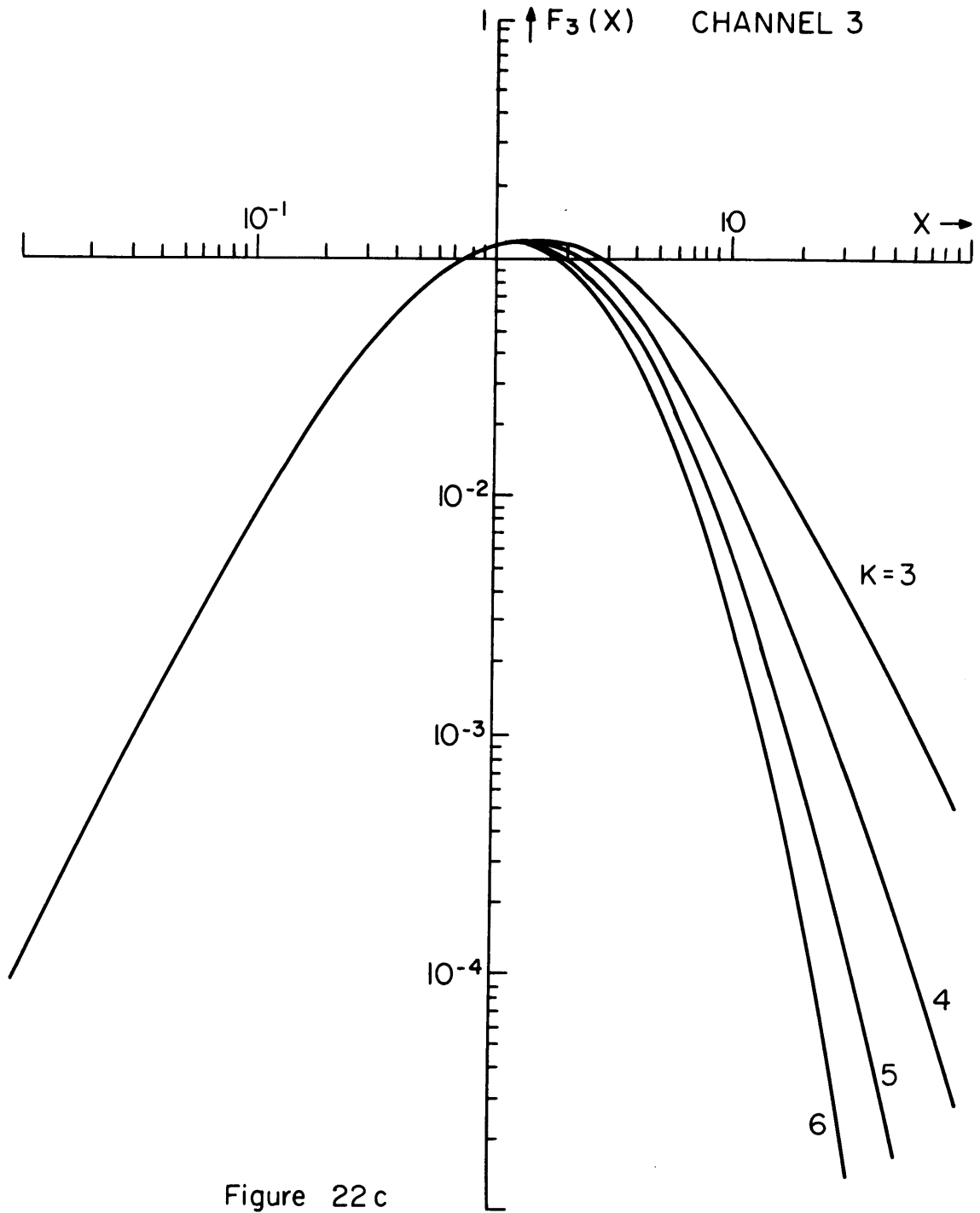


Figure 22 c

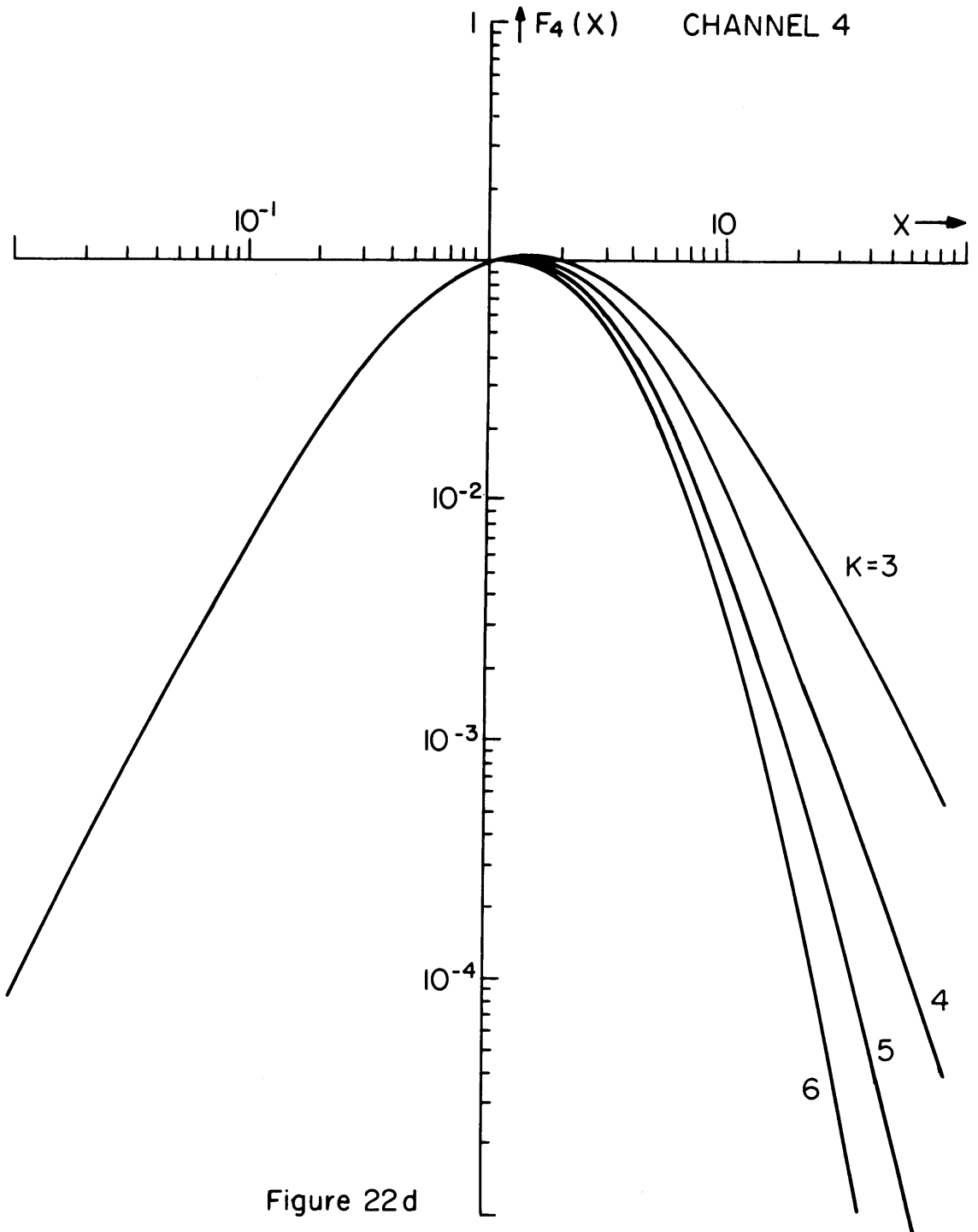


Figure 22d

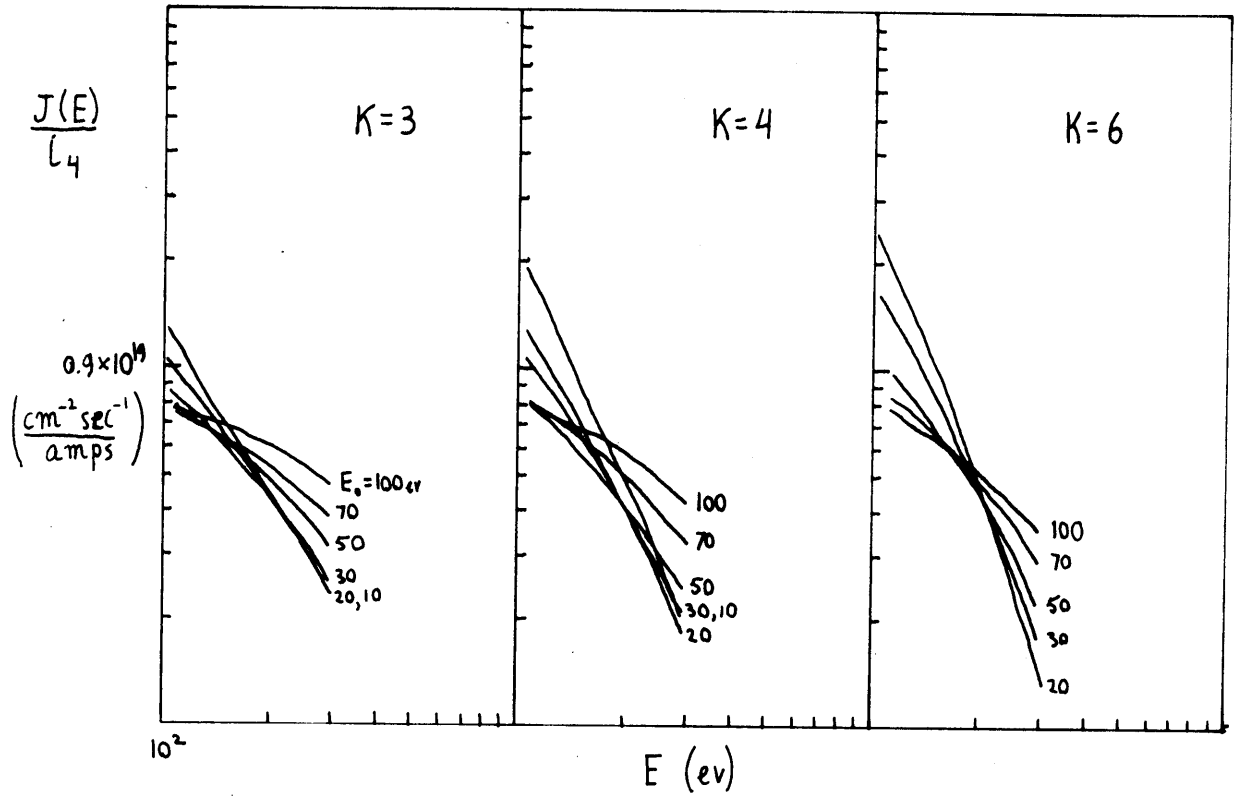


FIGURE 23

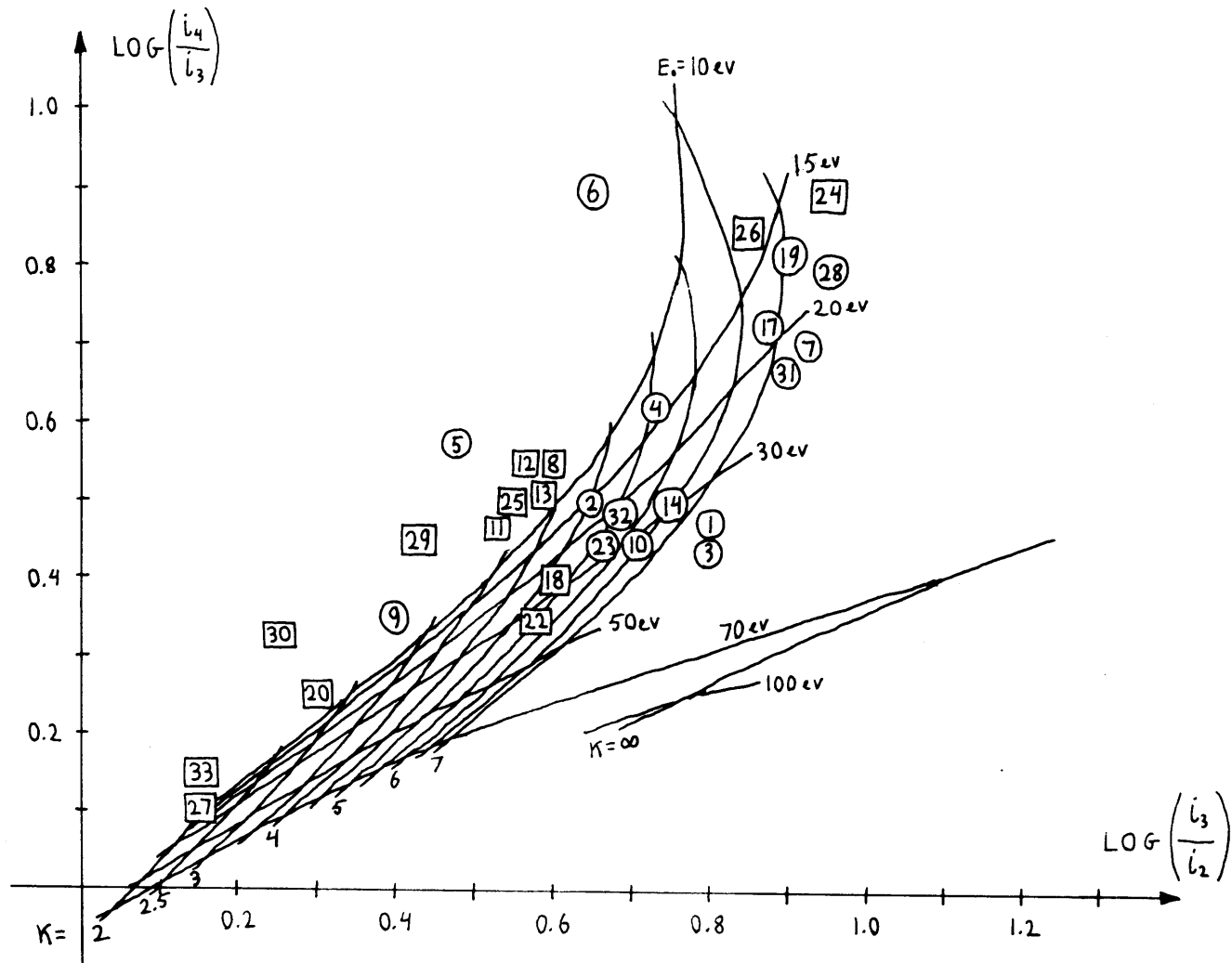


FIGURE 24

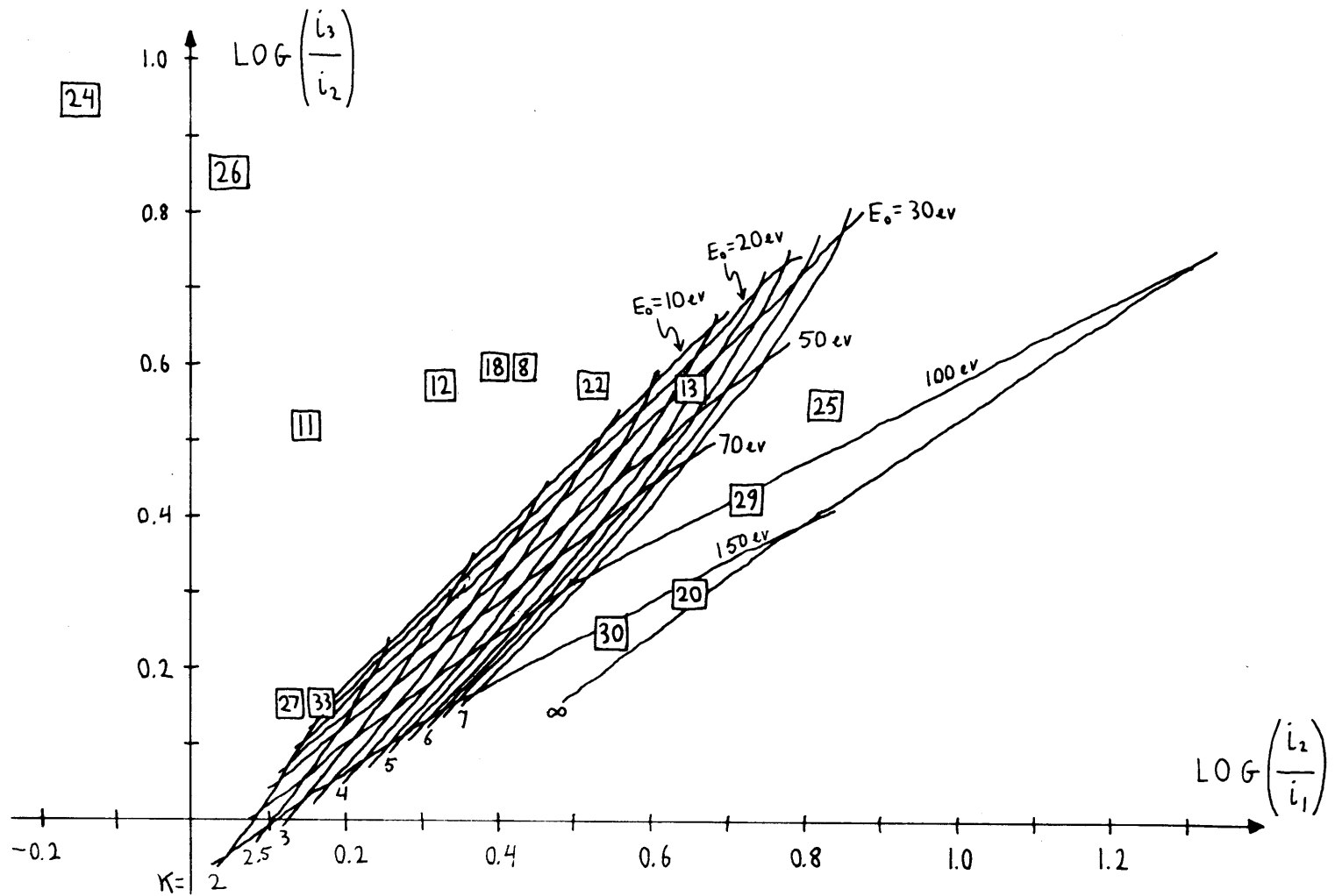


FIGURE 25

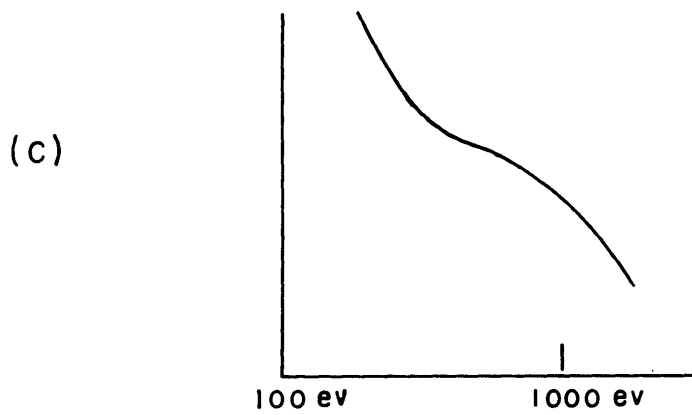
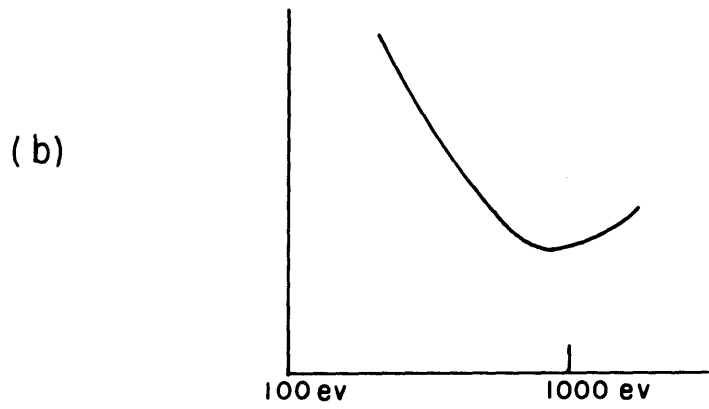
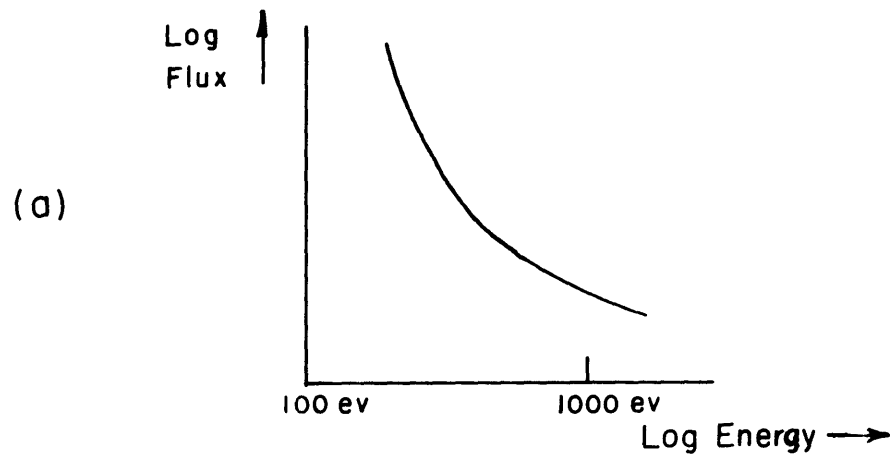


FIGURE 26

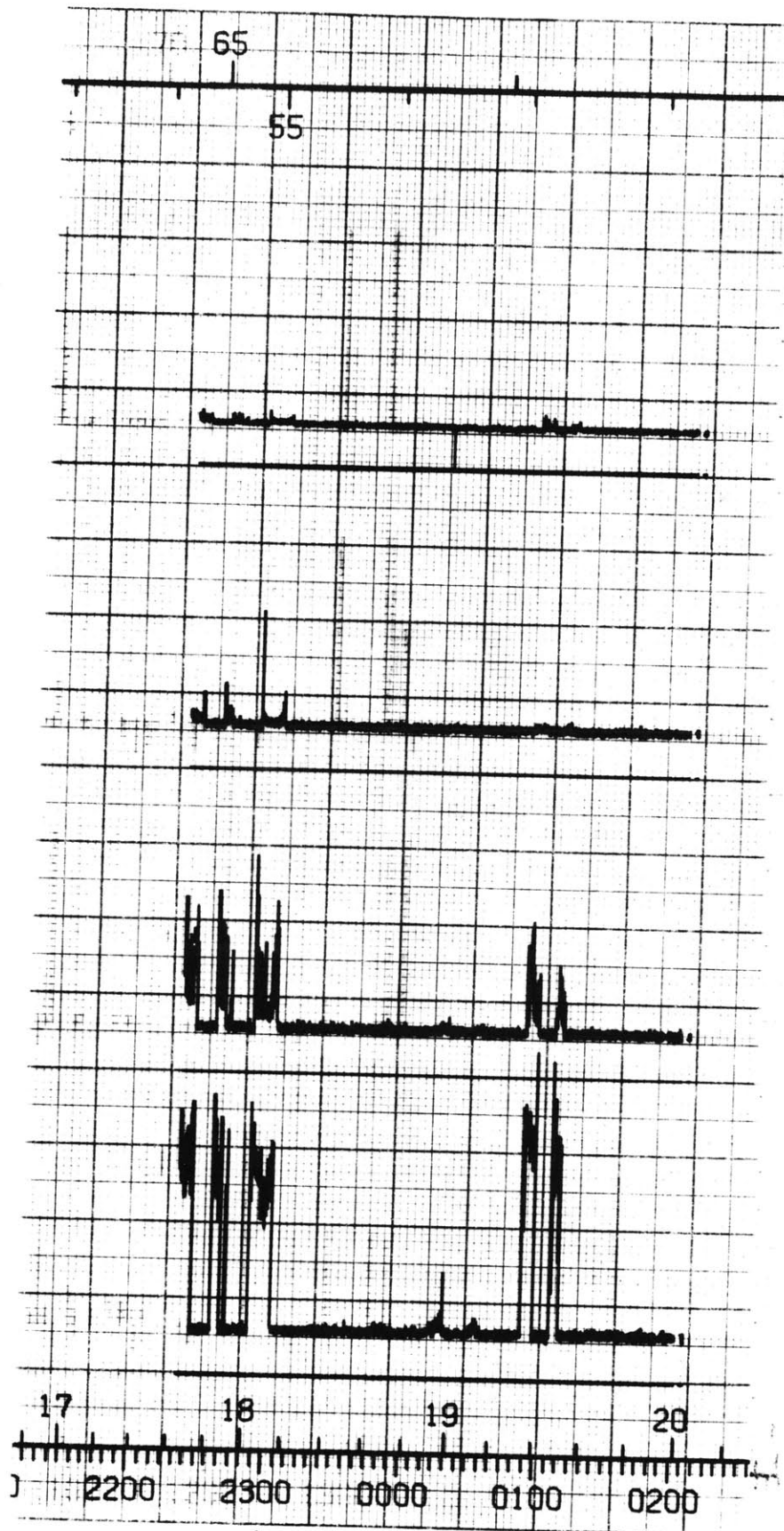


Fig. 27

11/30/64

ORBIT 15 INBOUND

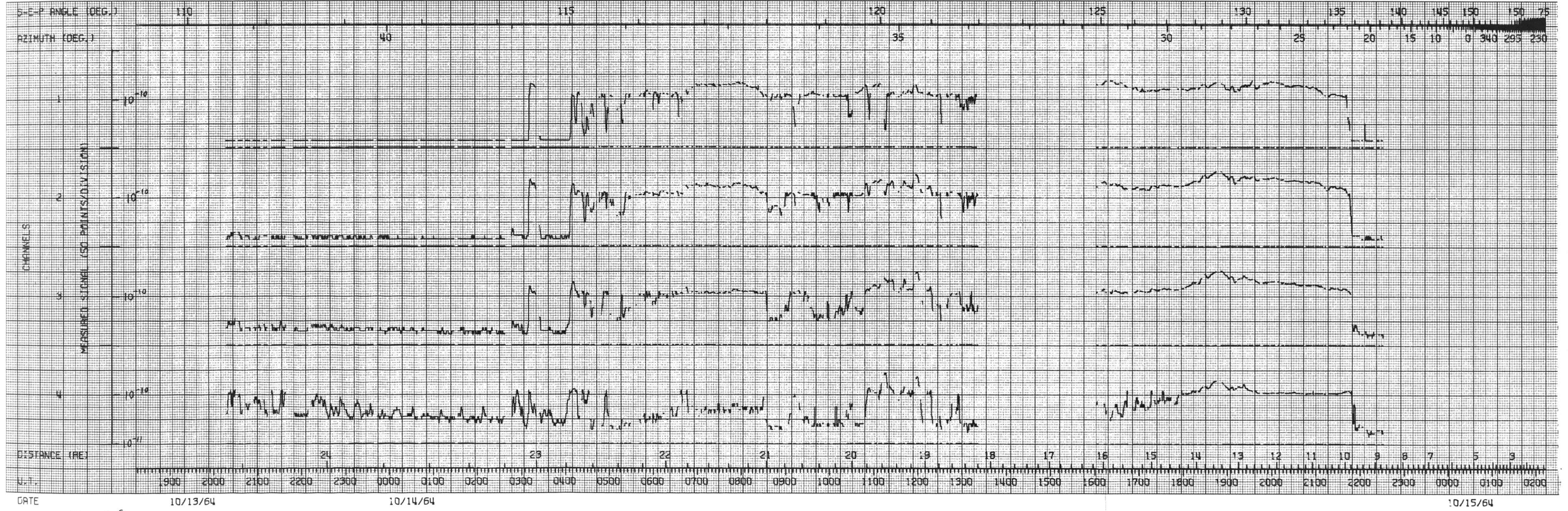
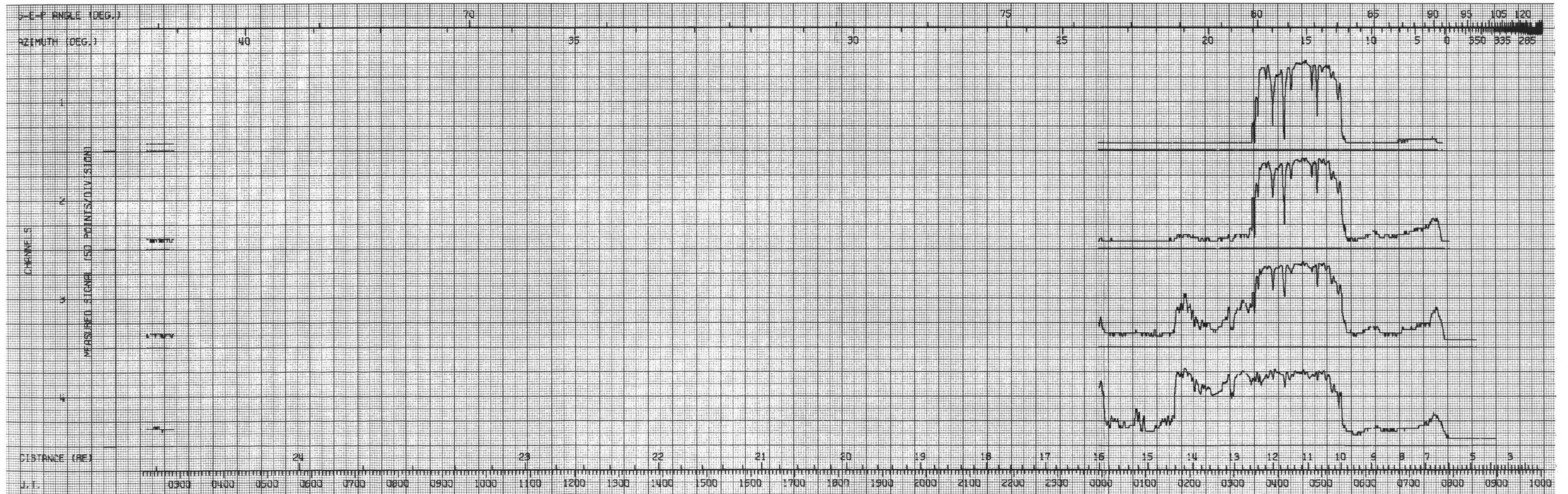


Fig-28

ORBIT 35 INBOUND

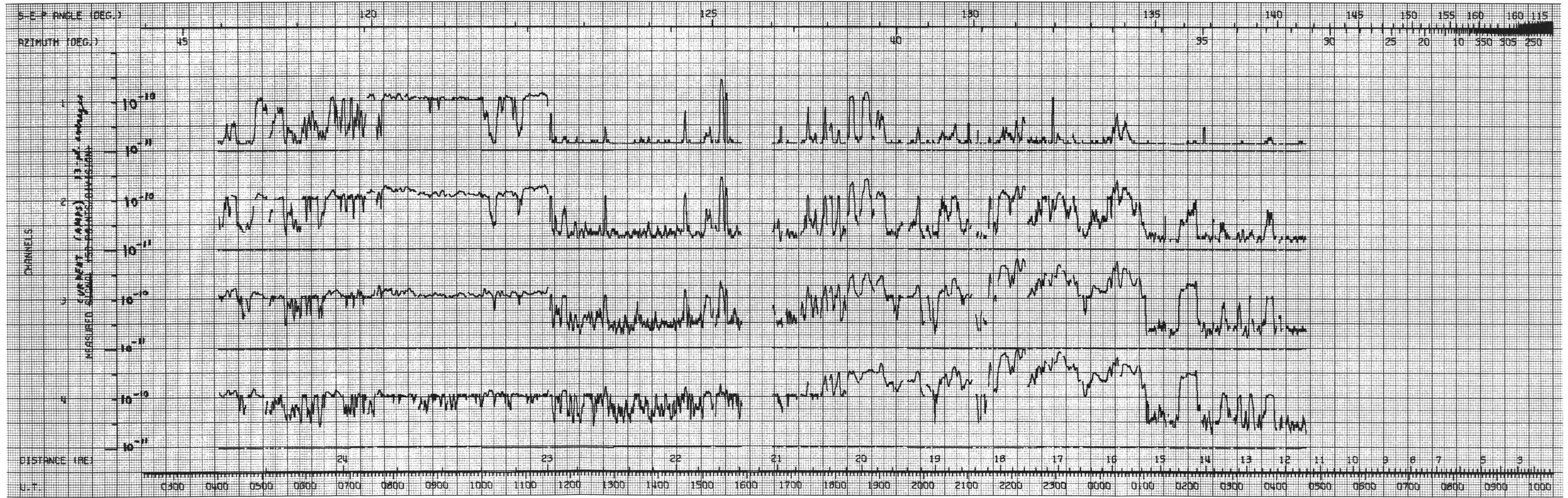


DATE 12/06/64

12/07/64

Fig. 29

ORBIT 11 INBOUND



DATE 10/03/64

10/04/64

Fig. 30

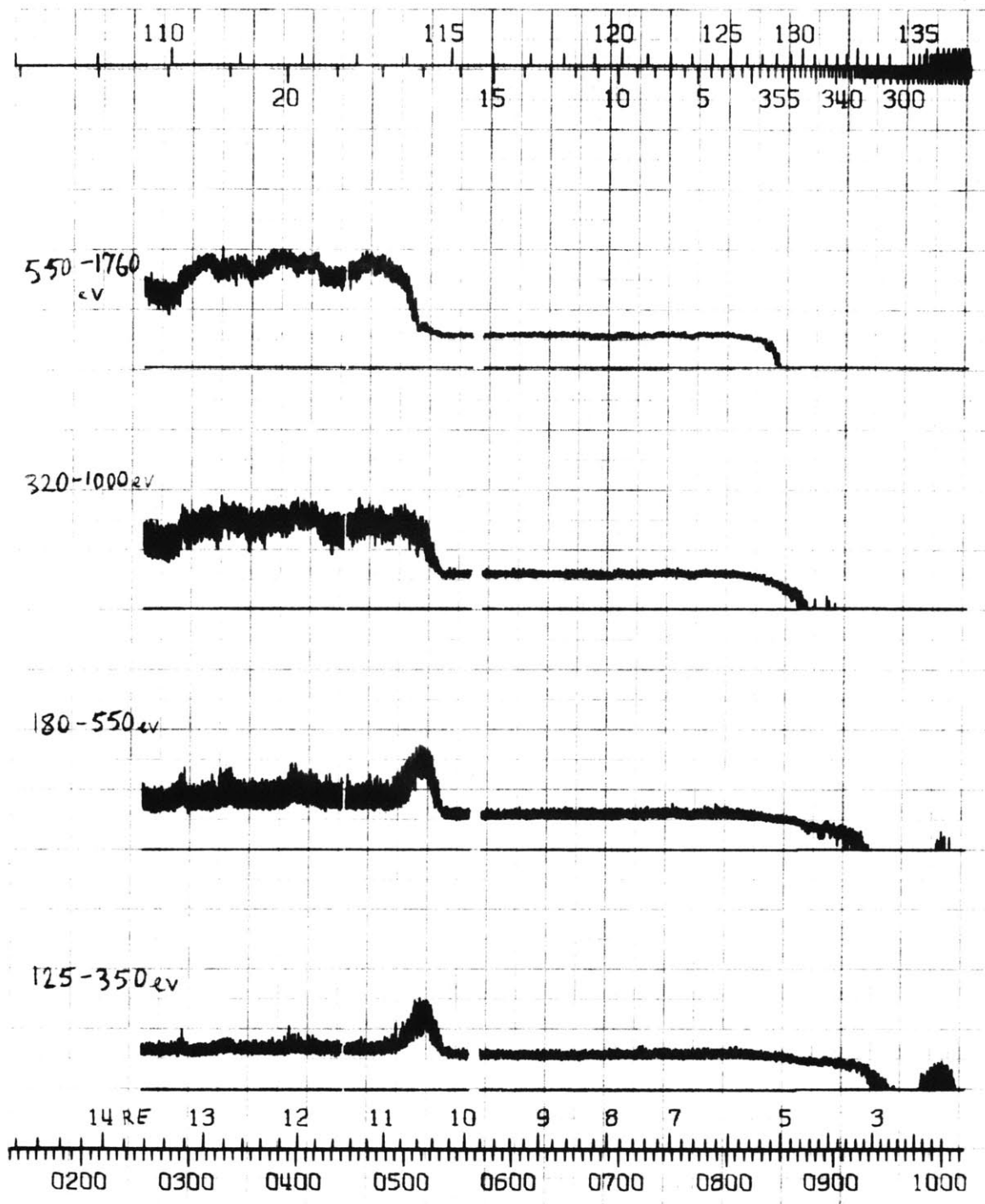
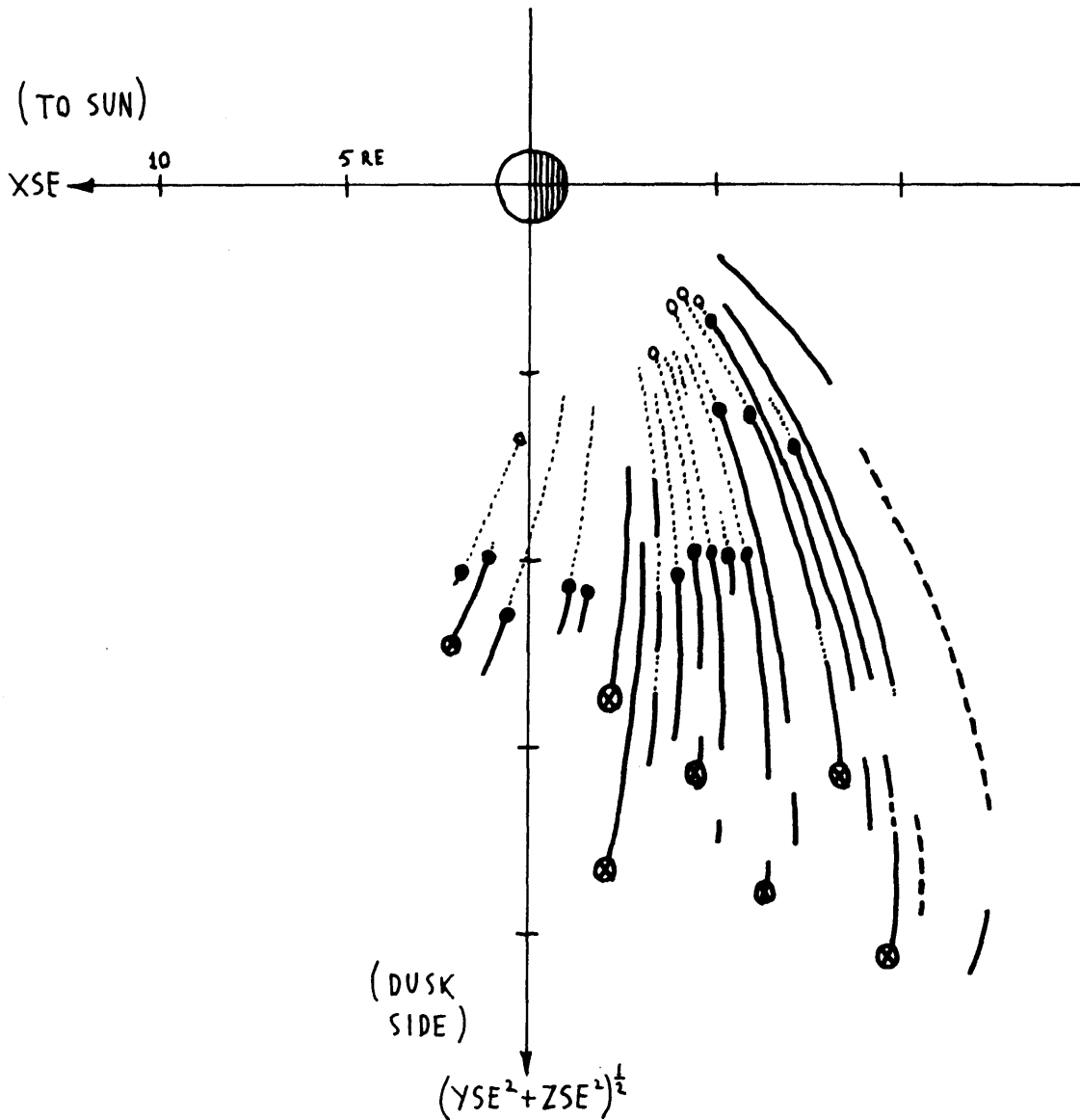


Fig. 31

11/5/64



- STRONG FLUXES, ENERGY < 100 EV
- ENERGY SEVERAL HUNDRED EV
- UNDETECTABLE OR WEAK FLUXES, LOW ENERGY
- MAGNETOPAUSE
- SHARP GRADIENT OF MEAN ELECTRON ENERGY
- BOUNDARY OF HIGH ION DENSITY REGION

FIGURE 32

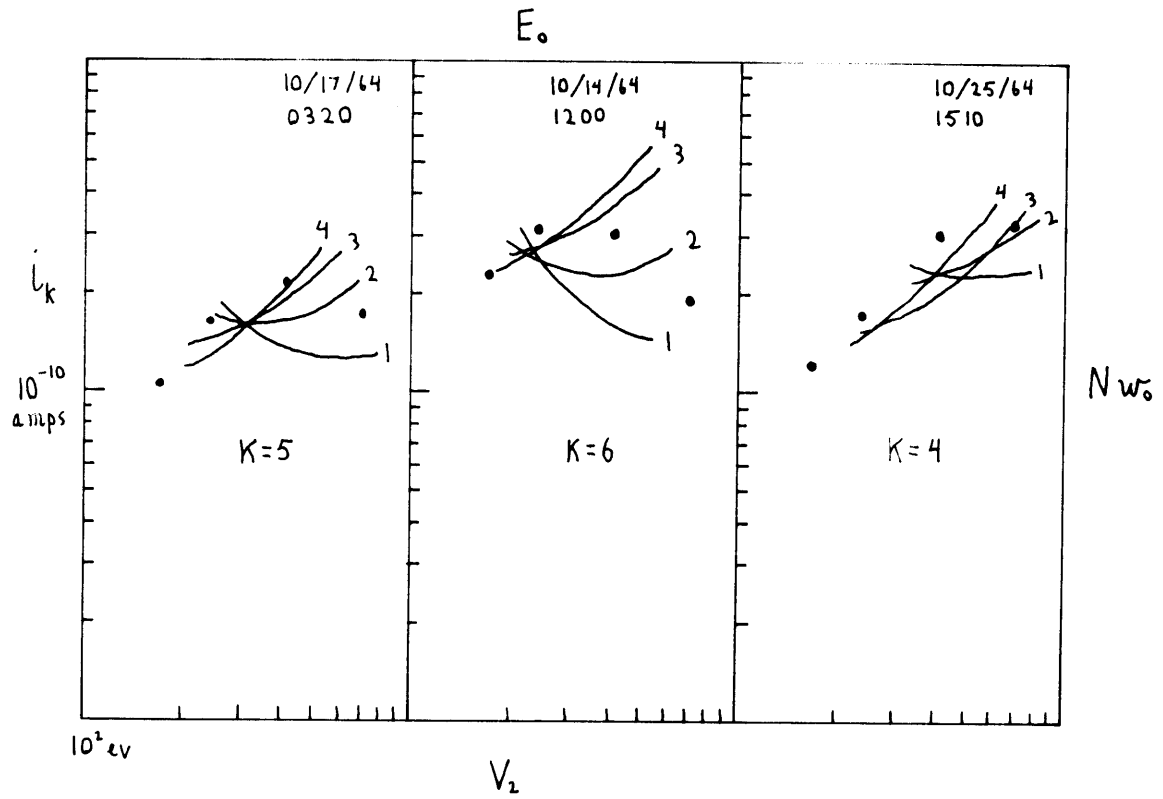
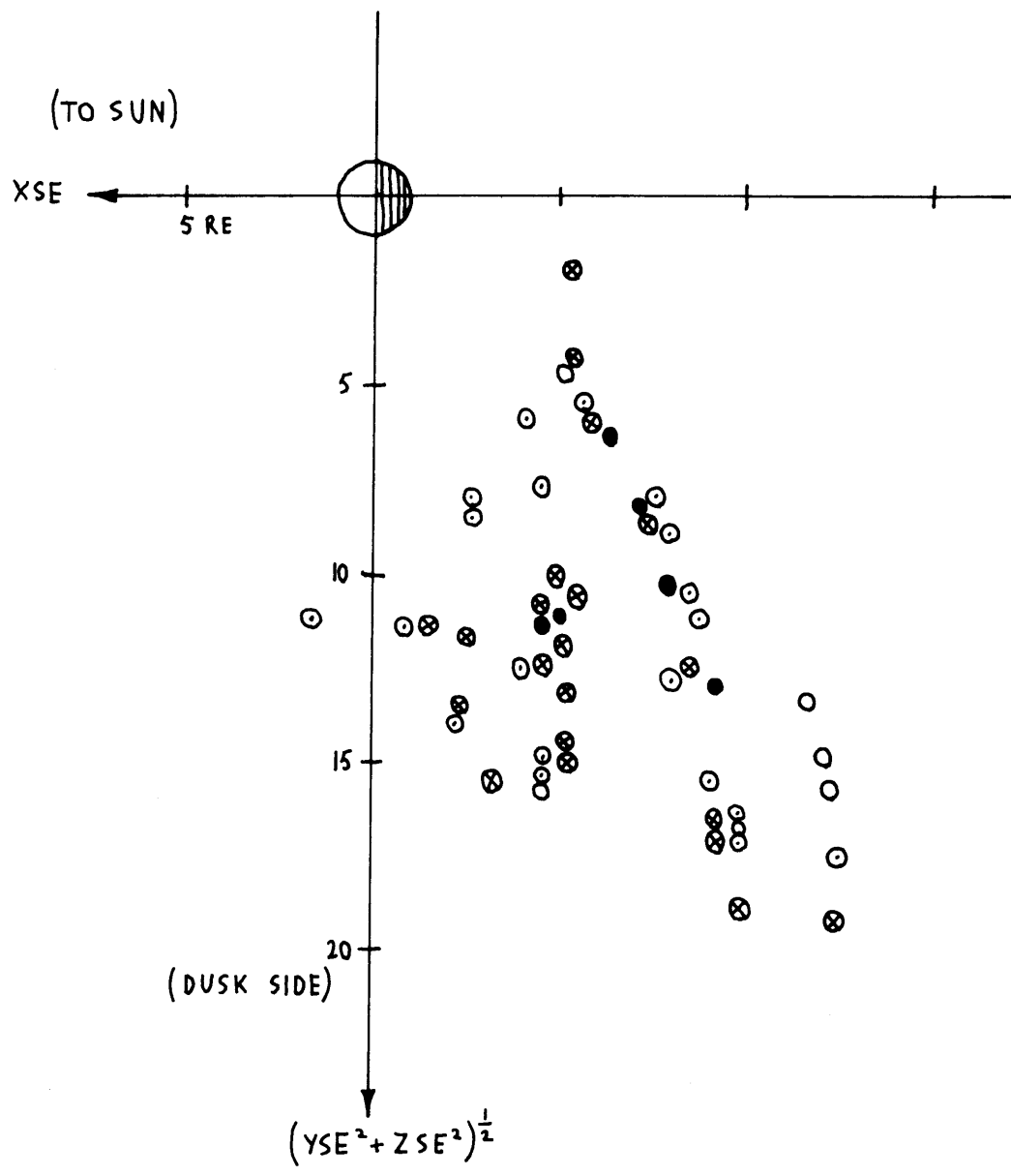


FIGURE 33



- $E_0 < 100 \text{ eV}$
- ⊙ $100 \text{ eV} < E_0 < 300 \text{ eV}$
- ⊗ $300 \text{ eV} < E_0 < 500 \text{ eV}$
- $500 \text{ eV} < E_0$

FIGURE 34

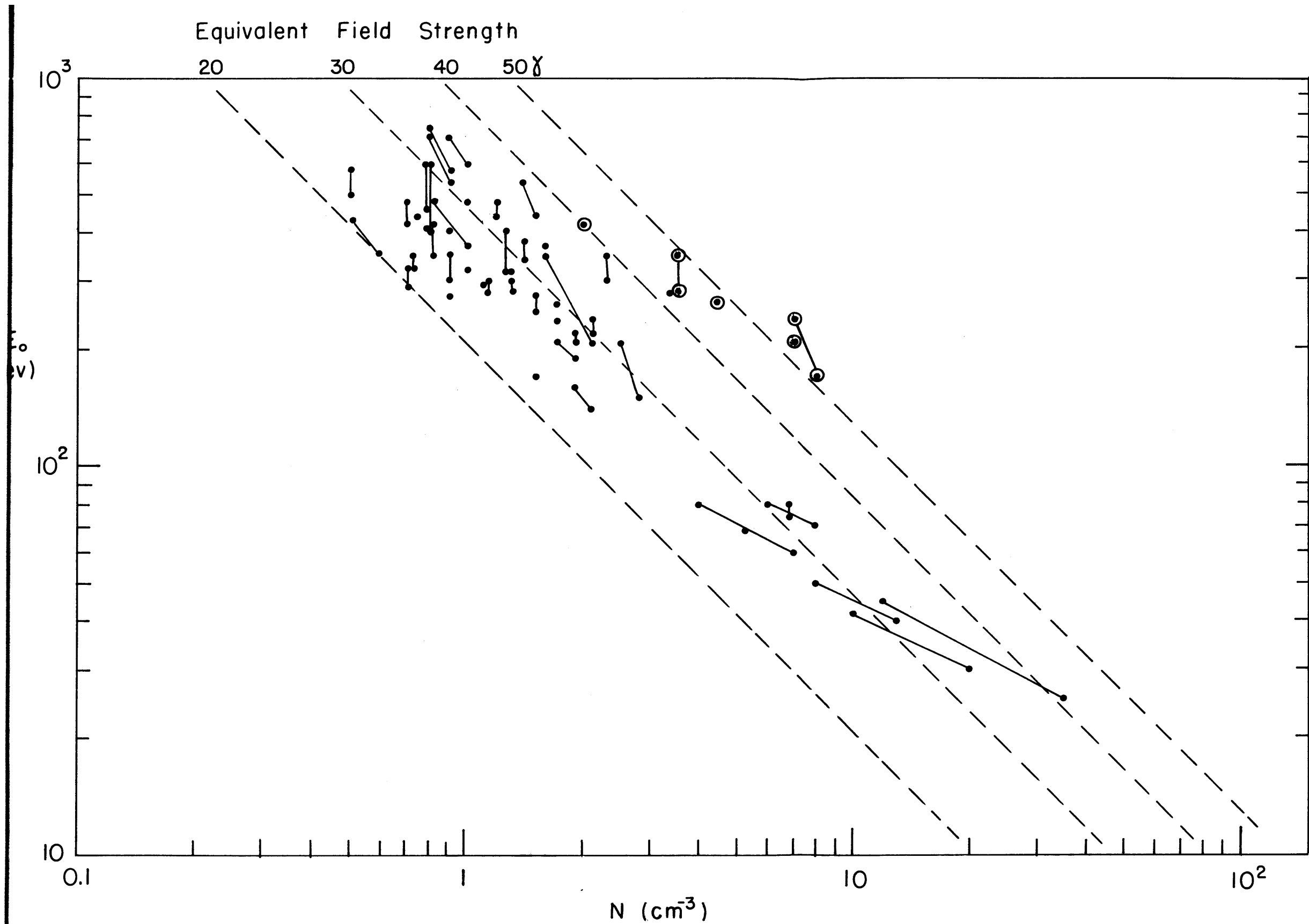


FIGURE 35

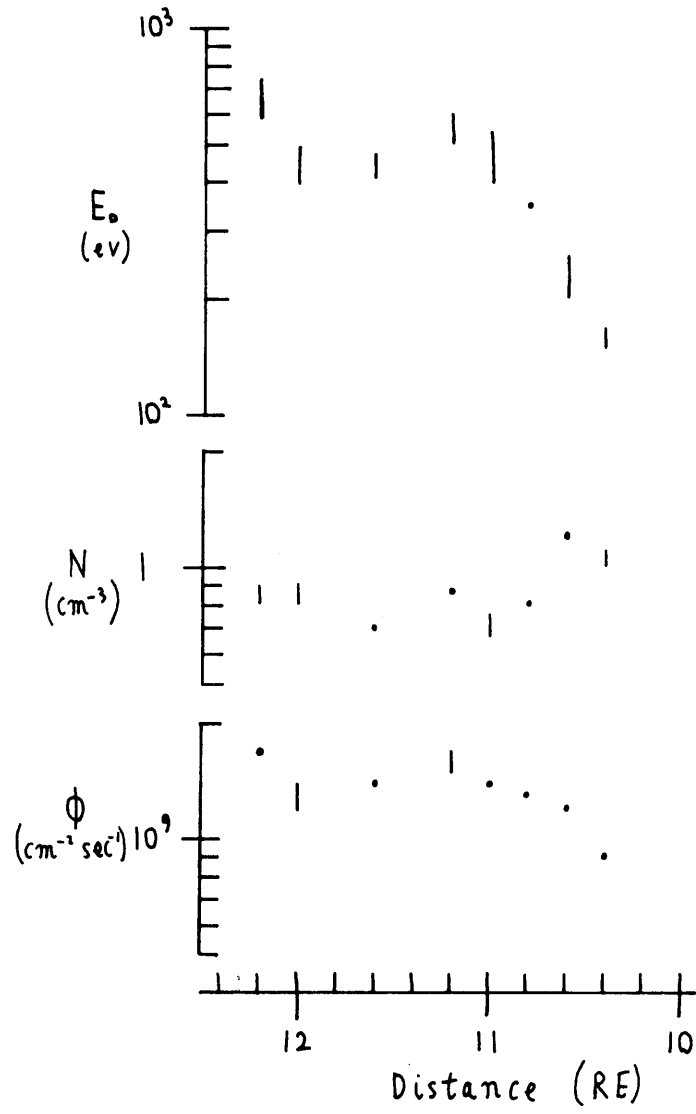


FIGURE 36

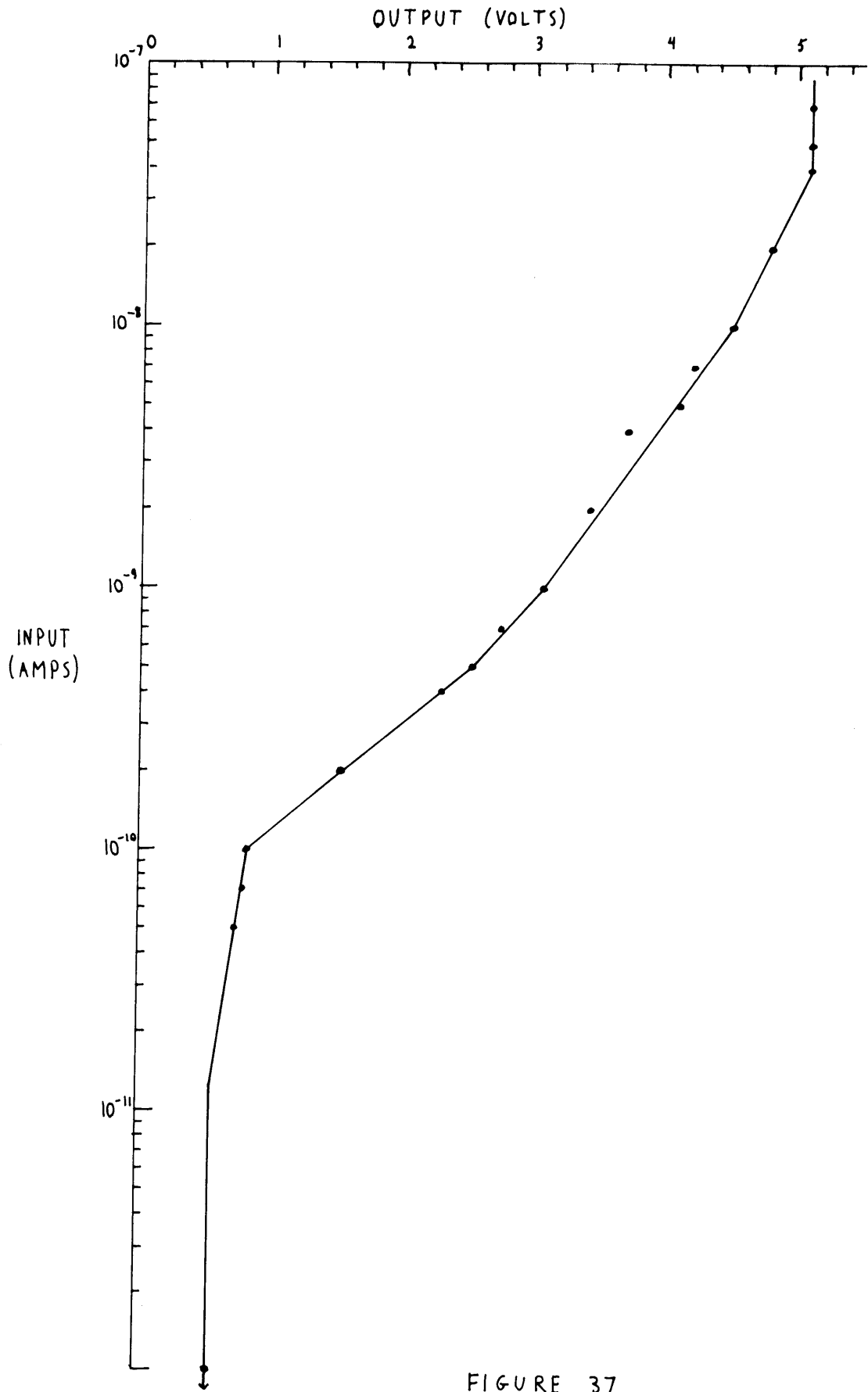


FIGURE 37

BIOGRAPHICAL NOTE

The author was born on September 25, 1939, in Kaunas, Lithuania. He came to the United States in 1954, after previous stays in Germany (1944-1950) and Colombia (1950-1954), becoming a U.S. citizen in 1959. After graduating from Central Catholic High School, Lawrence, Mass. he entered Harvard College and received the A.B. degree cum laude in physics in 1962. He then entered the M.I.T. graduate school, where from the beginning he was associated with the interplanetary plasma group, working first on instrumental problems of Faraday cup detectors and then on analysis of the OGO-A data. He contributed a paper based on some of the OGO-A results to the meeting of the American Geophysical Union in April, 1966.